Author's personal copy

Available online at www.sciencedirect.com

SciVerse ScienceDirect

Nuclear Data Sheets 113 (2012) 3054–3100

Nuclear Data Sheets

www.elsevier.com/locate/nds

Determination of Resonance Parameters and their Covariances from Neutron Induced Reaction Cross Section Data

P. Schillebeeckx,[1,*] B. Becker,[1] Y. Danon,[2] K. Guber,[3] H. Harada,[4] J. Heyse,[1] A.R. Junghans,[5] S. Kopecky,[1] C. Massimi,[6] M.C. Moxon,[7] N. Otuka,[8] I. Sirakov,[9] and K. Volev[1]

[1] *EC-JRC-IRMM, Retieseweg 111, B-2440 Geel, Belgium*
[2] *Rensselaer Polytechnic Institute, Troy, NY 12180, USA*
[3] *Oak Ridge National Laboratory, Oak Ridge, TN 37831-6171, USA*
[4] *Japan Atomic Energy Agency (JAEA), Tokai, Naka, Ibaraki 319-1195, Japan*
[5] *Helmholtz-Zentrum Dresden Rossendorf, D-01314 Dresden, Germany*
[6] *University of Bologna and Sezione INFN of Bologna, Via Irnerio 46, I-40126 Bologna, Italy*
[7] *Hyde Copse 3, Marcham, UK*
[8] *IAEA Nuclear Data Section,International Atomic Energy Agency, Wagramerstraße, Vienna, A-1400, Austria*
[9] *Institute for Nuclear Research and Nuclear Energy, BG-1784 Sofia, Bulgaria*

(Received 17 August 2012; revised received 27 September 2012; accepted 3 October 2012)

Cross section data in the resolved and unresolved resonance region are represented by nuclear reaction formalisms using parameters which are determined by fitting them to experimental data. Therefore, the quality of evaluated cross sections in the resonance region strongly depends on the experimental data used in the adjustment process and an assessment of the experimental covariance data is of primary importance in determining the accuracy of evaluated cross section data. In this contribution, uncertainty components of experimental observables resulting from total and reaction cross section experiments are quantified by identifying the metrological parameters involved in the measurement, data reduction and analysis process. In addition, different methods that can be applied to propagate the covariance of the experimental observables (*i.e.* transmission and reaction yields) to the covariance of the resonance parameters are discussed and compared. The methods being discussed are: conventional uncertainty propagation, Monte Carlo sampling and marginalization. It is demonstrated that the final covariance matrix of the resonance parameters not only strongly depends on the type of experimental observables used in the adjustment process, the experimental conditions and the characteristics of the resonance structure, but also on the method that is used to propagate the covariances. Finally, a special data reduction concept and format is presented, which offers the possibility to store the full covariance information of experimental data in the EXFOR library and provides the information required to perform a full covariance evaluation.

Editorial Note*: All papers in the present issue, including this paper, are printed in black and white. Color version is available online at www.sciencedirect.com, see also www.elsevier.com/locate/nds.*

CONTENTS

* Corresponding author, electronic address: peter.schillebeeckx@ec.europa.eu

0090-3752/$ – see front matter © 2012 Elsevier Inc. All rights reserved.
doi:10.1016/j.nds.2012.11.005

Author's personal copy

I. INTRODUCTION

Neutron induced reaction cross sections in evaluated data libraries are mostly based on a parameterisation by means of nuclear reaction theory. In the resolved resonance region (RRR), which also covers the thermal region, cross sections are parameterised based on the R-matrix formalism using parameters of individual resonances [1–3]. Each resonance is characterized by the resonance energy E_R, the total width Γ, the partial reaction widths (*e.g.* the neutron width Γ_n, the capture width Γ_γ, the fission width Γ_f, ...), the total angular momentum J and the orbital angular momentum of the original neutron-nuclear system ℓ and the channel spin s. For a complete consistent description of the total and reaction cross sections also scattering radii are required. However, no theory exists which can predict parameters of individual resonances. Resonance parameters, together with scattering radii, are extracted by adjusting them in a fit to results of time-of-flight (TOF) measurements using Resonance Shape Analysis (RSA) codes based on the R-matrix formalism [4–7].

In the unresolved resonance region (URR) cross sections can be parameterised by the Hauser-Feshbach formalism including a width fluctuation correction [8–10] or more rigorously by solving the triple integral over the Gaussian Orthogonal Ensemble (GOE) of resonances. Alternatively, they can be obtained by creating resonance structured cross sections through Monte Carlo simulations of resonance parameters [11]. Independent of the method that is used, they all rely on average parameters such as level densities and strength functions or transmission coefficients [12]. The average parameters can be derived from a statistical analysis of parameters of resolved resonances [1]. Some of them, such as the neutron strength functions or transmission coefficients for particle reaction channels, can even be obtained from optical model calculations [13, 14]. However, to arrive at a reasonable accuracy level, in particular for the capture reaction channel, an adjustment of the parameters by fitting to experimental data is required [14, 15].

This demonstrates that the quality of evaluated neutron induced reaction cross sections strongly depends on the experimental data that is used to determine nuclear reaction model parameters. To improve the quality of cross section data, including the production of full covariance information, the various sources of uncertainties together with the origin of possible biases have to be identified and quantified. A typical example of a bias effect is Peelle's Pertinent Puzzle (PPP) [16–22]. To avoid PPP various recipes have been proposed [16–19, 22]. Independent of the recipe that is used, the problem can only be avoided if detailed information concerning the covariance matrix of the experimental data is available [23].

In this contribution, the various steps to obtain cross section data in the resonance region are discussed, starting from the production of counting histograms to the determination of resonance parameters together with their covariances. In addition, a procedure is proposed to store the full information that is required to deduce reliable cross sections in the EXFOR library. This procedure provides a scheme to store the full covariance information due to both correlated and uncorrelated uncertainties.

In the paper we have tried to follow as much as possible the terminology defined in the "Guide to the Expression of Uncertainty in Measurement" or GUM(2008) [24] and in Ref. [25]. The uncertainty of a variable X is represented by u_X. All uncertainties which are quoted in this document are standard uncertainties, *i.e.* at one standard deviation.

Author's personal copy

II. TIME-OF-FLIGHT MEASUREMENTS AT A WHITE NEUTRON SOURCE

A. Time-of-Flight Facilities

To study the resonance structure of neutron induced reaction cross sections neutron spectroscopic measurements are required which determine with a high accuracy the energy of the neutron interacting with the material under investigation [26]. They can be carried out at a continuous source using a chopper [27] or at an accelerator driven white neutron source operating in pulsed mode [28].

Measurements using a chopper, mostly performed at a reactor, are limited to studies in the low energy region. However, they are essential to produce consistent cross sections from thermal energy up to the continuum. Thermal cross section data and scattering lengths, compiled in Ref. [29] and Ref. [30, 31], respectively, are important to adjust the contribution of bound states. Transmission measurements with a chopper have been used extensively to determine absolute capture cross section data at extreme low energies [32] and to verify deviations from the $1/v$ behavior of reaction cross sections in the low energy region [33].

To cover a broad energy range, the resonance region is best studied at a pulsed white neutron source that is optimised for TOF measurements [26, 28, 34]. Pulsed neutron sources can be realized at electron- and proton-based accelerators. In electron-based accelerators high-energy electrons generate Bremsstrahlung in a target made out of material with a high mass number (*e.g.* Ta, Hg or U) and neutrons are produced via photonuclear reactions. High-energy proton accelerators produce neutrons via the spallation process in target also made out of high mass number material. The energy spectrum of neutrons produced by spallation and photonuclear reactions is not directly exploitable for low energy neutron resonance spectroscopy. A moderator consisting of hydrogen rich material is used to increase the amount of low-energy neutrons and produce a broad neutron spectrum ranging from thermal energies up to the high energy region.

Due to their different constructions and operation modes, pulsed neutron sources have different characteristics. The flight path length together with the pulse width determine in part the neutron energy resolution of a facility. Other contributing factors are the construction, materials and dimensions of the neutron production target together with the corresponding slowing down process of the neutron in the target-moderator assembly. This process is energy dependent and can vary from neutron source to neutron source, depending on the target and moderator size. Electron driven sources have a relatively small neutron producing target-moderator assembly, compared to spallation sources. The latter are usually optimised for high neutron flux, as a result long tails on the resonances are observed for measurements at spallation sources. These tails can be confused with background in a capture measurement and with a biased normalization in a transmission measurement. On the other hand spallation sources have mostly a much higher instantaneous neutron flux. Hence, they are more suitable for measurements of radioactive material. Table I shows characteristics of some TOF facilities, which are dedicated to neutron cross section measurements. Some of them have several measurement stations such that experiments can be carried out in parallel.

Charged particle reactions, such as ^{7}Li(p,n)^{7}Be, together with a pulsed proton source can be used to perform TOF experiments in the URR and in the RRR for nuclei with a relatively low level density. A ^{7}Li(p,n)^{7}Be neutron source is normally operated with a fixed short pulse using a bunching system. At the threshold proton energy of 1.881 MeV neutrons are emitted in forward direction. If the proton energy is adjusted approximately 100 keV above the threshold, a continuous neutron spectrum with neutron energies from 3 keV to 200 keV is realized. Such a neutron source is especially suited to determine average total and capture cross section data in the URR. Accurate total and capture cross section data have been derived from measurements with a Li-glass scintillator and 4π BaF_2-detector, respectively, at the Van de Graaff accelerator of the Karlsruhe Institute of Technology [47, 48]. Similar capture measurements, using a NaI(Tl) spectrometer, have been carried out at Pelletron of the Tokyo Institute of Technology [49, 50].

B. Time-of-Flight Technique

The TOF technique can be applied to determine the velocity v of a neutron from the time t it needs to travel a given distance L. Experimentally this time is derived from the difference between a stop and a start signal, represented by T_s and T_0, respectively. At the GELINA facility of the EC-JRC-IRMM [37], for example, the start signal is produced when the pulsed electron beam passes through a coil just before the beam enters the uranium target. This signal represents the time the neutron is produced. The stop signal or arrival time of the neutron in a transmission experiment is provided by the neutron detector. In a reaction cross section experiment the arrival time is obtained from the detection of the reaction products which are emitted in the neutron induced reaction. The observed TOF t_m becomes

$$t_m = (T_s - T_0) + t_0, \tag{1}$$

where t_0 is a time offset. This time offset, which is mostly due to a difference in cable lengths, can be deduced from a measurement of the TOF of the γ-ray flash produced in the target.

The time-of-flight t_m can be related to the velocity v of the neutron at the moment it leaves the target and enters the detector or sample by

$$v = \frac{L}{t} = \frac{L}{t_m - (t_t + t_d)}, \tag{2}$$

Author's personal copy

TABLE I. Characteristics of TOF facilities used for cross section measurements. Similar comparisons of some of these facilities can be found in Ref. [35, 36].

Facility	Ref.	Type	Particle Energy (MeV)	Target	Pulse width (ns)	Frequency (Hz)	Flight path length (m)
GELINA	[37]	e^-	80 - 140	U	1	40-800	10-400
KURRI (short pulse)	[38]	e^-	20 - 46	Ta	2, 5, 10, 22, 33, 47, 68, 100	1 - 300	10, 13, 24
KURRI (long pulse)		e^-	7 - 32	Ta	100 - 4000	1 - 100	10, 13, 24
nELBE	[35]	e^-	40	Pb	0.01	500000	4
ORELA	[34]	e^-	140	Ta	2 - 30	1 - 1000	10 - 200
POHANG	[39]	e^-	75	Ta	2000	12	11
RPI	[40]	e^-	60	Ta	7 - 5000	500	10 - 250
J-PARC/MLF - ANNRI	[41, 42]	p	3000	Hg	600	25	21, 28
LANSCE - MLNSC	[43, 44]	p	800	W	135	20	7 - 60
LANSCE - WNR	[43, 44]	p	800	W	0.2	13900	8 - 90
n_TOF	[45]	p	20000	Pb	6	0.4	185

where L is the distance between the outer surface of the neutron-producing target and the front face of the detector or sample, t_t is the time difference between the moment that the neutron leaves the target and the moment of creation and t_d is the difference between the time of detection and the moment the neutron enters the detector or sample. The kinetic energy of the neutron is given by

$$E = mc^2(\gamma - 1), \tag{3}$$

where m is the rest mass of the neutron and γ represents the Lorentz factor

$$\gamma = \frac{1}{\sqrt{1 - (v/c)^2}}, \tag{4}$$

with c the speed of light.

The energy resolution ΔE of a TOF spectrometer is related to the velocity resolution Δv by

$$\frac{\Delta E}{E} = (\gamma + 1)\gamma\frac{\Delta v}{v}. \tag{5}$$

At low velocities ($\gamma \approx 1$) the relative energy resolution is twice the relative velocity resolution. The velocity resolution is a combination of the resolution broadening due to the TOF t and distance L represented by Δt and ΔL, respectively

$$\frac{\Delta v}{v} = \sqrt{\left(\frac{\Delta t}{t}\right)^2 + \left(\frac{\Delta L}{L}\right)^2}. \tag{6}$$

The distance L can be determined by metric measurements with an uncertainty of less than 1 mm ($\Delta L < 1$ mm at full width half maximum (FWHM)). The TOF t corresponding to the distance L depends on t_m, t_t and t_d.

C. Response Function of a Time-of-Flight Spectrometer

The response function of a TOF-spectrometer $R(t_m, E)$ is the probability that a neutron with energy E is detected with a time-of-flight t_m. It can be considered as a convolution of different independent components:

- finite duration of the accelerator burst (T_0);
- time resolution of the detector and electronics (T_s);
- neutron transport in the neutron producing target (t_t);
- neutron transport in the detector or sample (t_d).

The finite duration of the accelerator burst can mostly be represented by a simple analytical function, *e.g.* a normal or trapezium shaped distribution with a width that is independent of neutron energy. This distribution can be determined by measurements of the γ-ray flash using a scintillator with a fast time response. The random time jitter of the detector and electronics, which determines the time T_s, can be described by a normal distribution with a width independent of energy. Since these components are independent, their contribution can be combined in one normal distribution with a total width that is derived from the quadratic sum of the two components. To account for the bin width of the time-of-flight histogram a rectangular distribution is often assumed. Often TOF-spectra are divided into several zones, referred to as accordion, each with a fixed channel width.

1. *Moderated neutron beam*

In case of a moderated neutron beam the broadening in time is dominated by the neutron transport in the target-moderator assembly, *i.e.* the time component t_t. Consequently, response functions will strongly depend on the neutron physics properties of the target-moderator assembly (dimensions and materials). The distribution of this component can be deduced from Monte Carlo calculations or approximated by analytical expressions. Monte Carlo (MC) simulations to determine the probability distribution of the time the neutron spends in the target-moderator assembly have been carried out for *e.g.* ORELA [51], RPI [40], GELINA [52] and n_TOF [45, 46]. Fig. 1 shows response functions due to the neutron transport in the target-moderator assembly for the GELINA facility. The distributions are for a moderated neutron

Author's personal copy

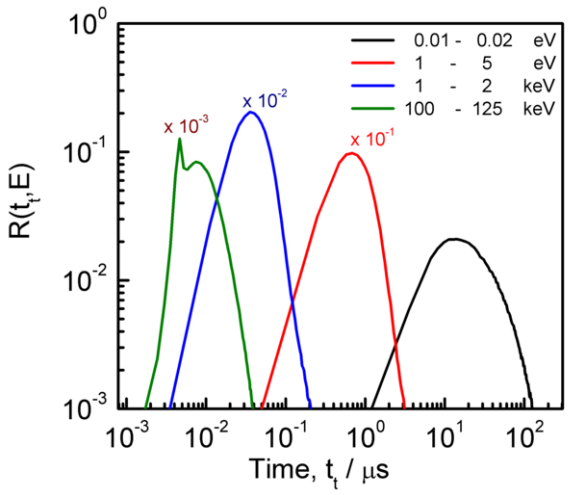

FIG. 1. The probability distribution of the time t_t that a neutron spends in the target-moderator assembly of GELINA.

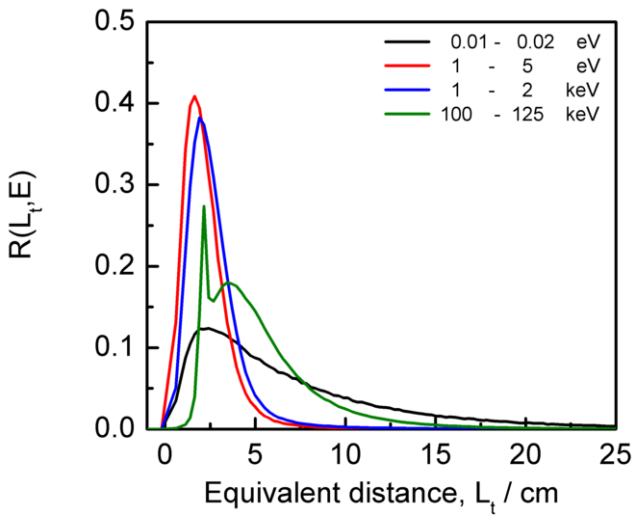

FIG. 2. The probability distribution of the equivalent distance L_t that a neutron travels in the target-moderator assembly of GELINA.

beam and a flight path that forms an angle of 0° with the normal to the exit face of the moderator. These distributions strongly depend on the neutron energy. Response functions of a TOF-spectrometer can be more conveniently represented by introducing an equivalent distance L_t travelled by the neutron in the target-moderator assembly [51, 53]. The equivalent distance is defined as $L_t = vt_t$, where v is the velocity of the neutron at the moment it escapes from the target-moderator assembly. This transformation of variables results in probability distributions of L_t which are less dependent on the neutron energy, as shown in Fig. 2. The energy dependences of the average equivalent distance and most probable distance, shown in Fig. 3, demonstrate that it is not evident to transform TOF-spectra into energy spectra.

Several examples of analytical expressions reflecting the neutron transport in the target-moderator system have been proposed [6, 51, 53, 55, 56]. They all have two common components: an exponential decay due to the primary neutron production in the target and a χ^2-distribution describing the distribution of the equivalent distance L_t, as suggested by Groenewald and Groendijk [54]. For neutron energies below 1 eV an additional storage term has to be taken into account as demonstrated by Ikeda and Carpenter [55]. The peak in the low energy region observed in Fig. 3 is due to this storage term. In case the flight path is not parallel with the normal to the exit face of the moderator additional broadening is caused by the angle between the moderator face and the flight path. Also this contribution can be described by an analytical function [6].

The resolution of a TOF-spectrometer can be experimentally assessed by a partial cross section measurement in the region of an isolated resonance using a relatively thin sample. The resonance should have a total width and Doppler broadening component which are small com-

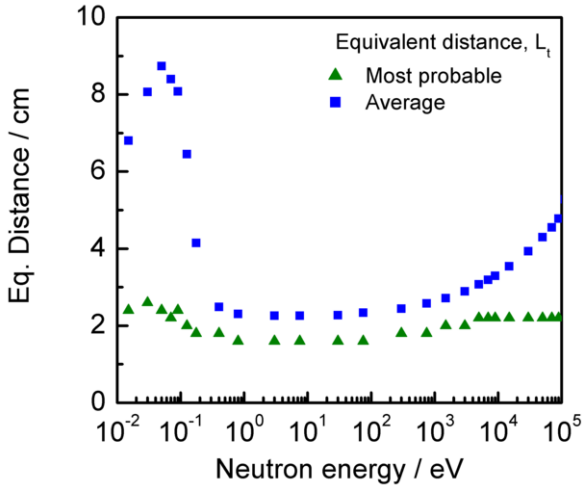

FIG. 3. The average and most probable equivalent distance as a function of neutron energy for the target-moderator assembly of GELINA.

pared to the width of the response of the spectrometer. An example is given in Fig. 4, which plots the experimental capture yield in the energy region of the 34 keV resonance of ^{56}Fe as a function of neutron energy. The yield was obtained from measurements at a 60 m station of GELINA. For this resonance the total width is $\Gamma \approx 2$ eV, the Doppler width (FWHM) is ≈ 13 eV and the TOF-resolution (FWHM) is ≈ 40 eV. Thus, the measured profile is dominated by the resolving power of the TOF-spectrometer. The good agreement between the experimental and calculated yield confirms the quality of the response functions. In the same figure the response

Author's personal copy

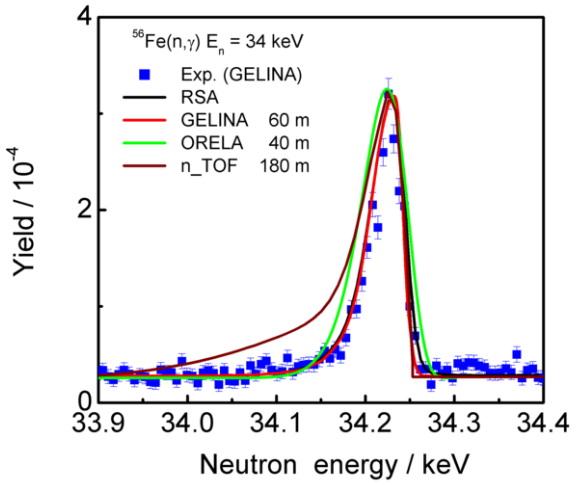

FIG. 4. The experimental yield in the region of the 34 keV resonance of ^{56}Fe obtained at a 60 m station of GELINA. The yield is compared with the result of a RSA. The response functions of GELINA, n_TOF and ORELA are also given.

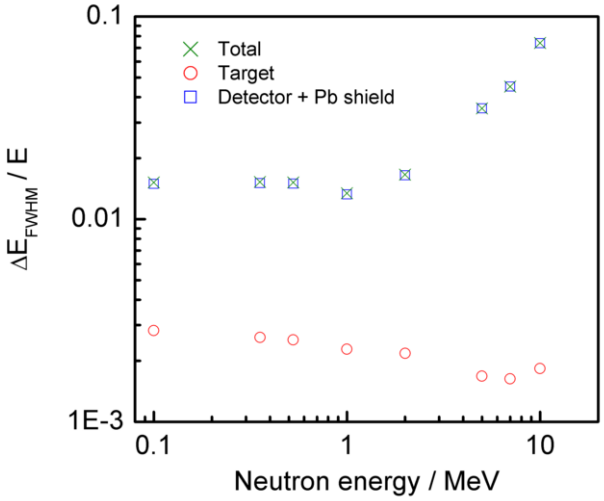

FIG. 5. The total energy resolution (at FWHM) (×) for transmission measurements at nELBE together with the contribution due to the neutron target (○) and the one from a 1.1 cm thick plastic scintillator [58] including a 1 cm Pb shield (□).

function of GELINA at 60 m is compared with the one of ORELA at 40 m and the one of n_TOF at 180 m. They have been normalized to the same peak height. This figure clearly demonstrates the difference in resolution of a facility based on a spallation source, such as n_TOF, and a white neutron source resulting from photonuclear reactions as GELINA and ORELA. Although the measurement station at the n_TOF facility has a flight path of 180 m, the observed width is broader compared to the profile obtained at a 60 m station of GELINA and a 40 m station of ORELA. In addition, a more pronounced tail on the low energy side of the resonance profile is observed. This difference is mainly due to the geometry of the neutron producing target-moderator assembly, which is more compact for a neutron source based on photonuclear reactions compared to a spallation type of neutron source. A more extensive comparison between the response of GELINA and n_TOF can be found in Ref. [57]. The difference between the response of ORELA and GELINA shown in Fig. 4, is mainly due to the difference in flight path length.

Reaction cross section measurements are mostly carried out on relatively thin samples and the impact of the time t_d can be neglected. However, in case of transmission measurements the finite size of the detector adds to the final response. This contribution is again best expressed in terms of an equivalent distance L_d defined by $L_d = vt_d$. Also this contribution can be estimated by Monte Carlo calculations or approximated by analytical expressions [6].

2. *Fast neutron beam*

For light nuclei or nuclei with a neutron or proton number near a closed shell the resolved resonance region extends to a few MeV and measurements are preferably performed at a fast neutron beam without the use of a moderator or by shielding against the moderator.

Response functions for neutron energies above 0.5 MeV for a fast (or direct) neutron beam at GELINA have a FWHM of about 0.5 cm due to the neutron transport in the target [52]. The final response is practically dominated by the shape of the pulsed electron beam and the time response of the detector and associated electronics. The pulsed electron beam can be approximated by a normal distribution with a FWHM of about 1 ns.

Monte Carlo simulations have been carried out to estimate the TOF-response of the fast neutron TOF facility nELBE [35]. The energy resolution due to the neutron producing target, $\Delta E/E \approx 2.35 \times 10^{-3}$ at FWHM, is mainly due to the geometrical extension of the target. Scattering of neutrons in the Pb absorber and neutron collimator leads to a moderate increase of the resolution. However, the total TOF-response in a transmission measurement at nELBE is strongly affected by neutrons which are scattered in the shielding material surrounding the neutron detector. This effect has been included in the MC-simulations. The total energy resolution together with the contribution of different components are shown in Fig. 5 for a 7 m flight path. The results of MC-simulations have been validated by transmission measurements on a natural Pb sample. The results of the transmission measurements are compared in Fig. 6 with a calculation that is based on a folding of an evaluated to-

Author's personal copy

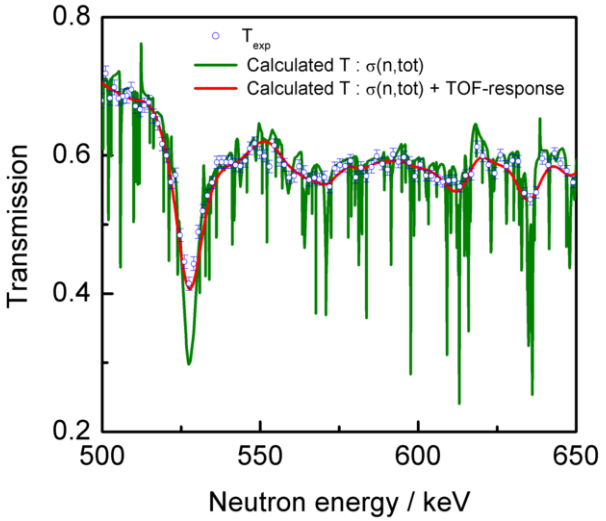

FIG. 6. Results of a transmission measurement on a 3 cm thick lead sample at nELBE. The experimental data are compared with calculated transmission curves based on the evaluated total cross section taken from ENDF/B-VII.1 [59]. The experimental energy resolution has been included by folding the transmission with a Gaussian response function based on the energy resolution shown in Fig. 5.

tal cross section with a Gaussian response using the total width obtained from Fig.5. The good agreement between experimental and calculated data in Fig. 6 confirms the result of the calculations.

D. Dead Time Corrections

All count rate spectra obtained from a TOF-experiment require a correction due to the dead time of the detection system consisting of the detector, electronics, digitizers and data acquisition system. In case of a fixed (non-extendable) dead time, the correction is well understood. Moore [60] derived an expression which takes into account the variation of the neutron beam intensity. To verify the accuracy of the correction, dedicated measurements have been performed at a capture measurement station of GELINA using a 1 mm thick ^{197}Au sample. TOF-spectra were taken with different fixed dead times from τ_d=240 ns up to τ_d=10000 ns. The uncorrected and corrected spectra together with the correction factors are shown in Fig. 7. The results in Fig. 7 together with a sensitivity study, which was performed to verify the influence of variations in beam intensity and dead time τ_d, indicate that uncertainties due to the dead time correction are $\leq 0.3\%$ when the dead time correction is less than a factor 1.3, the variation of the beam intensity is $\leq 15\%$ and the uncertainty on the dead time is $\leq 0.25\%$. Similar conclusions have been drawn in Ref. [61].

III. THEORETICAL CONSIDERATIONS

A. Nuclear Reaction Models in the Resonance Region

The R-matrix formalism, which was introduced by Wigner and Eisenbud [2], is a nuclear reaction formalism that is particularly suited for the parameterisation of resonance structured cross sections. A detailed description of the theory is given by Lane and Thomas [3]. Several approximations of the R-matrix formalism are used and an overview is given by Fröhner [1].

The R-matrix formalism links the properties of excited states of the compound nucleus, such as energy, spin, parity and partial reaction widths, to the cross sections. An effective and reasonable R-matrix approximation is the Reich-Moore (RM) one [62]. Its assumption that photon channels have only a diagonal contribution to the width matrix is justified by the great number of radiative channels and practically random signs of their width amplitudes.

For light nuclei, accurate cross sections can only be parameterised based on a full R-matrix analysis by *e.g.* codes like EDA [4] and RAC [5]. These codes are also able to treat direct and inverse channels, simultaneously. However, they do not account for experimental details such as the response function of the TOF-spectrometer, self-shielding, multiple interaction effects and detector and sample characteristics. More general purpose codes are REFIT [6] and SAMMY [7]. REFIT is based on the Reich-Moore approximation of the R-Matrix formalism and includes modules to account for various experimental effects such as sample inhomogeneities, self-shielding, multiple scattering, Doppler broadening, response of the TOF-spectrometer, neutron sensitivity of the capture detection system and γ-ray attenuation in the sample. SAMMY includes most of these effects and an option to perform full R-matrix analysis.

Formalisms to parameterise cross sections in the URR are based on average parameters. In the absence of direct reactions, the fluctuating cross sections depend only upon the transmission coefficients [8–10]. Independent parameters that describe the average total and partial cross sections for non-fissile nuclei are, for instance, the neutron strength functions S_ℓ, the scattering radius R' and the capture transmission coefficients at zero neutron energy $T^{J^\pi}_{\gamma,0}$ [14, 19]. In first approximation, the neutron strength functions can be considered as being energy independent. The J-dependence of $T^{J^\pi}_{\gamma,0}$ can be determined from the known J-dependence of the level density [14] with the common assumption that the effective radiation widths only depend on parity.

B. Doppler Broadening

When a nuclear reaction takes place the atomic nuclei are not at rest in the laboratory system, but they

Author's personal copy

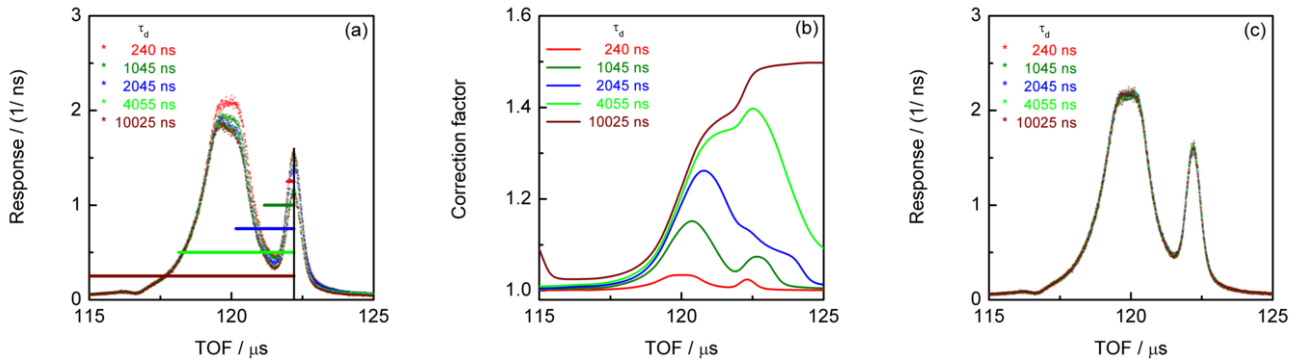

FIG. 7. TOF-spectra obtained at GELINA for a 1 mm thick ^{197}Au sample taken with different fixed dead time τ_d. The uncorrected spectra are shown in (a), the dead time correction factors in (b) and the dead time corrected spectra in (c). In (a) the region affecting the response at 122.2 μs for different values of τ_d are indicated.

have thermal motion in the lattice of the sample material. Since the thermal motion is a statistical process with an energy distribution, the cross sections will be broadened, which is known as Doppler broadening. A Doppler broadened cross section $\overline{\sigma}$ can be obtained from the convolution of the nuclear cross section σ with an energy transfer function $S(E', E)$ which accounts for the energy distribution of the target nuclei [63]

$$\overline{\sigma}(E) = \int dE' S(E, E')\sigma(E'). \tag{7}$$

Within the free gas model approximation (FGM) the target velocity distribution is given by a Maxwell-Boltzmann distribution. For energies much larger than the Doppler width $E \gg \Delta_D$, a Doppler broadened cross section can be approximated by a convolution of $\sqrt{\frac{E'}{E}}\sigma(E')$ with a Gaussian [1]

$$\overline{\sigma}(E) \approx \frac{1}{\Delta_D\sqrt{\pi}} \int_{-\infty}^{\infty} dE'\ e^{-\left(\frac{E'-E}{\Delta_D}\right)^2} \sqrt{\frac{E'}{E}}\sigma(E'), \tag{8}$$

The Doppler width Δ_D is defined as

$$\Delta_D = \sqrt{\frac{4Ek_BT}{M/m_n}}, \tag{9}$$

where k_B is the Boltzmann constant and M and m_n are the rest mass of the target nucleus and neutron, respectively. This width is related to the full width half maximum (FWHM) of the Gaussian by: FWHM $= 2\sqrt{\ln 2}\Delta_D$.

It has been shown by Lamb [64] that for a crystalline solid the transfer function $S(E, E')$ can be derived assuming a Maxwellian distribution of velocities for the target nuclei, similar to a mono-atomic free gas or a classical solid, by introducing an effective temperature T_{eff}. Using a simple Einstein model, the effective temperature T_{eff} is related to the temperature T of the sample and the Debye temperature Θ by [63]

$$T_{eff} = \frac{3}{8}\Theta \coth\left(\frac{3}{8}\Theta/T\right), \tag{10}$$

and replaces the temperature T in Eq. (9). This is usually accurate enough at room temperature where T_{eff} is only a few percent greater than Θ. It should be noted that the influence of the crystalline and molecular vibrations is mainly of importance at low temperatures and for low energy resonances. For an accurate description of the observed resonance profile in some cases more sophisticated theories are required. In case of a crystal, the phonon spectrum can be used to evaluate the interaction probability (see *e.g.* [65–68]).

For many elements the Debye temperature is significantly lower than the room temperature. In all these cases the effective temperature for the FGM is just slightly higher than the room temperature. The FGM provides then a good approximation to account for the Doppler effect. This can be demonstrated by results of transmission measurements for ^{241}Am carried out at a 25 m station of GELINA [69]. Using a Crystal Lattice Model (CLM) based on the DOPUSH code [67] only a slightly better description of the experimental resonance shape is obtained compared with the calculations using the FGM. This is illustrated in Fig. 8 for the 0.31, 0.57 and 1.27 eV resonances of ^{241}Am. When fixing the resonance parameters derived with the CLM and only adjusting the effective temperature, the optimum T_{eff} is, within the uncertainties due to counting statistics, in agreement with the one calculated using a Debye temperature quoted in the literature. In addition, the transmission data obtained at room temperature show that a change of T_{eff} by 1 meV (corresponding to approximately 12 K) results in a change in the total width of less than 1%. It is also worth noting that for the first three resonances of ^{241}Am the average radiation width extracted by applying the CLM agrees within 1% with

Author's personal copy

the one applying the FGM using the recommended Debye temperature and measured room temperature.

C. Theoretical Estimates of Experimental Observables

Cross section measurements can be divided into transmission measurements, from which the total cross section is determined, and reaction cross section measurements from which the partial cross section of a neutron induced reaction (n,r) is deduced.

1. Resolved resonance region

In a transmission experiment the observed quantity is the fraction of the neutron beam traversing the sample without any interaction. For a parallel neutron beam, which is perpendicular to a homogeneous slab of material, this fraction or transmission T is

$$T = e^{-\sum_k n_k \overline{\sigma}_{tot,k}}, \tag{11}$$

where $\overline{\sigma}_{tot,k}$ is the Doppler broadened total cross section and n_k is the number of atoms per unit area of nuclide k.

In a reaction cross section measurement the quantity of interest is the reaction yield, which is the fraction of the neutron beam inducing a reaction in the sample. The theoretical reaction yield $Y_{r,k}$ resulting from a neutron induced reaction (n,r) with nuclide k, can be expressed as a sum of primary $Y_{0,k}$ and multiple interaction events $Y_{m,k}$

$$Y_{r,k} = Y_{0,k} + Y_{m,k}. \tag{12}$$

The latter are due to a (n,r) reaction after at least one neutron scattering in the sample. For a parallel uniform neutron beam and a homogeneous slab of material, which is placed perpendicular to the neutron beam, the primary yield $Y_{0,k}$ is given by

$$Y_{0,k} = \left(1 - e^{-\sum_j n_j \overline{\sigma}_{tot,j}}\right) \frac{n_k \overline{\sigma}_{r,k}}{\sum_j n_j \overline{\sigma}_{tot,j}}, \tag{13}$$

where $\overline{\sigma}_{r,k}$ is the Doppler broadened reaction cross section. Only for very thin samples and/or small cross sections, such that $\sum_j n_j \overline{\sigma}_{tot,j} \ll 1$, the reaction yield is directly proportional to the reaction cross section, with $Y_{r,k} \approx n_k \overline{\sigma}_{r,k}$.

The calculation of the reaction yield, in particular the contribution of the multiple interaction events is one of the most complex parts of a resonance shape analysis code. For a parallel beam traversing a sample with a simple composition and geometry, *e.g.* discs or foils, the primary yield (Eq. (13)) is a straightforward function depending on area densities and Doppler broadened cross sections. In case of one scattering followed by a reaction event and a simple geometry, exact expressions can be derived based on asymptotic free gas scattering. For more than one scattering (m > 1), one usually makes the additional assumption that neutrons are uniformly distributed within the sample. These approximations are implemented in SAMMY and REFIT.

A second deterministic solution in REFIT is based on a more elaborated approximation for the Doppler effect to account for the thermal motion of the sample nuclei in the calculation of the energy of the scattered neutron. The difference between the two options can be seen in Fig. 9, showing the experimental yield around the 69 eV resonance of ^{232}Th resulting from capture measurements on a 1 mm thick and 80 mm diameter metal Th disk at GELINA. The experimental yield is compared with the calculated yield using the two options in REFIT [70].

To fully account for both the thermal motion of the sample nuclei and resonance structures in the calculation of the scattering kernel, a stochastic approach referred to as Doppler Broadened Rejection Correction (DBRC) was developed by Becker et al. [71]. This approach has been tentatively implemented in the Monte Carlo code SAMSMC [72], which was originally developed to verify deterministic calculations of $Y_{m,k}$ and is included as an auxiliary module in SAMMY. A comparison of the experimental and theoretical yields in Fig. 9 demonstrates that for the 69 eV resonance of ^{232}Th the yield calculated with the second option in REFIT is in very good agreement with the one obtained from SAMSMC including DBRC. Similar observations were made in Ref. [73]. Only in very special cases, the DBRC option is needed to describe experimental yields. In case of complex geometries, relatively thick samples and/or strong scattering resonances, experimental yields can only be reproduced by Monte Carlo simulations, as demonstrated in Ref. [70] for capture measurements on a thick Mn sample.

2. Unresolved resonance region

To deduce average cross sections in the URR from experimental observables corrections due to resonance structures are needed. The average total cross section is derived from

$$\langle T_{exp} \rangle = F_T e^{-n\langle \sigma_{tot} \rangle}. \tag{14}$$

The correction factor F_T, which is important for thick samples and strongly fluctuating cross sections, can be derived by creating a ladder of resonances based on statistical models and calculating the variance and higher moments of the resulting Doppler broadened cross sections. This method is implemented in the SESH code developed by Fröhner [11]. The code starts from average resonance parameters (*i.e.* level densities, neutron strength functions and average radiation widths) to create resonance structured cross sections. The factor F_T

Author's personal copy

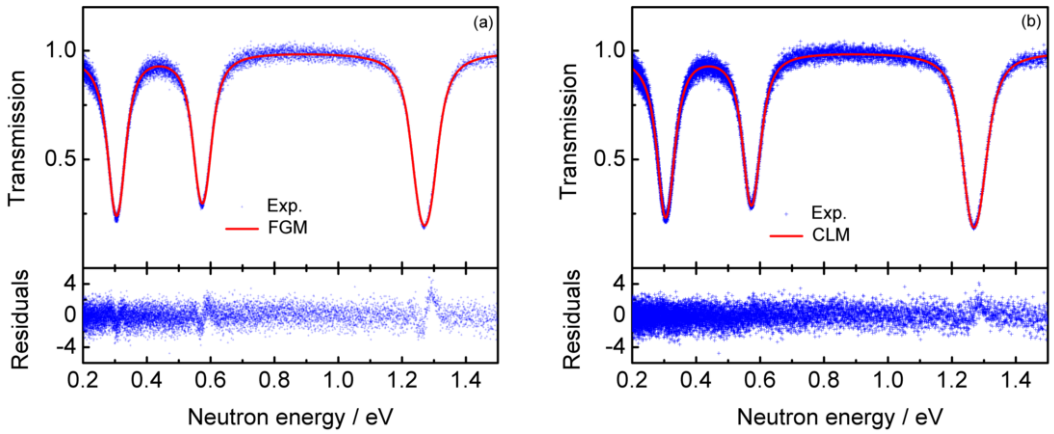

FIG. 8. The transmission around the 0.31, 0.57 and 1.27 eV resonances of ^{241}Am derived from measurements at a 25 m station of GELINA. The experimental transmission is compared with the result of a RSA based on the FGM (a) and the CLM (b).

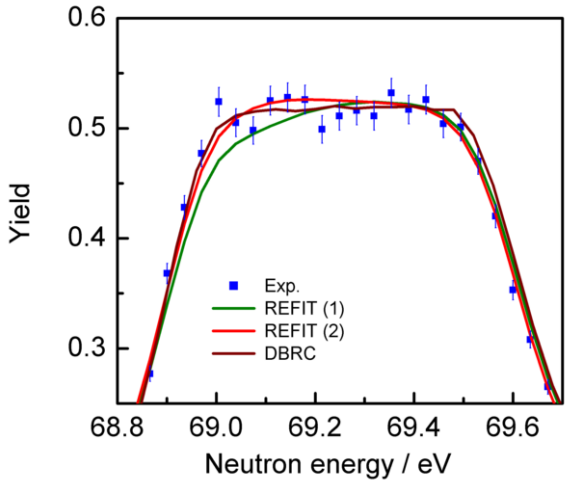

FIG. 9. Comparison of the experimental and calculated yield in the peak region of the 69 eV resonance of ^{232}Th for a 1 mm thick metal disc measured at GELINA [70]. The theoretical yield is given for three different treatments of the Doppler broadening (see text).

can also be calculated by Monte Carlo simulations using probability tables, produced *e.g.* by NJOY [74], to account for the resonance structures.

Average capture cross sections in the URR are mostly derived from results of measurements with relatively thick samples. In addition to the correction for self-shielding, which is again subject to resonance fluctuations, the experimental yield has to be corrected for events due to neutron scattering followed by capture. The relation between the average capture cross section $\langle\sigma_\gamma\rangle$ and the average experimental yield $\langle Y_{exp}\rangle$ is expressed as

$$\langle Y_{exp}\rangle = F_c n_x \langle\sigma_\gamma\rangle, \tag{15}$$

where F_c is a correction factor to account for the contribution due to neutron attenuation in the sample and multiple interaction events. Due to the finite dimensions and shape of the sample Monte Carlo simulations are recommended. The SESH code includes a module to perform such simulations. The correction can also be derived by a combined use of MCNP and probability tables. Fig. 10 reveals a good agreement between results obtained with SESH and MCNP/NJOY. Similar agreements are obtained for the correction factor F_T used in Eq. (14). Unfortunately, the SESH code is limited to simple geometries. The MCNP/NJOY procedure offers the advantage that more complex geometries and sample characteristics can be considered and various systematic effects (*e.g.* the influence of the energy dependence of the neutron flux, the sample diameter) can be verified to estimate their contribution to the uncertainty.

IV. TOTAL CROSS SECTION MEASUREMENTS

A. Principles

Transmission measurements are the simplest, however, also the most accurate type of cross section measurements. Experimentally the transmission T_{exp} is obtained from the ratio of TOF spectra resulting from a sample-in C_{in} and a sample-out measurement C_{out}, after subtraction of the background contributions B_{in} and B_{out}, respectively [76]

$$T_{exp} = N_T \frac{C_{in} - B_{in}}{C_{out} - B_{out}}. \tag{16}$$

Author's personal copy

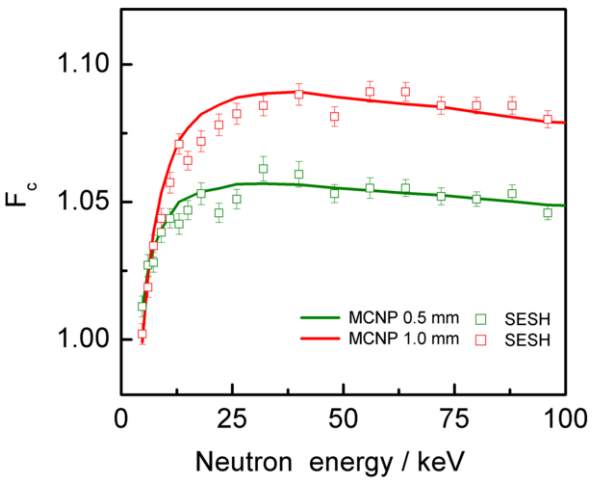

FIG. 10. Factors F_c, to correct for self-shielding and multiple interaction events, for a 0.5 mm and 1.0 mm thick ^{197}Au sample obtained with SESH are compared with those from MCNP/NJOY.

The experimental spectra in Eq. (16) are corrected for losses due to the dead time in the detector and electronics chain (see section II D), and all spectra are normalized to the same neutron intensity and TOF-bin width. The factor N_T accounts for the ratio of the total intensities of the incident neutron beam during the sample-out and sample-in cycles. This factor is mostly derived from neutron detectors monitoring the total neutron production. Thus, its uncertainty depends on the stability of both the neutron monitors and the neutron transmission detectors. Typically an uncertainty better than 0.5% can be reached. This uncertainty can be reduced by alternating sequences of sample-in and sample-out measurements.

Eq. (16) reveals that the experimental transmission is deduced from a ratio of counting spectra. Therefore, it is independent of the detector efficiency and no absolute measurement of the neutron flux is required. For neutron energies below 1 MeV Li-glass scintillators enriched in ^{6}Li are mostly used [76–79]. At higher energies plastic and liquid scintillators (e.g NE213 or EJ-301 type) [58, 77, 80] are used. They are, however, more sensitive to γ-rays compared to Li-glass scintillators. In the case of liquid scintillators pulse-shape analysis can be performed to reject events from γ-rays and to reduce their contribution to the background [80]. The time resolution of such detectors depends on the neutron transport within the detector. Thus, the probability distribution of t_d (or of the equivalent distance L_d) will depend on the size, material density and cross sections of the main components with which the neutron interacts in the detector.

The experimental observable T_{exp} (Eq. (16)) is a direct measure of the theoretical transmission (Eq. (11)) if the measurements are performed in a good transmission geometry, that is:

- the sample is perpendicular with respect to a parallel incoming neutron beam;
- all neutrons that are detected have passed through the sample; and
- neutrons scattered by the sample are not detected.

In addition, it requires a constant homogeneous spatial distribution of the sample material. The conditions of an ideal or good transmission geometry can be achieved by a proper collimation of the neutron beam at both the sample and detector position.

B. Background

1. *Moderated spectrum*

The background in a TOF transmission measurement can be considered as a sum of a time independent and time dependent components [76, 81]

$$B(t) = B_0 + B_\gamma(t) + B_{no}(t) + B_{ns}(t) + B_{ne}(t). \quad (17)$$

For measurements at a moderated neutron beam, the contribution $B_\gamma(t)$ is primarily due to the detection of 2.2 MeV γ-rays resulting from neutron capture in hydrogen present in the moderator. Since the energy deposited by a 2.2 MeV γ-ray in a Li-based scintillator is comparable to the energy deposited by the charged particles produced in the ^{6}Li(n,α) reaction, this component is hard to suppress by pulse-height discrimination. The time distribution of the 2.2 MeV γ-rays is directly related to the slowing down process of the neutrons in the moderator. Monte-Carlo simulations have shown that for the GELINA facility this component can be described by an exponential decay with a decay time of about 25 μs [76]. The time distribution of this component was confirmed by measurements with polyethylene filters in the beam. The polyethylene filter is used to enhance the ratio of γ-ray to neutron beam intensity. The decay constant resulting from a similar study with a Li-glass scintillator carried out at ORELA was 25.4 μs [81]. Additional γ-ray background results from high energy γ-rays and Bremsstrahlung scattered in the target-moderator assembly. Since their energy spectrum is dominated by Compton scattered γ-rays around 250 keV, their contribution can be significantly reduced by a proper pulse height threshold. In addition, their arrival time corresponds to the one of fast neutrons. The second time dependent component $B_{no}(t)$ results from overlap neutrons, *i.e.* neutrons which are detected but have been produced in a previous cycle. This contribution can be reduced by inserting a ^{10}B or Cd overlap filter in the beam. The optimum type and thickness of such filters are defined by the overlap energy and the application. The component $B_{no}(t)$, which strongly depends on the operating frequency and the kind of overlap filter that is used, can

Author's personal copy

be estimated from measurements in the same experimental conditions, however, at a lower operating frequency of the accelerator or by an extrapolation of the time response at the end of a cycle. A third time dependent component $B_{ns}(t)$ originates predominantly from beam neutrons which are scattered inside the detector station. To deduce their time dependence, measurements can be carried out in experimental conditions that exclude the impact of both overlap neutrons and 2.2 MeV γ-rays. Such conditions can be realized by a proper combination of the operating frequency and filters, *e.g.* for a 25 m and 50 m station by measurements at 100 Hz with a Cd-overlap filter and a Pb filter to reduce the γ-ray background. A small background component $B_{ne}(t)$ is due to neutrons scattered in the surroundings (environment) or at other flight paths in case of a multi-user facility. The time dependence is mostly very weak and its contribution is hard to be distinguished from the time independent background B_0. The overall contribution B_0 + $B_{ne}(t)$ can be determined by measurements with the beam closed.

Finally, the background as a function of TOF can be determined by an analytical expression applying the black resonance technique. The free parameters in the analytical expression are determined by a least square fit to resonance dips observed in the TOF-spectra from measurements with black resonance filters. The thickness of the filter is chosen to ensure that the transmission through the filter at the resonance energy is less than 10^{-4}. Ideally, the black resonances have a large capture to scattering cross section ratio and a total width that is larger than the resolution. The filters should be placed far away from the detector position. Elements that can be used as black resonance filters are *e.g.* Cd, Ag, W, Mo, Co, Al, Na and S. At higher energies relatively thick Si or Ti are applicable.

Unfortunately, the presence of both the sample and black resonance filter will alter the background. In particular, the time dependent components $B_\gamma(t)$, $B_{no}(t)$ and $B_{ns}(t)$ are very sensitive to the absorption and scattering characteristics of the filter and sample. To avoid bias effects in the background, the change in background level due to the presence of the sample and the filters has to be taken into account [82]. An extrapolation to zero thickness for each individual filter is time consuming since it should be repeated for each sample. The limitations of the combination of measurements with two black resonance filters to extrapolate to zero filter thickness is discussed in Ref. [82] and [83]. This method underestimates the background when more than one component is present and will produce a neutron width which is biased to lower values [83]. These limitations can be avoided by the black and white filter method proposed by Syme [82]. In addition to a black resonance with a zero transmission, it relies on calculated transmissions. The best results are obtained when regions are included where the transmission through the filter is almost unity, *e.g.* at s-wave resonances with a strong resonance - potential scattering interference.

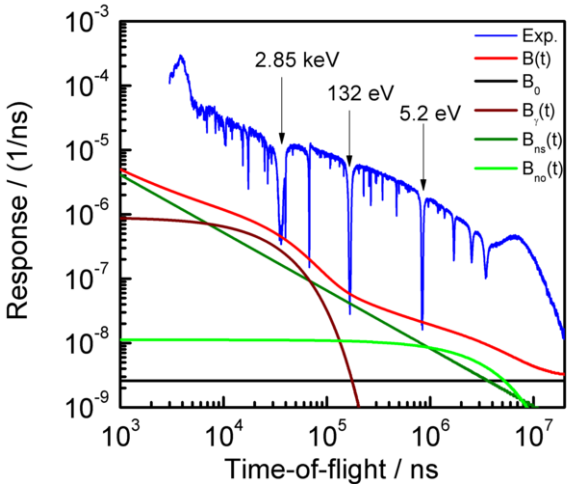

FIG. 11. The response of a Li-glass detector as a function of TOF for measurements at GELINA, is shown together with the total background and the contribution of the different components. The response is the result of a sample-in measurement on ^{241}Am [69].

Nevertheless, the best accuracy is obtained by measurements with fixed background filters in the beam. Using fixed background filters the impact of the material placed in the beam can be taken into account and the stability of the background level can be controlled at any time. For samples which have resonances that black out, the corresponding transmission in the sample-in spectra can be used as self-indicating black resonance dips. In most cases the time dependence of the components can be considered as fixed, such that only the amplitudes are sensitive to the presence of the filters and sample.

Fig. 11 shows the result of a sample-in measurement on ^{241}Am together with the different background components. The measurements have been carried out at a 25 m station of GELINA with the accelerator operated at 50 Hz using a Li-glass detector [69] . The main objective of these measurements was the determination of parameters of the 0.31, 0.57 and 1.27 eV resonances of ^{241}Am. Therefore, the measurements were performed with a fixed Na, Bi, Co and Ag filter in the beam. The function that was used is typical for measurements with a Li-glass scintillator at a moderated neutron beam

$$B(t) = a_0 + a_1 e^{-\lambda_1 t} + a_2 t^{\lambda_2} + a_3 \left(t + t_0\right)^{\lambda_3} . \quad (18)$$

The exponential is due to the 2.2 MeV γ-rays. The second time dependent component results from neutrons scattered in the surroundings. Depending on the measurement conditions it can be approximated by a power function or an exponential decay. For these measurements the best description was obtained with a power function. The second power function accounts for the contribution of overlap neutrons, which has been estimated by an ex-

Author's personal copy

trapolation of the spectrum at the end of the cycle. The parameter t_0 is related to the operating frequency of the accelerator, *e.g.* $t_0 = 20$ ms for 50 Hz measurements. The time dependence of the $B_{ns}(t)$ component was verified by measurements with a Cd filter to eliminate the contribution due to overlap neutrons.

The final uncertainty on the background based on Eq. (18) is due to uncertainties on the free parameters resulting from a fit and to systematic effects related to the model. All the covariances, resulting from both the fit and the model, can be propagated in the data reduction procedures described in Ref. [23]. These procedures can also take into account uncertainty components which are common to sample-in and sample-out measurements. The covariance matrix of the parameters resulting from the fit depends mainly on the counting statistics in the TOF-histogram and is determined by conventional uncertainty propagation (see Eq. (28) of section VIII A). Results of different measurements can be combined by applying a Bayesian procedure as described in section VIII A. The contribution due to counting statistics is mostly inferior compared to the uncertainties related to the model. The latter have been estimated by dedicated measurements using additional black resonance filters. A statistical analysis of the difference between the observed black resonance dips and the estimated background indicates that the accuracy of the modeled background is better than 5%. This accuracy can not be taken as an overall accuracy for the background in transmission measurements. It is strictly linked to the complete measurement procedure, involving the use of fixed black resonance filters to account for the filter and sample dependence. The quoted value is based on an experimental validation, which in some cases is more time consuming than the measurement itself.

2. *Fast spectrum*

The methodology of transmission measurements in the high energy range is very similar to what was described before with some modifications. The treatment of the background is different compared to the low energy region where black resonances can be used. In addition, the background structure depends strongly on the laboratory conditions where the measurements are performed.

Transmission measurements on C, Be, Ti and Fe in the energy region from 0.5 - 20 MeV using liquid scintillators are described in Ref. [84]. The experiments were performed at a 100 m and 250 m flight path station of RPI with the electron accelerator operated at 55 MeV with a frequency of 400 Hz and a pulse width of 6 - 8 ns. The main background component for these measurements was due to neutrons which are thermalised and captured in the detector resulting in a 2.2 MeV γ-ray contribution to the background. This background component was estimated from measurements without a sample, combined with Monte Carlo simulations. The results for the 100 m measurements are shown in Fig. 12. For these measurements the signal to background ratio reaches a maximum between 1 and 2 MeV. An example of a Be cross section derived from measurements at 100 m is shown in Fig. 13 [84]. The resonances in the MeV region are clearly observed and there is a very good agreement with results in evaluated data files for neutron energies above 0.5 MeV. Below this energy region a small systematic difference is noticed.

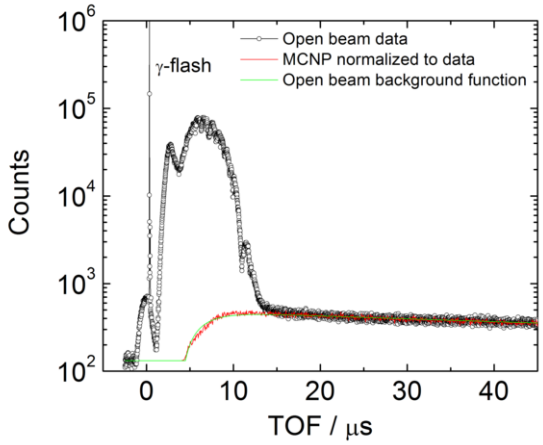

FIG. 12. The response of a liquid scintillator resulting from transmission measurements at RPI as a function of TOF is shown together with the background contribution estimated from a measurement without sample and from Monte Carlo simulations. The upper limit in TOF (45 μs) corresponds to a neutron energy of 25.8 keV.

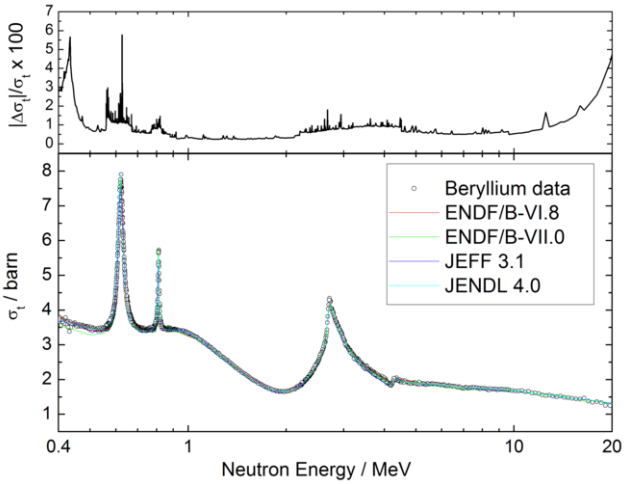

FIG. 13. Results of transmission measurements on Be performed at RPI are compared with the data in the evaluated data files.

Author's personal copy

The background at the nELBE facility does not show a significant time dependence. The behaviour of the background was verified by measurements with a 30 cm thick polyethylene sample in the beam. For neutron energies below 6.4 MeV the background is $\leq 1\%$. Its contribution is estimated in the TOF-interval ($4\ \mu s \leq t_m \leq\ 9.8\ \mu s$). In this way the sample dependence can be taken into account. The uncertainty due to counting statistics is typically 0.1%. A sample-out spectrum together with the background contribution is shown in Fig. 14.

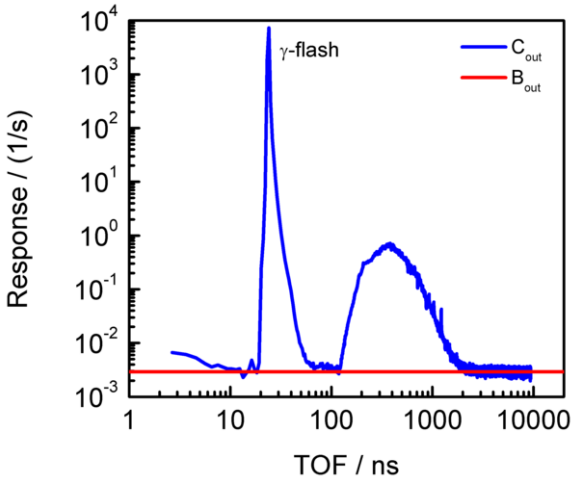

FIG. 14. Results of transmission measurements performed at nELBE. The γ-flash is observed at 24 ns and the neutron spectrum starts at about 100 ns corresponding to a neutron energy of 10.5 MeV. The end of the spectrum corresponds to a neutron energy of 850 eV.

C. Sample Properties

In the literature a variety of studies dealing with the ideal sample thickness and measurement time to optimise results of transmission measurements can be found [85–89]. For a flat cross section without any background contribution, the sample thickness which optimises the results from the point of view of counting statistics uncertainties corresponds to a transmission of approximately 0.08 [85, 86]. This value changes when the results are affected by a background contribution. The optimum transmission (or sample thickness) increases (decreases) with increasing background-to-signal ratio [87–89]. The optimum transmission shows hardly any changes for relative background contributions below 0.005 and increases rapidly for a relative background between 0.01 and 1. Above a background-to-signal ratio of 1 the optimum transmission is constant at around 0.35. However, under such extreme experimental conditions it is difficult to extract a reliable transmission. Danon and Block [89] investigated the transmission value which minimizes the

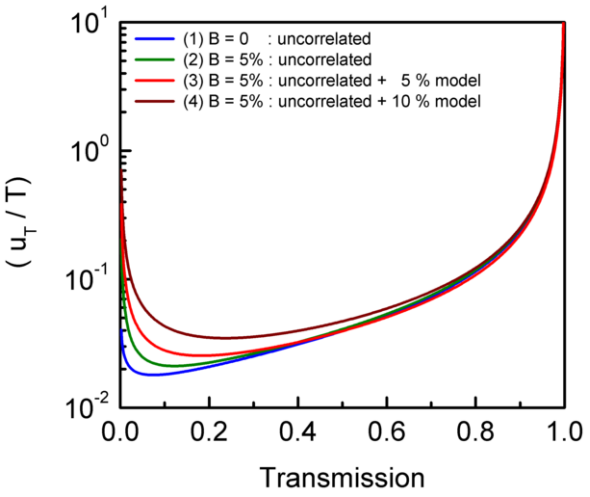

FIG. 15. The calculated relative uncertainty as a function of transmission for different background conditions and contributing uncertainty components (see text).

uncertainty on the area of a resonance dip. They found that for a resonance the optimum transmission is significantly lower than the one for a constant cross section.

The above mentioned studies only considered the influence of uncorrelated uncertainties due to counting statistics. The conclusions change significantly when systematic effects resulting in a correlated component, *e.g.* an uncertainty related to the background model, are included in the study. This can be seen in Fig. 15 which compares for a flat cross section the relative uncertainty of the transmission (u_T/T) as a function of transmission for different conditions: (1) no background; (2) with a background contribution, however, only accounting for counting statistics uncertainties; (3) including an additional 5% correlated uncertainty due to the background model; and (4) including an additional 10% correlated uncertainty. The relative background contribution for cases (2), (3) and (4) was 0.05. Fig. 15 shows that the transmission that minimizes the uncertainty, increases when also a correlated uncertainty component is considered. In addition, the minimum for the optimum sample thickness becomes shallower. Hence, the penalty for not having the ideal sample thickness becomes smaller.

Even more important than the optimum transmission and measurement times, are the sample characteristics to ensure that the direct link between experimental and theoretical transmission can be made. The constraints for an optimum transmission geometry require homogeneous samples without holes. In case of non-ideal samples the resonance parameters will be biased, unless the sample characteristics, in particular sample inhomogeneities, are taken into account in the data analysis [90]. This is illustrated in Fig. 16, showing the transmission around the 2.65 eV resonance of ^{242}Pu as a function of neu-

Author's personal copy

tron energy. The data are the result of transmission measurements using a PuO_2 powder sample enriched to 99.93 wt% in ^{242}Pu, mixed with carbon powder and canned in a copper container [90]. The average area density of ^{242}Pu was 2.51 10^{-5} at/b. The measurements were performed with the sample at 77 K and 300 K. The experimental data are compared with results of a least squares adjustment which was applied to extract Γ_n and Γ_γ. For the Doppler broadening the CLM [67] was used. To account for the powder grain size, a special model was implemented in REFIT, as discussed in section VIII B. This model [90] includes a log-normal distribution describing the variation in the area density and a parameter reflecting the fraction of holes in the sample. Table II shows that there is a strong difference between the parameters (Γ_n and Γ_γ) which are derived from a fit with and without accounting for sample inhomogeneities. In addition, the residuals in Fig. 16 show that the quality of the fit improves significantly when the powder grain size is included in the analysis. The improved quality is observed for both the 77 K and 300 K data. The parameters reported in the literature [91–94] are also given in Table II. The parameters resulting from the fit which accounts for the sample inhomogeneities are in much better agreement with the literature data. In Ref. [92] and [94] special attention was given to the homogeneity of the samples used. In Ref. [92] the plutonium oxide powder was pulverized after precipitation to reduce the grain size of the powder. The sample used in Ref. [94] was formed by dissolving PuO_2 in a deuterated nitric-acid solution. In Ref. [91] and [93] powder samples were used. However no detailed information on the powder characteristics are given. The results in Table II demonstrate that ignoring sample inhomogeneities in the analysis leads to an overestimation of the total width and an underestimation of the peak cross section (or smallest width), with bias effects between 10% and 30%. Unfortunately, in case of very strong resonances it is difficult to produce a homogeneous sample with such a thickness that a reasonable transmission can still be reached. Although in the RSA sample inhomogeneities can be taken into account, the use of solutions in the form of very low enriched materials or sol-gel based samples as in Ref. [69] are definitely preferred above powder samples. For the determination of the resonance parameters of ^{155}Gd and ^{157}Gd, Leinweber et al. [95] performed transmission measurements at RPI on gadolinium samples prepared as a liquid solution with heavy water. Due to the neutronic properties the use of heavy water is preferred compared to normal water.

TABLE II. Resonance parameters of the 2.65 eV resonance of ^{242}Pu.

		Γ_n / meV	Γ_γ / meV
Egelstaff et al.	[91]	1.70 ± 0.80	
Coté et al.	[92]	1.90 ± 0.20	25.10 ± 2.60
Auchampaugh et al.	[93]	1.92 ± 0.10	25.48 ± 1.00
Young and Reader	[94]	2.00 ± 0.08	25.00 ± 1.50
Kopecky et al.	[90]		
homogeneous		1.45	36.50
inhomogeneous		1.90	25.00

V. REACTION CROSS SECTION MEASUREMENTS

A. Principles

The theoretical expected count rate $C_{r,k}$ in a reaction cross section experiment due to the presence of nuclide k in a sample, which is placed perpendicular to a parallel incident neutron beam, is related to the reaction yield $Y_{r,k}$ by

$$C_{r,k} = K_r Y_{r,k} \varphi, \tag{19}$$

where φ is the incident neutron flux. For an isotropic emission of reaction products the parameter K_r can be considered as an effective efficiency which is the product of a set of parameters

$$K_r = \epsilon_r \Omega_r P_r A_r, \tag{20}$$

where

A_r: is the effective area of the sample as seen by the incident neutron beam or the effective beam intersection area;

P_r: is the probability that the reaction product escapes from the sample;

Ω_r: is the solid angle between the sample and the detection system; and

ϵ_r: is the efficiency of the detection system to detect an event resulting from a (n, r) reaction by nuclide k.

In case of anisotropic emission of the reaction products corrections have to be applied. Such corrections require angular differential distributions which can be expressed as a finite sum of Legendre polynomials [96]. The impact due to anisotropic emission of primary γ-rays on the determination of the angle-integrated cross section are largely reduced (or even avoided) by using two detectors placed at 110° and 150° with respect to the incident neutron beam [97]. By weighting the measured spectra appropriately, anisotropic effects in the total response are largely avoided up to multipolarities L = 3. In some cases detectors are placed at 125° [98]. However, such a geometry minimizes the effect only under more

Author's personal copy

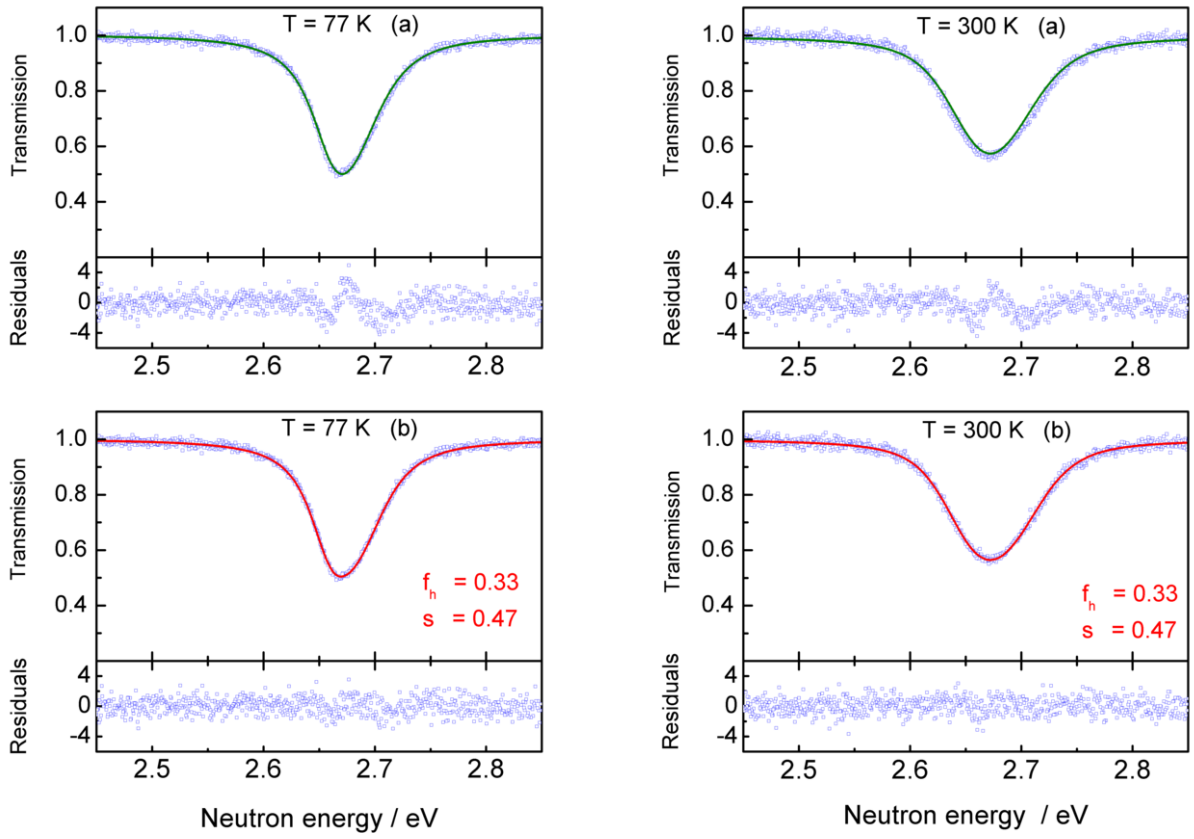

FIG. 16. The transmission as a function of energy for a PuO_2 powder sample enriched in ^{242}Pu and mixed with carbon powder at 77 K and 300 K measured at GELINA. Results of a RSA supposing a homogeneous (a) and inhomogeneous (b) sample are given. The parameter s reflects the degree of inhomogeneity and f_h the fraction of holes (see section VIII B)

specific conditions. For example, in case of a primary dipole emission (multipolarity L = 1) the angular differential distribution is determined by the sum of the zero and second order Legendre polynomial and the latter is zero at 125° [96, 97].

Based on Eq. (19) and Eq. (20) the experimental yield Y_{exp}, *i.e.* the observable of a reaction cross section experiment, is defined as the total observed count rate C_r which is corrected for its background contribution B_r and divided by the neutron flux φ and the parameter K_r

$$Y_{exp} = \frac{C_r - B_c}{K_r \varphi}. \tag{21}$$

In most cases the parameters (A_r, P_r, Ω_r, ϵ_r) related to the detection of the reaction product and the absolute value of the neutron flux at a given energy are lumped together into one normalization factor N_r and the experimental yield is expressed as

$$Y_{exp} = N_r \frac{C_r - B_r}{\varphi'}. \tag{22}$$

The normalization factor N_r is determined at an energy where the theoretical yield is well known and only the shape of the neutron flux, *i.e.* its relative energy dependence denoted by φ', needs to be determined. Such a procedure is only valid when the parameters (A_r, P_r, Ω_r, ϵ_r) are energy and nuclide independent. This assumption strongly depends on the experimental conditions, such as the type of neutron production facility, measurement methods and sample properties. In case the neutron beam shows an energy dependent spatial profile the beam interception fraction A_r is energy dependent and corrections are required, see *e.g.* Ref. [99, 100]. They can be derived from measurements with position sensitive devices such as the Micromegas-based detector used at the n_TOF facility [101]. When more than one nuclide is present in the sample and the parameter K_r is nuclide dependent, due to *e.g.* the detection efficiency or the escape probability, the parameter K_r is mostly related to the main nuclide of interest. In case the contributions of other elements or isotopes are not considered in the background, corrections have to be included in the data analysis (see section VIII B).

The discussion in the previous paragraphs reveals the complexity of reaction cross section experiments compared to a total cross section measurement. In most

Author's personal copy

cases, additional flux and normalization measurements are required. Moreover, the relation between the reaction yield and reaction cross section is more complex compared to the relation between transmission and total cross section. Consequently, uncertainties of cross section data resulting from yield measurements are expected to be larger compared to uncertainties of cross sections deduced from transmission measurements.

B. Neutron Flux Measurements

For the analysis of any reaction cross section measurement the absolute or relative neutron flux as a function of neutron energy is essential. Such measurements rely on neutron induced reactions for which the cross sections are known. Since the accuracies of these cross sections directly translate into the accuracy of the experimental yield Y_{exp}, reactions for which the cross sections are considered as a standard are preferred. Details about standard cross sections for neutron induced reactions can be found in Ref. [21]. Additional cross section standards at 0.0253 eV neutron energy or at a velocity of 2200 m/s are given in [32]. It should be noted that in the evaluation of the thermal capture cross section of ^{197}Au(n,γ) only transmission measurements were considered, that is, no measurements made relative to another cross section were included [32].

A flux measurement based on such standard cross sections is nothing else than a reaction cross section measurement. Therefore, Eq. (21) becomes

$$Y_{exp} = \frac{K_\varphi}{K_r}\frac{C_r - B_r}{C_\varphi - B_\varphi}Y_\varphi, \tag{23}$$

where Y_φ is the theoretical yield for the flux measurements and C_φ and B_φ are the total and background count rate for the flux measurement. To prevent artificial structures in Y_{exp}, due to structures in Y_φ and the finite response of the TOF-spectrometer, standard reactions with a smooth cross section as function of neutron energy are preferred. In the region below a few hundred keV flux measurements are predominantly based on the ^{6}Li(n,t)α, ^{10}B(n,α)^{7}Li and ^{10}B(n,$\alpha\gamma$)^{7}Li reactions. At energies above 0.5 MeV the ^{235}U(n,f) reaction is mostly used. The ^{238}U(n,f) reaction is especially useful in the MeV region, because the cross section has a threshold near 1 MeV eliminating the influence of low-energy neutrons.

1. $^6Li(n,t)\alpha$

The ^{6}Li(n,t)α reaction is used in combination with *e.g.* a Li-glass scintillator [102] or surface barrier Si-detectors [103]. Its cross section is smooth and nearly inversely proportional to the velocity for neutron energies below a few keV. It exhibits a p-wave resonance near 240 keV. Since the angular differential cross section is not considered as a standard, the application in a low geometry is limited to the region where the emission is isotropic.

A Si-based neutron monitor combined with a thin layer of ^{6}LiF containing material is used at n_TOF and LANSCE for low neutron energies. A Li-glass scintillator offers a high detection efficiency, an intrinsic independence from angular distribution effects and a time resolution better than 1 ns. The background components for such a detector are similar to those discussed in section IV B. A 0.5 mm thick detector is routinely installed at the capture measurement stations of ORELA with background levels $\leq 1\%$ for energies below 100 keV. The main disadvantage of a Li-glass scintillator is the presence of significant quantities of silicon and oxygen and other impurities such as Ce for an accurate calculation of the yield Y_φ.

2. $^{10}B(n,\alpha)^7Li$

The ^{10}B(n,α)^{7}Li reaction is mostly used as a neutron converting reaction in combination with proportional counters or ionization chambers [104]. The use as an absolute flux monitor is limited due to the complexity to determine the area density of the ^{10}B layers with a high accuracy [105]. However, combined with a normalization procedure, very accurate reaction yields can be determined, since only the energy dependence of the cross section is required. This energy dependence is very smooth and known with a very good accuracy below 200 keV. Detecting the charged particles by an ionization chamber requires thin layers resulting in relatively low count rates. However, it reduces significantly (or even eliminates) effects due to the self-shielding (and multiple interaction) contribution in the calculation of the yield Y_φ.

At GELINA this reaction is used for capture and fission cross section measurements below 200 keV [98, 106, 107]. A double Frisch-gridded ionization chamber is used with a common cathode loaded with two layers of ^{10}B. The ^{10}B layers with an area density of about 40 μg/cm^2 are evaporated back-to-back on a 30-μm thick aluminum backing. The chamber is almost transparent for the neutron beam. The bias on the amplitude spectrum, taken from the anode, is set low enough to accept the signals from both the ^{7}Li and α-particles. This choice, together with a back-to-back configuration, rules out a systematic bias effect related to the forward-to-backward emission ratio [108]. The background for flux measurements with such a chamber is determined by an analytical expression applying the black-resonance technique as discussed in section IV B. The main difference with the Li-glass scintillator is that the contribution of the 2.2 MeV γ-ray can be neglected. The response of such a chamber and the background contributions for measurements at a 12.5 m station at GELINA are shown in Fig. 17. The results are for measurements at 50 Hz and 800 Hz. The measurements at 50 Hz were optimised for measurements below 100 eV. Fixed Na, Bi and Co background filters were used. Those at 800 Hz were optimised to determine the

Author's personal copy

average capture cross section for ^{197}Au(n,γ) in the URR between 4 keV and 90 keV. Therefore they were carried out with a fixed Na and S black resonance filter in the beam. Based on measurements using different combinations of black resonance filters, the uncertainty due to the background model was evaluated. Under the constraint of using at least one fixed background filter, this uncertainty is $\leq 3\%$.

3. $^{10}B(n,\alpha\gamma)^7Li$

A neutron flux derived from the reaction ^{10}B(n,$\alpha\gamma$)^{7}Li is based on the detection of the 478-keV γ-ray. This reaction is used by Gilliam et al. [109] for an absolute determination of the neutron flux for cold and thermal neutron beams with an accuracy of 0.1%. The method is based on a combination of α- and γ-counting using a boron target that totally absorbs the impinging neutrons. For energy dependent cross section measurements a ^{10}B containing sample combined with a γ-ray detector is used to determine the shape of the neutron flux. Often a NaI detector is used [110]. In case of capture cross section measurements, the capture sample can be replaced by a sample containing ^{10}B. At RPI the incident neutron flux is determined by replacing the capture sample by a 2.54 mm thick, 97.9 wt% enriched $^{10}B_4C$ sample and recording the 478-keV γ-ray in the capture detection system consisting of a 16-segment NaI(Tl) detector [111]. Peak-to-background ratios between 180 and 400 from 12 eV up to 600 eV, respectively, are obtained [79]. However, the thicker the sample the more systematic effects, due to self-shielding, multiple interaction and γ-ray attenuation in the sample, have to be taken into account in the calculation of Y_φ. The same method, however, using a compact 4π BGO (1.5 l) [112] and later a 4π 16-segment BGO (8.5 l) [113] spectrometer was used at KURRI. The ^{10}B sample was 52 mm in diameter, 0.49 g/cm^2 in area density and enriched to 93% in ^{10}B. An analytical correction for neutron self-shielding and multiple interaction was applied in Ref. [114] based on the approximation in Ref. [115]. The ^{10}B(n,$\alpha\gamma$)^{7}Li reaction has also been utilized using an advanced Ge spectrometer at KURRI and J-PARC [116]. By using a high-flux pulsed neutron beam at J-PARC, a thin ^{nat}B sample can be used. Because of the superior energy resolution of the Ge-spectrometer the peak-to-background conditions have been improved.

4. $^{235}U(n,f)$

The ^{235}U neutron induced fission cross section is a very valuable standard for energies above 150 keV because after fission two fragments with a high kinetic energy are available for detection; the cross section is of reasonable magnitude with uncertainties below 1%; and ^{235}U is very suitable for use in parallel plate [117, 118] or Frisch-gridded ionization chambers [119]. The latter provides a better pulse-height resolution. However, their time resolution is limited to about 40 ns. Thin ^{235}U layers can be very well characterized for their total area density and area density distribution. Depending on the isotopic composition of the uranium layer, uncertainties better than 0.3% can be reached by low geometry α-counting. Hence, ^{235}U loaded ionization chambers can also be used as absolute flux monitors. The largest uncertainty component for absolute measurements results from the detection efficiency, especially when using parallel plate chambers. Nevertheless, accuracies of 2% can be reached. By combining results of ^{235}U loaded chambers with flux measurements based on the ^{6}Li(n,t)α, ^{10}B(n,α)^{7}Li or ^{10}B(n,$\alpha\gamma$)^{7}Li reaction, the neutron flux in a broad energy range can be derived [107]. A transparent detector loaded with ^{10}B and ^{235}U based on the micromegas concept has been developed to monitor the neutron flux at n_TOF [120].

C. Normalization

The normalization factor is one of the most important correlated uncertainty components in a reaction cross section experiment. This factor is determined by normalizing at an energy where the theoretical yield is well known. One can rely on:

- a neutron induced reaction for which the total and reaction cross sections are known;
- an isolated resonance with well defined resonance parameters; or
- a saturated resonance with $\Gamma_n \ll \Gamma_\gamma$.

In case of the first option, the lowest uncertainty is obtained when standard reaction cross sections are involved. Normalization at a known resonance can be performed completely independent of any other cross section when the neutron width of the resonance is much smaller than the reaction width. In that case the reaction cross section is sensitive to the neutron width, which can be very accurately determined from transmission data. A normalization independent from any reference cross section can also be realized by normalizing at a saturated resonance [98, 121]. For a saturated resonance the product of the area density and cross section is high enough such that all incident neutrons with energies near the resonance energy interact with the sample. This procedure is practically only suitable for capture studies. Most of the measurements of neutron induced charged particle reactions are performed by detecting the charged particles produced in the reaction. For such studies extremely thin targets are required and no saturated resonance can be observed in the measured spectrum.

The accuracy of the normalization will strongly depend on how well the parameters (A, P, Ω, ϵ) for the normalization reaction match those for the reaction under

Author's personal copy

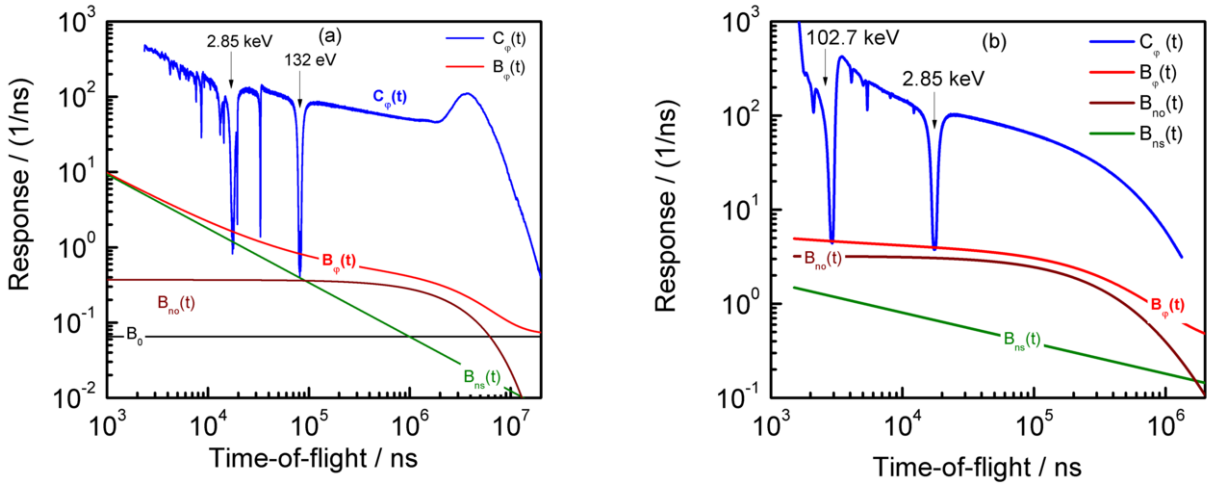

FIG. 17. The response of a ^{10}B ionization chamber as a function of TOF at a 12.5 m station at GELINA is shown together with the background contributions. The results are for measurements at 50 Hz (without overlap filter) (a) and 800 Hz (with overlap filter) (b) operating frequency.

study. Differences in the effective sample area and thickness require often significant corrections. Consequently, the sample characteristics, *i.e.* area density and homogeneity, are of primary importance and are systematic effects which will introduce correlated uncertainty components.

A substantial reduction of the correlated uncertainty due to the normalization is achieved when an internal normalization can be realized, *e.g.* normalization at a resonance present in the TOF-spectrum under investigation. Under such circumstances all experimental conditions remain unchanged. Consequently, all systematic effects due to the positioning of the sample with respect to the neutron beam and detection system, and variations of detector and accelerator operating conditions are eliminated.

VI. NEUTRON INDUCED CHARGED PARTICLE AND FISSION REACTIONS

As discussed in section V A the count rate in a charged particle or fission cross section experiment is related to the reaction yield by a combination of Eq. (19) and Eq. (20). Since the count rate for flux measurements is described by the same equations, the reaction yield can be expressed by Eq. (23) with the ratio K_φ/K_r given by

$$\frac{K_\varphi}{K_r} = \frac{\epsilon_\varphi}{\epsilon_{r,k}} \frac{\Omega_\varphi}{\Omega_r} \frac{P_\varphi}{P_{r,k}} \frac{A_\varphi}{A_r}. \qquad (24)$$

The parameters ϵ, Ω and P strongly depend on the sample and detector characteristics and on the reaction products. At GELINA [122] a double Frisch gridded ionization chamber filled with ultrapure methane is used, with the sample being investigated mounted back-to-back with a sample to monitor the flux. In some cases a separate experiment was done with the sample for the reaction cross section measurement being replaced by a well characterized sample for which the cross section is well known [127]. Due to the working principle of an ionization chamber [119] the intrinsic detection efficiency is close to 100% and the solid angle is close to 2π, both for the reaction and the flux measurement. This greatly simplifies Eq. (24). By using samples with the same dimensions for the reaction and the flux measurement, the interaction area also cancels out.

Through the use of thin samples, the escape probability of the reaction products is close to 1. However, even for thin layers one still has to take into account absorption in the sample itself for reaction products emitted nearly parallel to the sample. Reaction products that loose a significant part of their energy before escaping from the sample will show up as a low energy tail in the pulse height spectrum of the detector. In the case of (n,f) cross section measurements on a material with a significant α-activity, the low energy tail of the fission fragments is very likely to overlap with the signals produced by the α-particles. In this case, a lower threshold is applied to the pulse height spectrum in order to avoid contributions of α-particles. The loss of fission fragments due to this threshold can be estimated by extrapolation of the shape of the fission fragment spectrum or by energy loss calculations in combination with MC simulations. The separation between α-particles and fission fragments depends on the characteristics of the detector that is being used, the α-activity and the thickness of the sample. Fig. 18 shows a pulse height spectrum for a multi layer parallel plate chamber loaded with ^{235}U, where fission fragments and α-particles are well separated.

Author's personal copy

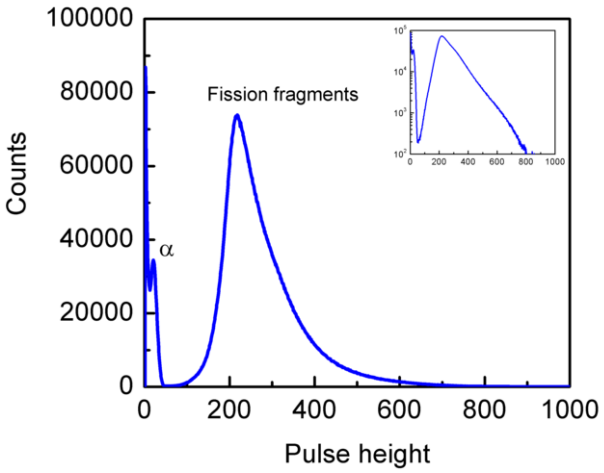

FIG. 18. An amplitude spectrum obtained with a parallel plate ionization chamber for fission cross section measurements on ^{235}U.

At the n_TOF facility the detection setup for neutron induced fission reactions is based on Parallel Plate Avalanche Counters (PPACs) [123] and Fast Ionization Chambers (FIC) [124]. PPACs consist of a number of fissile layers mounted parallel to each other and with electrodes in between the fissile layers. ^{235}U and ^{238}U layers are mounted in the same chamber and used as references. By using thin target backings both fission fragments can be measured in coincidence, which allows to reduce most of the background produced by α-emission of the radioactive samples. Simulations combining MC methods and stopping power calculations are used to determine detection efficiencies. These are typically between 0.85 and 0.90. Since the samples being used in the PPACs do not all have the same diameter, an experimental determination of the beam profile and an additional correction factor are needed in order to take into account the effective interaction area between the different samples and the neutron beam. The FICs are not working in proportional mode and in these chambers only one fission fragment is detected per fission reaction. Computer simulations based on energy loss calculations are used to determine the FICs capability of discriminating between α-particles and fission fragments.

At ORELA a multi-layer chamber containing 40 coatings on 21 plates has been used [125] to determine the fission cross section of ^{233}U. This chamber allowed a clear separation between fission fragments and α-particles. The neutron flux was determined using a 1 mm thick ^{6}Li-glass detector positioned upstream from the fission chamber. Due to the non-negligible thickness of the flux monitor, the transmission of the neutron beam was determined experimentally. Also the transmission through the air gap in between the detectors was taken into account.

Tovesson and Hill [126] used a parallel plate ionization chamber (PPIC) at LANSCE to measure the ^{237}Np(n,f) cross section relative to ^{235}U. These chambers are close to 100% efficient for fission detection. By optimizing the plate spacing and the gas pressure in the PPIC a high level of separation between fission fragments and α-particles could be achieved. A ^{235}U, ^{238}U and blank sample were mounted in the same chamber for respectively flux monitoring, measuring beam related background events and determining charged particle emission from the sample backings. Charged particles have been measured at LANSCE by Koehler et al. [128] using both a Si surface barrier detector and a double Frisch-gridded ionization chamber.

Due to the high energy of fission fragments, background contributions from low energy particles can be reduced significantly. For other charged particle reactions this might be more problematic. The determination and description of the background for neutron induced charged particle reactions can be performed as described in section V B 2.

In the case of very active samples a more limited detection geometry can be used in order to avoid strong overlap between fission fragments and α pile-up. Typically a vacuum chamber in combination with a Si surface barrier detector is used, with the sample mounted at 45° relative to the incoming beam and with the detector mounted out of the collimated beam [122]. To reduce the impact of the γ-ray flash a compensated ionization chamber was developed by Koehler et al. [129] and used for (n,p) and (n,α) cross section measurements at ORELA [130].

Special care should be taken during the sample preparation and a good characterization of the samples used is essential [131]. For a measurement of (n,f) cross sections, a small presence of other fissile material can give a large contribution to the observed response. Another important aspect is the variation of sample characteristics with time due to physical and chemical instability of the material or due to radioactive decay. When determining *e.g.* the ^{243}Am(n,f) cross section, the in-growth of ^{239}Pu due to successive decay processes following the α-decay of ^{243}Am has to be accounted for [132]. Even starting from a pure ^{243}Am target, the contribution of ^{239}Pu at thermal energy after 60 weeks is already 50% of the observed fission rate. These contributions can be corrected for, provided that the nuclear data necessary are known. Both the uncertainties on the amount of parasitic nuclei and on the nuclear data will contribute to the uncertainty of the final result of the reaction cross section measurement.

In summary, when homogeneous, well characterized samples are used for both the reaction under study and the one for the flux measurement, such that quantities in Eq. (24) are well defined, uncertainties of 2% can be reached.

Author's personal copy

VII. NEUTRON INDUCED CAPTURE REACTIONS

A. Principles

Neutron induced capture cross section measurements rely either on post-irradiation activation analysis or on the detection of prompt γ-rays emitted in the (n,γ) reaction. Capture cross sections in the resonance region are best determined by a prompt γ-ray detection system that is optimised for TOF measurements. An ideal prompt γ-ray detection system fulfills the following requirements [133]:

- the detection efficiency for a capture event is independent of the γ-ray cascade, *i.e.* independent of the multiplicity of the γ-ray spectrum and the γ-ray energy distribution;
- the sensitivity to neutrons scattered by the sample is low compared to the sensitivity to γ-rays produced by the capture reaction in the sample;
- the detector has a sufficient time resolution ($\leq$ 1 ns);
- for the study of a fissioning system, the γ-rays from neutron capture can be separated from those resulting from neutron fission; and
- in case of a radioactive sample, the prompt γ-rays can be separated from the γ-rays emitted due to the radioactive decay.

Three different principles based on the direct detection of prompt γ-rays can be distinguished: γ-ray spectroscopic, total γ-ray absorption and total energy detection principle. They will be discussed with an emphasis on capture cross section measurements in case the fission channel can be neglected. Techniques to determine capture cross section data for fissile nuclei will be mentioned, however, without discussing their accuracy.

The choice of the principle and related detection system depends on the reaction to be studied, the energy region of interest, the amount of available sample material and the required accuracy and resolution. For studies of neutron induced capture reactions using highly radioactive samples, pulse pile-up and count losses due to the dead time of the detector and electronics can be reduced by using digital signal processing techniques [61, 134, 135].

B. Normalization and Background

The best accuracy is obtained by normalizing to a saturated resonance [98, 121]. Based on theoretical capture yields, Borella et al. [98] have demonstrated that a normalization factor deduced from the yield of a saturated resonance, with $\Gamma_n \ll \Gamma_\gamma$, is nearly independent of the resonance parameters and target thickness. This is confirmed in Table III which reports the normalization factor N obtained from an analysis of a saturated resonance at 4.9 eV obtained from measurements with a 0.1 mm thick metallic ^{197}Au disc. The resonance parameters derived by Massimi et al. [136] are also given. The normalization constant has been determined for different energy ranges and adjusting the values of Γ_n and Γ_γ together or separately. The data in Table III reveal that the normalization factor is independent of the resonance parameters as long as the fit region is limited to the saturation region of the resonance. Consequently, it is hard to derive reliable parameters from a saturated resonance. The last line in Table III shows that by extending the fit region the results do definitely not improve.

TABLE III. Results of an analysis of the 4.9 eV resonance of ^{197}Au from measurements at GELINA [136]. The normalization factor N is given for different fit conditions. The flag columns indicate the adjusted parameters.

N	Γ_γ	Γ_n	Flag			χ^2/ν	Region
	meV	meV	N	Γ_γ	Γ_n		eV
1.0003	128.9	14.5	x	x	x	1.19	4.8 – 5.0
1.0003	121.5	15.2	x		x	1.18	4.8 – 5.0
0.9995	123.0	15.0	x	x		1.17	4.8 – 5.0
1.0052	147.5	12.8	x	x	x	1.39	3 – 7
Ref. [136]: $\Gamma_\gamma = 121.4 \pm 0.03$, $\Gamma_n = 14.96 \pm 0.02$							

The normalization uncertainty is significantly reduced when the γ-ray cascade at the normalization energy is very similar to the cascade of the reaction being studied. This eliminates all systematic effects related to the efficiency to detect a capture event. Such a self-normalization can be realized when a saturated resonance is present in the spectrum [99, 100, 106, 137] or by a simultaneous analysis of capture and transmission data when resonances with $\Gamma_n \ll \Gamma_\gamma$ can be observed in both the transmission and capture spectrum [138]. However, it will never completely eliminate systematic effects due to sample properties and normalization as suggested in Ref. [139].

The background for capture measurements consists of three contributions: (1) a time independent component due to ambient radiation and possible long lived radioactivity in the sample and its surroundings; (2) a time dependent component independent of the sample and (3) a time dependent component depending on the sample characteristics. The first component can be estimated with a good accuracy from measurements just after the accelerator is switched off, or in a TOF region where the neutron flux is negligible. The time dependent component independent of sample properties, results from neutrons which are scattered inside the measurement station and at other flight paths. This contribution can be deduced from measurements without a sample in the beam. The last component is the most difficult one to quantify. This component depends on the neutron and γ-ray

Author's personal copy

scattering properties of the sample, on the neutron sensitivity of the detection system and the characteristics of the measurement station. The neutron sensitivity in this discussion is the detector response due to neutrons which are scattered from the sample and create a capture reaction in the sample-detector environment. One has to differentiate between a direct and a delayed component. The direct or prompt component originates from scattered neutrons which cause an immediate capture reaction in the detector assembly. This contribution follows the resonance structure of the cross section and is hard to distinguish from the response due to a (n,γ) reaction in the sample. The delayed component is due to neutrons that scatter from the sample, enter the measurement station or detector and slow down in the construction material of the measurement station or detector before they create a capture reaction in the detector. The time and sample dependent component may be influenced by overlap neutrons. This impact depends on the operating frequency and overlap filter that is used. The best way to determine its contribution is by measurements at a lower frequency as in *e.g.* Ref. [42, 140].

Since potential scattering is always present and for all resonances $\Gamma_n > 0$, neutron scattering always occurs. One way to assess the background due to scattered neutrons is by additional measurements with material for which the contribution due to capture can be neglected, *e.g.* ^{208}Pb or carbon. To separate the direct from the delayed component several measurements using various black resonance filters are required. When in beam γ-rays scattered by the sample also contribute to the background, the problem becomes even more complicated. The contribution due to in-beam γ-rays strongly depends on the type of neutron producing facility and will contribute in the low TOF (high energy) region. The 2.2 MeV γ-ray is an important background component for the capture measurements at n_TOF reported in *e.g.* Ref. [99, 100, 137]. This background contribution can be reduced by using borated water as a moderator [141].

The sample dependent background due to the neutron sensitivity of the detection system is a systematic effect which can create a substantial bias if it is not correctly taken into account in the data reduction or analysis. It plays on important role for all resonances with a $\Gamma_n \gg \Gamma_\gamma$. The consequences of deducing resonance parameters of large s-wave resonances from measurements suffering from a substantial neutron sensitivity have been discussed in Ref. [133, 142, 143]. After a substantial reduction of the neutron sensitivity of their detection system, Koehler et al. [143] determined capture widths for the 289 and 325 keV s-wave resonances in ^{88}Sr which were a factor five smaller than the previously reported values. Corvi [133] compared the capture widths for structural materials derived from measurements at GELINA with a C_6D_6 with those at ORELA with a C_6F_6. For large s-wave resonances the widths from ORELA were a factor 2 larger than those from GELINA. Beer et al. [142] observed a linear increase of the ratio of capture areas

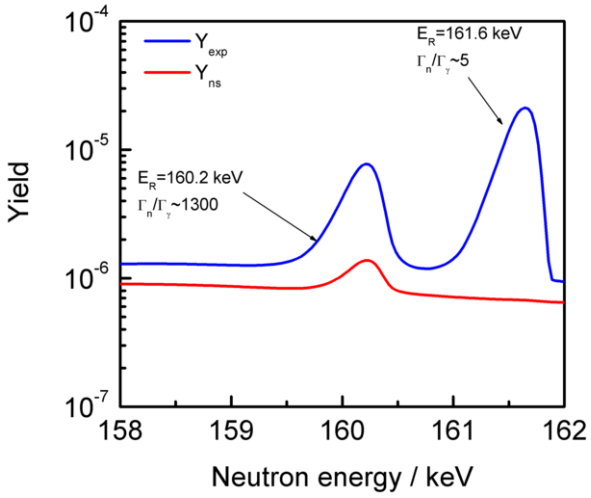

FIG. 19. The experimental yield (Y_{exp}) obtained from capture measurements on a 1.08 mm thick ^{206}Pb sample at a 60 m station of GELINA is compared with the contribution due to the neutron sensitivity of the detector (Y_{ns}).

reported by Macklin et al. [144] and their values with the ratio Γ_n/Γ_γ. These examples show that Γ_γ will always be biased to larger values when no correction for the neutron sensitivity is applied.

Sometimes a capture width $\Gamma_{\gamma c}$, corrected for the direct neutron sensitivity component, is derived from the expression

$$\Gamma_{\gamma c} = \Gamma'_\gamma - K_{ns}\Gamma_n, \tag{25}$$

where Γ'_γ is the radiation width resulting from an analysis without correction for the neutron sensitivity of the detection system, which is denoted by K_{ns}. Such a correction is only valid for very thin samples [145] and can result in a substantial bias on Γ_γ[98]. Fig. 19 shows the experimental yield around the 160 keV resonance of ^{206}Pb together with the expected contribution due to the neutron sensitivity of the detector assembly. The overall contribution of the neutron sensitivity to the total area of the 160 keV resonance is about 3%. Taking into account the neutron sensitivity in the resonance shape analysis $\Gamma_\gamma =$ 53.5 meV was derived. Applying the correction procedure of Eq. (25) the resulting $\Gamma_{\gamma c} = 48.3$ meV is underestimated by 10%. This underestimation is due to the fact that the multiple interaction events are not taken into account when Eq. (25) is applied. The correction can only be applied based on a proper calculation of the scattered neutron yield (see section VIII B).

The best solution is to reduce the neutron sensitivity as much as possible by a proper design of the detection system [146] and by avoiding scattering material close to the detection systems. An elegant method to avoid additional corrections due to the neutron sensitivity is by making the target-to-sample distance shorter than the

Author's personal copy

sample-to-detector distance [147]. With such an experimental set-up the impact of the direct neutron sensitivity can be discriminated by the TOF. However, due to the limited TOF-resolution, this approach can only be applied for specific applications, *e.g.* to study a limited number of well separated resonances.

C. Detection Systems

1. γ-ray spectroscopy

Using detectors with a high resolving power for the γ-ray energy, *e.g.* high purity Ge-detectors, capture cross sections can be determined in case the γ-ray transitions of the cascade are well known. The capture cross section can be derived from [148–151]

- the sum of all the partial cross sections of primary transitions depopulating the capture state;
- the sum of the partial capture cross sections of the transitions feeding the ground state; or
- the sum of all the observed partial cross sections weighted with the energy of the transition divided by the total γ-ray energy liberated in the capture event [150].

These principles have been applied by *e.g.* Raman et al. [151] to derive the thermal capture cross section of ^{28}Si and by Borella et al. [152] for the determination of the thermal capture cross section of ^{209}Bi to the ground state and the isomeric state.

Partial capture cross sections for a specific transition are deduced from the full-energy net peak area corrected for electron conversion, γ-ray attenuation, detection efficiency and neutron flux. Systematic effects are reduced when an internal normalization is applied by *e.g.* taking a well-defined stoichiometric compound which includes an element for which a partial transition cross section is known. Under these conditions the effective area, the absolute detection efficiency and absolute neutron flux cancel out and only their relative energy dependence has to be determined [131, 152]. In Ref. [152] a bismuth-nitrate sample was used and the data were normalized to the partial capture cross section $\sigma_{1884,N} = 14.52 \pm 0.07$ mb for the 1884 keV transition after thermal neutron capture in ^{14}N of Ref. [153]. This is common practice for measurements at a thermal or cold neutron beam where a limited amount of material is needed. However, in case the full resonance region is investigated larger samples are required and the amount of matrix materials has to be limited to avoid large corrections due to self-shielding and multiple interaction, as discussed in Ref. [131, 154]. When the full resolving power of the γ-ray spectrometer is exploited and the resonances and γ-ray transitions of the sample under investigation do not coincide with those in the detector material, the results are in principle not affected by the neutron sensitivity of the detection system.

The above mentioned methods are only applicable when the level scheme up to the capture state is well established and all transitions in the cascade are represented by a detected γ-ray. Therefore, γ-ray spectroscopic methods are very powerful to determine capture cross section data for light nuclei or for nuclei with a proton and neutron number close to a magic shell as demonstrated in Ref. [151]. Thermal capture cross section data for Pb isotopes using Ge-detectors are reported in Ref. [155]. Köhler et al. [156] performed high-resolution capture cross section measurements for ^{207}Pb(n,γ) at a 130 m station of GELINA using a detection system consisting of four BGO detectors. The resolving power of the BGO detectors was good enough to determine separately the partial capture yields to the ground state and to the 3^- first excited state at 2.61 MeV. The partial yields were used to determine the total capture yield and to verify the spin and parity assignment of resonances.

In case not all γ-ray transitions can be determined the results are biased and only lower limits can be derived. To verify the impact of missing transitions, the principle of γ-ray intensity balance [157, 158] or crossing intensity sum, as described by Belgya [159], can be applied. The missing contributions can also be based on statistical models to simulate the full γ-ray cascade. Codes that can be used are *e.g.* DICEBOX [160], DECAYGEN [161] and γDEX [162]. The γ-ray cascade simulations rely on nuclear level statistical models and nuclear data input (low-lying level scheme, average radiation widths, level densities). The accuracy of the cross section depends on the statistical nature of the γ-ray cascade.

For the thermal neutron capture cross section of ^{107}Pd, a lower limit of 9.16±0.27 b was determined by the sum of the partial cross sections of the transitions feeding the ground state in Ref. [157]. The γ-ray intensity balance for the first excited state, that is, comparing the sum of γ-ray intensities feeding the level with those depopulating the level, was used to estimate the missing contribution. Based on a 7% difference a capture cross section of 10 b was recommended. The same method was applied to determine the capture cross sections for ^{91}Zr and ^{93}Zr [158].

2. Total absorption

The total γ-ray absorption principle relies on the detection of the energy sum of the γ-rays emitted in a capture event. The ideal detector has a 4π geometry and a 100% absolute detection efficiency allowing for the detection of the entire electromagnetic cascade. Thus, the energy deposited in the detector is directly proportional to the total energy available in the capture event and independent of the γ-ray cascade.

The first total absorption detectors were large liquid (organic) scintillation tanks [163–167] covering a solid angle of almost 4π, however, with a very poor γ-ray energy

Author's personal copy

resolution and a relatively modest time resolution limited to about 5 ns. Due to their size, they suffer from a large natural background and they have an intrinsically high neutron sensitivity due to neutron capture in hydrogen. An upper limit on the energy deposition is imposed to reduce the background from high energy cosmic rays. The contribution of neutrons captured in the detector can be limited by lining the inside of the detector with a material containing ^{6}Li or by loading the liquid with boron [164–167], together with a lower discrimination threshold of about 500 keV to reject the low energy γ-rays caused by neutron absorption in ^{10}B. Unfortunately such liners are only effective for low energy neutrons. Since the neutron sensitivity is predominantly due to neutron capture in hydrogen, this background component can be reduced significantly by applying a lower discrimination level of at least 2.5 MeV to reject signals produced by 2.2 MeV γ-rays emitted after neutron capture in hydrogen [171]. This reduction in background is to the expense of having a detection efficiency that is strongly dependent of the cascade, especially for systems with a low neutron separation energy. Another problem is the effective detection efficiency deviating from 100% due to both the lower discrimination level and the intrinsic efficiency for a γ-ray to interact within the detector. To correct for the fraction in the spectrum that is lost due to the lower discriminator level an extrapolation to zero level is applied. Even after correction for the overall loss in detection efficiency, the accuracy of these systems is limited to 5% - 10% and depends strongly on the reaction under study [165, 167].

Organic liquid scintillators have extensively been used to determine capture cross sections of fissile material. To separate capture events from fission events different methods have been applied. In Ref. [168–170] a Cd-loaded scintillator is used. Fission events are identified by the delayed pulses produced by neutron capture of fission neutrons in the scintillator. Corrections are required for fission events that are not followed by the detection of a delayed neutron. This fraction is estimated by additional measurements with a fission counter. In Ref. [170–177], an additional ionization chamber was used and a fission event was characterized by a coincident signal from the liquid scintillator and the fission chamber. A considerable improvement in the signal-to-background ratio was achieved by operating the two optically separated halves of the liquid scintillator in coincidence [177]. In Ref. [173, 178] the shape of the energy deposition spectrum is studied to separate fission from capture events. The capture-to-fission cross section ratio was derived from a combination of spectra with a low and high discriminator level. All these references [168–178] provide the main experimental database to evaluate capture-to-fission ratios for ^{233,235}U and ^{239}Pu.

The size of a total absorption detector can be reduced and the detection efficiency even increased by using inorganic scintillators. A system based on 48 NaI(Tl) crystals was used at the Kurchatov Institute by Muradyan et al. [179]. A similar system, containing 16 NaI(Tl) crystals, is used for capture cross section measurements in the thermal and epi-thermal energy region at the TOF-facility of RPI [79, 95, 111]. A detection assembly of 16 BGO-crystals is installed at KURRI [38, 114]. A BaF_2 detection system made of 42 individual crystals with a truncated pyramidal shape [180] was used at FZK Karlsruhe to determine capture cross sections in the URR [47, 48]. A similar system is installed at the n_TOF facility for capture cross section measurements [99, 181]. The Detector for Advanced Neutron Capture Experiments (DANCE), which is a 4π array consisting of 162 BaF_2 elements, is installed at the Los Alamos Neutron Science Center (LANSCE) to carry out neutron capture cross section measurements [182]. The initial design of this detector and the one installed at n_TOF is described in Ref. [183]. A 4π $LaBr_3$(Ce) spectrometer was designed and optimised as a high-resolution total absorption detector and its performance was investigated by Monte Carlo simulations in Ref. [184]. The advantages and drawbacks of NaI(Tl), BaF_2 and BGO scintillators are discussed in Ref. [185]. Most of these systems have a multi-sectional structure and thus the ability to measure the multiplicity of the γ-ray cascade.

An example of the total energy deposited in a BaF_2 detector is shown in Fig. 20. The spectra are the result of capture cross section measurements on ^{197}Au carried out at n_TOF [99]. The distribution of the deposited energy E_d, for neutron energies between 1 eV and 5000 eV and normalized to the incident beam intensity, presents several structures. They correspond to the Q-value of different (n,γ) reactions. The peak around 6.5 MeV corresponds to the excitation energy of the compound nucleus ^{198}Au. The other structures are due to radioactive decay and to neutron induced reactions contributing to the background. Their origin can be identified and their impact quantified by the results of dedicated background measurements without a sample, with a pure scattering sample (*e.g.* carbon) and with the beam switched off. The optimum conditions, which maximize the capture-to-background ratio, are derived from energy deposition spectra for different multiplicities. These conditions depend on the reaction being studied, thus they are specific for each experiment. For ^{197}Au(n,γ) cross section measurements the best compromise between minimizing the background and maximizing the efficiency was found for multiplicities $m_C \geq 2$ and an energy deposition 2.5 MeV $< E_d <$ 7.5 MeV. These conditions eliminate practically the contribution of the 478 keV and 2.2 MeV γ-ray due to the ^{10}B(n,$\alpha\gamma$) and ^{1}H(n,γ) reaction, respectively. It also results in a significant reduction of (n,γ) reactions in the ^{135,137}Ba isotopes with neutron separation energies above 7 MeV. Nevertheless, Fig. 21 reveals that neutron capture in Ba will always contribute as a neutron sensitivity background component. A method to correct for this background contribution is explained in [47]. The contribution of neutron capture in Ba is defined by the TOF-spectrum obtained with the carbon sample which is normalized by the ratio of the TOF-

Author's personal copy

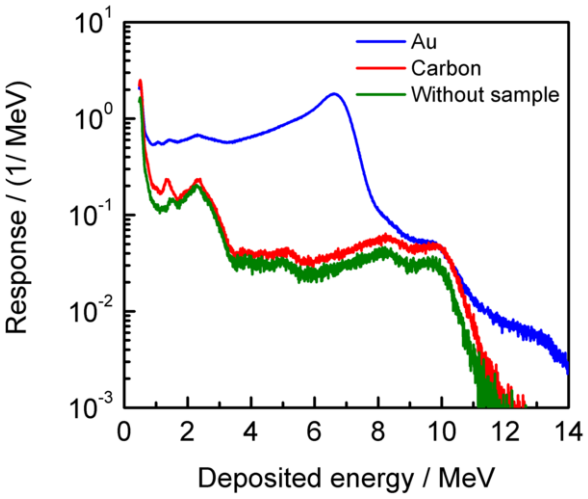

FIG. 20. Distribution of the energy deposited in the BaF_2 detector installed at n_TOF. The results of measurements with a Au and carbon sample are compared with the one without sample. The data are from Ref. [99].

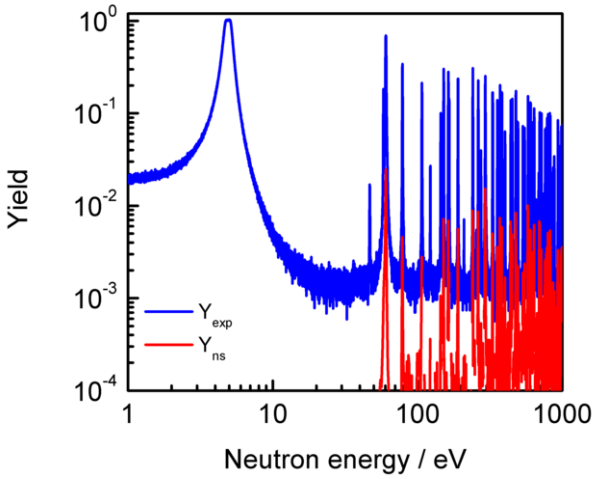

FIG. 21. The experimental yield as a function of neutron energy for a 0.122 mm thick Au sample is compared with the background contribution due to the neutron sensitivity of the detector (Y_{ns}). The data result from measurements with the BaF_2 detector at n_TOF [99].

spectra of the Au and carbon sample for an energy deposition 8.5 MeV $< E_d <$ 10.5 MeV. This method supposes that neutron capture in ^{197}Au does not contribute to the high energy region 8.5 MeV $< E_d <$ 10.5 MeV. The experimental yield obtained with the ^{197}Au sample and the background contribution due to neutron scattering is shown in Fig. 21. This comparison shows that the background contribution can reach 20%.

Since an ideal detector with a 100% γ-ray detection efficiency does not exist, a correction is needed when the normalization is performed using a capture reaction which has a different γ-ray cascade from the reaction under study. Such a correction becomes even more important when a constraint is imposed on the multiplicity and energy deposition to reduce the background and when the γ-ray cascade changes from resonance to resonance. In most cases the correction factors rely on statistical model calculations to simulate the γ-ray cascade (*e.g.* DICEBOX [160], DECAYGEN [161], γDEX [162]) combined with Monte Carlo simulations for the γ-ray transport in the sample and the detector. The accuracy of the correction factors depends on the statistical nature of the γ-ray cascade and on the quality of the geometry input file for the MC simulations of the γ-ray transport. Wang et al. [111] have reported efficiency calculations for the RPI detection system. Without imposing criteria on the multiplicity, they observed a difference of about 10% between the detection efficiency for ^{149}Sm(n,γ) and ^{150}Sm(n,γ). Similar calculations have been carried out for DANCE [186] and for the detection system installed at n_TOF [187]. Guerrero et al. [187] found a reduction in the detection efficiency of about 40% going from the condition ($m_C > 0$ and $E_d > 100$ keV) to ($m_C > 2$ and $E_d > 2500$ keV). Mostly thin samples are used such that corrections for γ-ray attenuation are not an issue.

The main drawback of total absorption systems is their neutron sensitivity. It can only be reduced at the cost of the above discussed corrections which strongly depend on the character and knowledge of the γ-ray cascade. However, their ability to measure the multiplicity distribution (due to their multi-sectional structure), their high detection efficiency and relative good γ-ray energy resolution make them especially adapted for capture cross section measurements of radioactive samples, to separate capture events from fission events and to study characteristics of the γ-ray cascade. The DAISY detector of Ref. [179] has been used as a multiplicity spectrometer to separate fission from capture events and for spin assignments of resonances. At LANSCE [188] and n_TOF [189] the 4π BaF_2 total absorption detector is combined with a fission chamber to derive capture cross sections for fissile nuclei. By imposing conditions on both the multiplicity and the energy deposition the separation between fission and capture events can be improved. The difference in response of the energy deposition between a capture and fission event is used in Ref. [190] as a separation criterium without the need of using a fission chamber.

3. *Total energy detection*

When the contribution of neutron induced fission reactions can be neglected, the most accurate capture cross section data can be measured by applying the total energy detection principle using C_6D_6 detectors combined with the pulse height weighting technique (PHWT) [98, 110, 191]. Application of the total energy detection

Author's personal copy

principle requires a γ-ray detector with a relatively low γ-ray detection efficiency which is proportional to the γ-ray energy. Under these conditions the efficiency to detect a capture event is directly proportional to the sum of the energies of the γ-rays emitted in the cascade. This makes the efficiency independent of the γ-ray cascade.

The Moxon-Rae detector achieves approximately the proportionality between the γ-ray energy and detection efficiency by a special design of the detector [192]. A Moxon-Rae detector consists of a γ-ray - to - electron converter coupled to a thin plastic scintillator mounted on a photomultiplier. The use of this type of detectors has been abandoned due to its extreme low detection efficiency and the non-proportionality of the γ-ray detection efficiency below 1 MeV [147]. To account for this non-proportionality, correction factors are required depending on the detector characteristics and the γ-ray cascade. Even after applying such a correction factor uncertainties due to systematic effects are at least 5% [193, 194].

An alternative is the PHWT by means of a weighting function. This technique is based on an original suggestion by Maier-Leibnitz. It was first applied by Macklin and Gibson [110] using C_6F_6 detectors. However, the use of the less neutron sensitive C_6D_6 detectors is definitely preferred [143, 146]. Such systems are extensively used at KURRI [195], GELINA [69, 98, 106, 107], n_TOF [100, 137] and ORELA [143, 196]. The total energy detection principle is applicable for any conventional γ-ray detector, *e.g.* Ge [116], BGO [114, 197], NaI [49] which have a much better γ-ray resolution. However, these systems suffer from a high neutron sensitivity compared to C_6D_6 detectors. To prevent the scattered neutrons entering the detector, neutron absorption material can be used. The neutron sensitivity can be partly reduced by using a ^{6}LiH shielding, *e.g.* for a Ge-spectrometer in Ref. [116] and for a NaI spectrometer in Ref. [49].

Plag et al. [146] discussed in detail the various components contributing to the neutron sensitivity of a C_6D_6 detector and realized a detector with an extreme low neutron sensitivity. A capture detection system based on such detectors is installed at n_TOF. More conventional C_6D_6 detectors are used at GELINA and ORELA. Typical background conditions of the capture systems installed at GELINA are shown in Fig. 22. The total weighted response for a ^{197}Au sample, together with the different background components, are shown for a measurement at a 12.5 m capture station. Since the measurements focused on the average capture cross sections in the URR between 4 keV and 90 keV, a fixed Na filter was placed in the beam for a continuous control of the background. Due to the presence of an additional S filter the contribution of in-beam γ-rays scattered by the sample was negligible. The total background B_w is estimated by

$$B_w = a_0 + k_1 C_{w,OPB} + k_2 R_n (C_{w,Pb} - C_{w,OPB}), \quad (26)$$

where a_0 is the total time independent contribution, and $C_{w,OPB}$ and $C_{w,Pb}$ are the weighted counts from measurements with no sample and with an almost purely scattering ^{208}Pb sample, respectively. The weighted counts are all normalized to the same total neutron intensity. The background is clearly dominated by the time dependent and sample independent background component $C_{w,OPB}$. The contribution of the sample dependent component is over the whole energy range less than 1%. The correction factor R_n accounts for the difference in scattering yield of the gold and lead samples. In case the uncertainty on the calculated scattering yield is too high, the correction for neutron sensitivity has to be done iteratively as part of the resonance analysis as described in section VIII B.

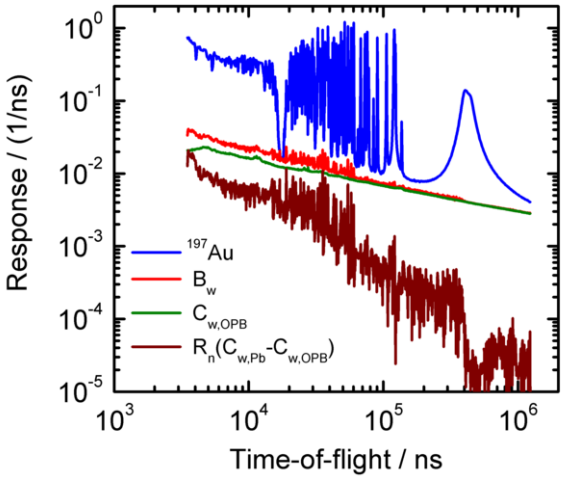

FIG. 22. The response of a C_6D_6 detector system as a function of TOF for a 1.0 mm ^{197}Au sample [198] obtained at GELINA is compared with the contribution of the different background components.

The factors $k_1 = 1.00 \pm 0.03$ and $k_2 = 1.00 \pm 0.05$ are used to introduce uncertainties due to systematic effects in the background model. The quoted uncertainties have been evaluated by supplementary measurements on a 0.01 mm and 0.5 mm thick Au sample. The uncertainties were derived from a comparison of the background level at resonance dips due to the fixed Na filter and by additional measurements with other black resonance filters (Co, W and Ag). These uncertainties differ from those reported in Ref.[23], which were only based on results obtained with the 0.01 mm sample. A comparison of the results in Fig. 21 and Fig. 22 puts in evidence the substantial difference in contribution of the neutron sensitivity of a BaF_2 detection system compared to a C_6D_6-system.

Over the last decade, an intense effort has been made to improve the quality of weighting functions and consequently the accuracy of $\sigma(n,\gamma)$ data based on the total energy detection principle in combination with the PHWT using C_6D_6 detectors. Various authors [98, 199–201] have demonstrated that accurate weighting functions

Author's personal copy

can be obtained from Monte Carlo simulations provided that the geometry description reflects the experimental conditions and the γ-ray transport in the sample and detector is taken into account. Due to experimental limitations it is impossible to record spectra at extreme low values of the deposited energy and a finite discriminator level E_D is applied. To account for the missing part in the observed spectrum two approaches can be followed. In a first approach, see *e.g.* Ref. [202], the weighting function is calculated for a theoretical discriminator level $E_L = 0$ MeV and a correction is applied for the missing contribution of both the γ-rays for which the energy is below the experimental level E_D and the γ-rays that contribute only partly to the observed spectrum. The other approach, followed in [98, 203], is to calculate the weighting function for $E_D = E_L$, *i.e.* assuming that for each γ-ray the response below E_D is zero. For this approach only corrections for γ-rays with an energy less than E_D have to be made. Applying the first approach, the quality of the weighting function is superior. However, more information about the γ-ray emission spectrum is required. The corrections for the two approaches are based on a simulation of the γ-ray cascade. Therefore, the validity of the first approach is questionable for nuclei with a simple γ-ray cascade such as light nuclei or nuclei close to a magic shell. For such nuclei the γ-ray cascades can not be estimated starting from statistical models. In addition, they differ strongly from resonance to resonance, as shown in Ref. [107] for ^{206}Pb. Since the emission probability of γ-rays with an energy smaller than E_D will be very low for such nuclei, the correction factor for the second approach is very close to unity independent of the resonance. The correction required for the 1.15 keV ^{56}Fe, 5.2 eV ^{109}Ag and 4.9 eV ^{197}Au resonances applying the second approach is limited to about 0.1%, 1% and 2%, respectively, for $E_D = 150$ keV [98].

The γ-ray attenuation can accurately be taken into account in the calculation of the weighting function, as demonstrated in Ref. [98, 201]. Since the γ-ray attenuation depends on the place where the capture reaction takes place in the sample, it will strongly depend on the total cross section. This implies that the weighting function depends on the resonance strength and may differ from resonance to resonance. For weak resonances a homogeneous distribution of the γ-rays is valid, while for strong resonances one needs to account for the flux attenuation. Thus, in the RRR each resonance requires in principle its own weighting function. This is from a practical point of view not realistic. Moreover, the primary and multiple interaction events contributing to the yield will have a different spatial distribution in the sample. Consequently the attenuation of the corresponding emitted γ-rays will be different and in the RRR a direct correction can not be applied. Therefore, the following procedure was proposed in Ref. [98]: the experimental yield is deduced using a weighting function calculated for γ-rays which are homogeneously distributed in the sample and a correction factor depending on the area density and total cross section is applied in the data analysis as will be discussed in section VIII B. These corrections can be determined by Monte Carlo simulations based on a combination of statistical models and a neutron and γ-ray transport code, *e.g.* DICEBOX, DECAYGEN, or γ-DEX combined with MCNP or GEANT. For ^{197}Au(n,γ) the correction factor derived from such calculations has been validated with experimental results in Ref. [98]. Correction factors for primary capture events in a 2-mm thick metal natural cadmium sample are shown in Fig. 23. This figure shows that the correction factor can not be approximated by a simple analytical function and surprisingly does not approach a constant value for large values of $n\sigma_{tot}$, as observed experimentally for ^{197}Au [98]. Fig. 23 also illustrates that the difference in separation energy for ^{112}Cd and ^{113}Cd, 6540 keV and 9043 keV, respectively, does not create a significant difference in correction factor. As already noted by Wisshak et al. [204] the correction for γ-ray attenuation will depend on the detection system including the position of the detectors with respect to the sample.

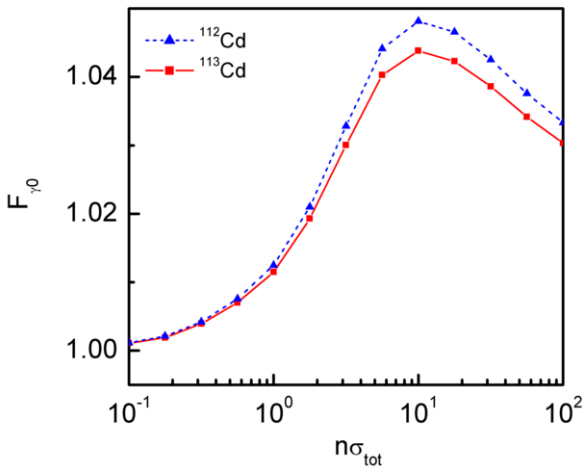

FIG. 23. Correction factor $F_{\gamma 0}$ to account for the γ-ray attenuation in the sample. The factor for ^{112}Cd and ^{113}Cd is given as a function of the product of the area density and the total cross section.

An experimental validation of the total energy detection principle combined with the PHWT for C_6F_6 detectors was performed by Yamamuro et al. [191]. Normalization factors derived from the saturated resonances 4.3 eV in ^{181}Ta, 4.9 eV in ^{197}Au and 5.2 eV in ^{109}Ag, were consistent within 2%. At GELINA a series of measurement campaigns have been dedicated to validate weighting functions determined by Monte Carlo simulations and to assess uncertainties of various systematic effects influencing results of capture cross section measurements. In Ref. [98] results of normalization measurements based on the saturated resonance at 4.9 eV in Au and 5.2 eV in Ag using samples with different thicknesses are reported.

Author's personal copy

TABLE IV. Γ_n of the 1.15 keV resonance of ^{56}Fe resulting from (n,γ) measurements with C_6D_6 at GELINA [98]. Uncertainties are only due to counting statistics. In the analysis Γ_γ = 574 meV was used.

Sample	Fe g/cm^2	X	Ø mm	Γ_n meV
Fe1	0.105		60	62.6 ± 1.0
Fe2	0.394		60	62.5 ± 0.8
Fe3	0.905		60	62.2 ± 0.7
^{206}PbFe*	0.394	1.213	60	63.1 ± 0.8
PbFe*	0.422	1.103	60	62.6 ± 0.8
PbFe*	0.422	2.725	60	62.6 ± 0.8
Fe4	0.202		80	61.2 ± 0.8
Fe5	0.795		80	60.3 ± 0.8
Fe6	0.998		80	61.2 ± 0.8
Fe_2O_3	1.404	0.603	80	59.1 ± 0.7
AuFe	1.708	0.118	80	61.3 ± 0.8

* Sandwich

These results demonstrate that the normalization factors agree to better than 0.5% independent of the sample characteristics provided that the weighting functions account for the combined effect of the neutron flux and γ-ray attenuation in the sample. The accuracy that can be reached in the determination of a capture area can be derived from the data in Table IV. This table summarizes the results of measurements with different samples to determine the neutron width of the 1.15 keV resonance of ^{56}Fe [98]. Since this resonance is well isolated and has a capture width Γ_γ = 574 ± 40 meV which is about ten times larger than the neutron width Γ_n = 61.7 ± 0.9 meV [205], it is an almost ideal resonance to test the accuracy of capture measurements. Based on an analysis of variance (ANOVA) [24], an uncertainty of 1.7% due to systematic effects was evaluated. This uncertainty acts as a correlated component for capture measurements when the normalization is based on an additional normalization measurement of a saturated resonance. Measurements were also carried out with a Fe-Au sandwich sample. For these data an internal normalization was applied. The resulting neutron width, Γ_n = 61.3 ± 0.8 meV, is in perfect agreement with the standard transmission value Γ_n = 61.7 ± 0.9 meV determined by Perey et al. [205] and with the value Γ_n = 61.8 ± 1.9 meV derived by Macklin [206] from a bright capture experiment using Fe-samples with different thicknesses. Based on these results the 1.15 keV resonance is used at GELINA to normalize capture data for measurements above a few hundred eV.

This uncertainty can still be reduced when the γ-ray cascade of the normalization resonance or reaction is very similar to the one of the reaction being studied. This is demonstrated in Fig. 24 which compares the yield for a 0.5 mm thick ^{197}Au metal disc with a calculated yield using the resonance parameters in the ENDF/B-VII.1 file [59]. The parameters in this file have been adjusted to reproduce the standard cross section σ(n,γ) = 98.66±0.14 b at 0.0253 eV of [21, 32]. The yield was derived from a weighting function considering a homogeneous distribution of the γ-rays in the sample and a correction for the γ-ray attenuation was applied on the calculated yield (see section VIII B). The agreement between the calculated and experimental yield is better than 0.5%. From the data a thermal capture cross section of 99.0± 1.0 b was derived. The quality of the capture data in the URR is discussed in detail in Ref. [106]. The capture cross section data of ^{232}Th in the URR was deduced by normalizing the data to the quasi-saturated ^{232}Th resonances at 21.8 eV and at 23.5 eV. A detailed study of the impact of both the parameters of these resonances and the applied weighting function revealed that the capture cross section in the URR was determined with an uncertainty better than 1.7%.

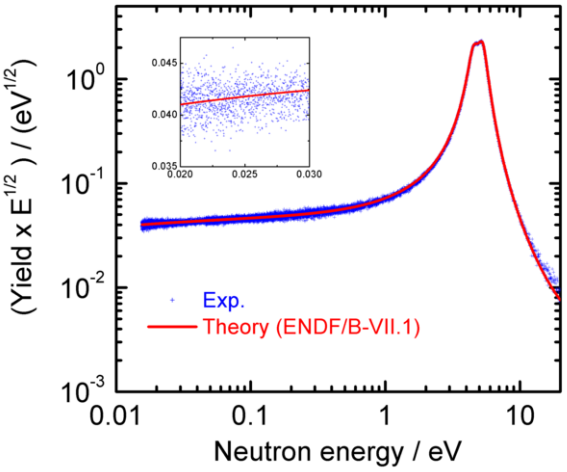

FIG. 24. The capture yield (multiplied by E$^{1/2}$) as a function of neutron energy, derived from capture measurements on a 0.5 mm thick ^{197}Au sample at a 12.5 m energy station of GELINA [70, 136], is compared with the theoretical yield based on ENDF/B-VII.1 parameters.

One can conclude that from measurements with a C_6D_6 detection system based on the total energy detection principle capture yields can be deduced from thermal energy up the URR with uncertainties better than 2%. This conclusion, however, is fully linked to the experimental conditions and is only valid under the following constraints:

- a continuous control of the shape of the neutron flux using a back-to-back ^{10}B-loaded ionization chamber and taking care of the flux profile;
- the use of fixed background filters to control in particular the sample dependent background component, the type of filter is adapted to the energy region of interest;
- the uncertainty of the dead time correction can be neglected;

Author's personal copy

- simulated weighting functions which account for the discriminator level and have been validated by experiment;

- special analysis procedures to account for γ-ray attenuation in the sample and neutron sensitivity of the detection system.

Low efficiency C_6D_6 have been used by Corvi et al. [207] to determine the capture-to-fission ratio for ^{235}U in the energy region from 2 keV to 85 keV. The detection system consisted of 4 C_6D_6 detectors combined with a parallel plate fission chamber loaded with 2.5 g ^{235}U. Two different normalizations for the capture data were applied: an internal normalization at thermal energy using the ^{235}U(n,γ) cross section as a reference and a normalization at the 4.9 eV saturated resonance of ^{197}Au based on an additional measurement. The agreement between the two normalization factors was within 3%. Borella et al. [107] determined for 22 resonances of ^{206}Pb below 70 keV partial radiation widths by unfolding the C_6D_6 pulse height spectra. From these data photon strength functions were derived. In addition for the p-wave resonances at 25.4 keV, 36.2 keV and 47.5 keV primary E2 transitions to the 569.7 keV $5/2^-$ state were observed.

D. Sample Properties

A sample for capture cross section measurements is ideally a thin homogeneous metal foil or disc, which is light tight such that the thin sample approximation is valid. In a real experiment a compromise between signal-to-background conditions and systematic effects due to self-shielding and multiple interaction has to be made to define the optimum thickness. In addition, samples in metallic form are not always available and samples have to be prepared starting from powder material. In some cases mixed powder samples are even needed to avoid saturation and to keep a certain degree of homogeneity. To reduce systematic effects on the normalization, mixed samples are often used [131].

When the self-shielding is significant and powder samples are used similar precautions as for transmission measurements have to be taken into account. Fig. 25 shows theoretical capture yields for $^{242}PuO_2$ samples with a different degree of homogeneity and fraction of holes. The difference in the observed profiles will have a strong effect on the parameters that are deduced from such data. To avoid bias effects on the parameters the sample characteristics have to be taken into account in the resonance shape analysis. When using a mixture or compound, the use of nuclei with a high neutron scattering probability and hygroscopic materials should be avoided. They complicate the corrections for self-shielding and in particular multiple interaction as discussed in Ref. [131, 154].

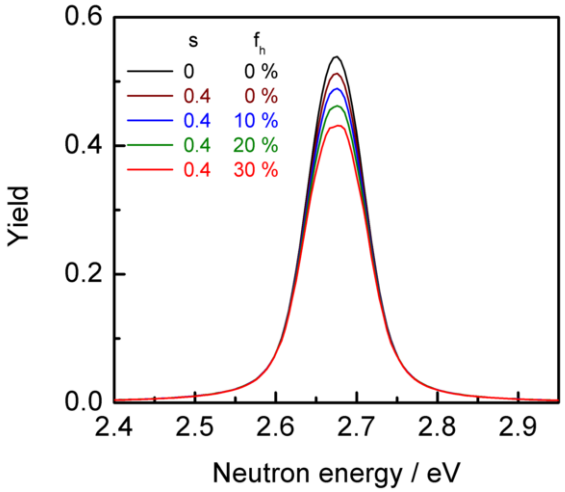

FIG. 25. The theoretical capture yield as a function of neutron energy is shown for PuO_2 powder samples with a different degree of homogeneity and holes fraction represented by s and f_h, respectively.

VIII. FROM EXPERIMENTAL OBSERVABLES TO RESONANCE PARAMETERS

A. Adjustment Procedures

Parameters of nuclear reaction models can be obtained from experimental data by a least squares adjustment, that is by minimizing the expression

$$\chi^2(\vec{\theta}) = \left(\vec{Z}_{exp} - \vec{Z}_m(\vec{\theta})\right)^T \mathbf{V}^{-1}_{\vec{Z}_{exp}} \left(\vec{Z}_{exp} - \vec{Z}_m(\vec{\theta})\right), \quad (27)$$

where $\vec{Z}_m(\vec{\theta})$ is the model describing the experimental data $\vec{Z}_{exp}$, with covariance matrix $\mathbf{V}_{\vec{Z}_{exp}}$, and $\vec{\theta}$ are the model parameters. The minimum condition of Eq. (27) is equivalent to a maximum likelihood when the probability distribution of the observable is a normal distribution [1, 19]. Without any additional information on the probability distribution of $\vec{Z}$ this can always be supposed based on the principle of maximum entropy [1, 19]. In case the data consists of counting histograms, the covariance in Eq. (27) is based on a Poisson distribution. The latter can be approximated by a Gaussian distribution when its mean is larger than 30 [25]. In case this condition is not fulfilled parameters are better determined by maximum likelihood to avoid bias effects [208]. The fitted parameters, describing in the best way the experimental data, can be found in an iterative way by searching for the steepest decent. For a linear model the minimum is also found for

$$\vec{\theta} = \left(\mathbf{G}^T_{\vec{\theta}} \mathbf{V}^{-1}_{\vec{Z}} \mathbf{G}_{\vec{\theta}}\right)^{-1} \left(\mathbf{G}^T_{\vec{\theta}} \mathbf{V}^{-1}_{\vec{Z}} \vec{Z}_{exp}\right). \quad (28)$$

Author's personal copy

The covariance of the estimated parameters based on conventional uncertainty propagation (CUP) is given by

$$\mathbf{V}_{\vec{\theta}} = \left(\mathbf{G}_{\vec{\theta}}^T \mathbf{V}_{\vec{Z}}^{-1} \mathbf{G}_{\vec{\theta}}\right)^{-1}. \quad (29)$$

The sensitivity matrix $\mathbf{G}_{\vec{\theta}}$ has as elements the partial derivatives of $\vec{Z}_{exp}$ with respect to $\vec{\theta}$. The quality of the fit can be verified by comparing the χ^2 per degree of freedom with its expectation value in case the observable follows a normal distribution. For an adequate description of the data this value approaches unity for a large number of degrees of freedom ν [25].

As noticed in Ref. [1, 19] the parameters which minimize Eq. (27) are the result of a Bayesian inference when the prior information on the parameters $\vec{\theta}_0$ with covariance $\mathbf{V}_{\vec{\theta}_0}$ is considered as a part of the experimental data $\vec{Z}_{exp}$ with covariance matrix $\mathbf{V}_{\vec{Z}_{exp}}$. The experimental data input is formed by stacking the informative prior ($\vec{\theta}_0$, $\mathbf{V}_{\vec{\theta}_0}$) and the new experimental data ($\vec{y}_{exp}$, $\mathbf{V}_{\vec{y}_{exp}}$). The vector $\vec{y}_{exp}$ contains the results of transmission and/or reaction cross section measurements. Such a Bayesian evaluation can be applied without any restriction on the correlation between the different elements of the observable $\vec{Z}$. Therefore, the results Eq. (28) and Eq. (29) can be considered as the solution of the most generalized least squares (GLS) adjustment.

The solution in case the prior information ($\vec{\theta}_0$, $\mathbf{V}_{\vec{\theta}_0}$) is not being considered as a part of the experimental data [7]

$$\vec{\theta} = \vec{\theta}_0 + \mathbf{V}_{\vec{\theta}_0} \mathbf{G}_{\vec{\theta}}^T (\mathbf{G}_{\vec{\theta}} \mathbf{V}_{\vec{\theta}_0} \mathbf{G}_{\vec{\theta}}^T + \mathbf{V}_{\vec{y}})^{-1} (\vec{y}_{exp} - \vec{y}_m(\vec{\theta}_0)), \quad (30)$$

with covariance

$$\mathbf{V}_{\vec{\theta}} = \mathbf{V}_{\vec{\theta}_0} - \mathbf{V}_{\vec{\theta}_0} \mathbf{G}_{\vec{\theta}}^T (\mathbf{G}_{\vec{\theta}} \mathbf{V}_{\vec{\theta}_0}, \mathbf{G}_{\vec{\theta}}^T + \mathbf{V}_{\vec{Y}})^{-1} \mathbf{G}_{\vec{\theta}} \mathbf{V}_{\vec{\theta}_0} \quad (31)$$

is only valid when the informative prior $\vec{\theta}_0$ is independent of the new data $\vec{y}_{exp}$. By including the prior as an experimental input parameter, one can also avoid that unrealistic low uncertainties are produced when a sequential Bayesian evaluation is applied incorrectly on a set of correlated data using Eq. (30) and Eq. (31). Under the condition of total ignorance or with a non-informative prior both sets of equations (Eq. (28) and Eq. (29)) and (Eq. (30) and Eq. (31)) result in the same analytical expressions. In case of non-linear models the sets of equations (Eq. (28) and Eq. (29)) and (Eq. (30) and Eq. (31)) can be solved in an iterative way to find the optimum parameters.

Results of a least squares adjustment might be biased when the model is non-linear and the estimator of the covariance matrix is not well defined, *e.g.* due to the presence of a correlated normalization component together with a strong scattering of the data around the estimated value [17, 22]. This problem, known as Peelle's Pertinent Puzzle (PPP), has been studied extensively in the literature [16–23]. Mostly the problem of estimating an independent quantity from a weighted average of values which are only correlated due to a normalization factor is discussed. Zhao and Perey [16] examined PPP also in case of a linear dependent quantity. Becker et al. [23] considered the problem of experimental observables which are similar to results of transmission and reaction cross section measurements. In addition, they discussed PPP when the scattering in the data is due to the physics and originates from fluctuations in the data due to the resonance structure. In the URR, this effect can cause a dramatic underestimation of the cross section when fitting is done with a full covariance matrix and the correlated contribution due to the normalization is based on the experimental data. This is illustrated in Fig. 26, which compares the average capture cross section deduced from measurements at a 30 m and 60 m station of GELINA [209] with a theoretical cross section based on the Hauser-Feshbach statistical reaction theory, described in Ref. [14]. The model parameters in the fit are the energy independent neutron strength functions for $\ell = 0, 1, 2$ and γ-ray transmission coefficients as model parameters. The 30 m and 60 m data show the same fluctuations with amplitudes that are substantially larger than the uncertainties resulting from counting statistics. These fluctuations are due to resonance structures. Using a full covariance matrix in the least squares adjustment, leads to a clear underestimation of the result when the covariance due to the normalization is based on the experimental fluctuating data (black line in Fig. 26). On the other hand by including the normalization as an additional experimental data input as proposed in Ref. [19], a good description of the data is obtained (red line in Fig. 26). The same solution is obtained using the full covariance matrix, but accounting for the normalization uncertainty iteratively based on the calculated cross section as suggested in Ref. [16–18, 22]. Interesting to note is that PPP does not affect the shape.

Different methods can be applied to take into account all uncertainty components whilst avoiding PPP:

A: include the normalization component in the covariance matrix based on a theoretical estimate of the data and apply CUP [16–18, 22],

B: include the correlated uncertainty component as an experimental data input and model parameters in the GLS and apply CUP [19],

C: by a Monte Carlo sampling scheme coupled to GLS proposed in Ref.[210] or

D: by a marginalization procedure coupled to GLS proposed in Ref. [211].

To account for all uncertainty components in the evaluation of ($\vec{\theta}$, $\mathbf{V}_{\vec{\theta}}$), a distinction has to be made between experimental effects resulting from the data reduction and

Author's personal copy

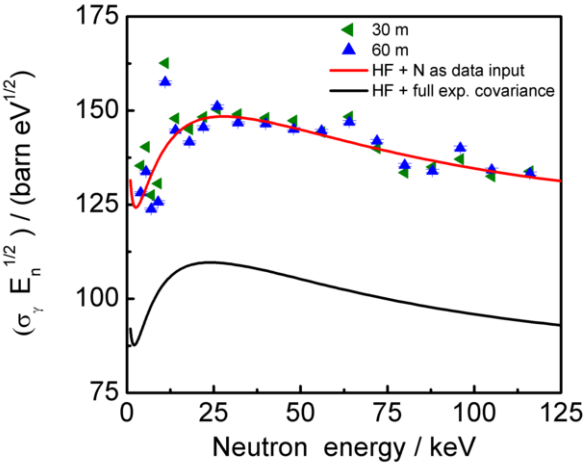

FIG. 26. The average capture cross section (multiplied by $E^{1/2}$) for ^{103}Rh as a function of neutron energy derived from measurements at GELINA [209]. The results of a least squares adjustment are also given (see text).

those due to the model. Evidently the covariance of parameters which can not be included in the model can only be propagated through the covariance matrix of the experimental observable.

B. Resolved Resonance Region

In the RRR the theoretical estimate $Z(t,\vec{\eta},\vec{\kappa})$ used in Eq. (27) is the result of a folding to account for the response function of the TOF-spectrometer

$$Z(t,\vec{\eta},\vec{\kappa}) = N_Z \frac{\int R(t,E,\vec{\kappa}) Z'(E,\vec{\eta},\vec{\kappa}) dE}{\int R(t,E,\vec{\kappa}) dE}, \qquad (32)$$

where N_Z is an adjustable normalization factor. $R(t,E,\vec{\kappa})$ is the response function of the TOF-spectrometer, which depends on *e.g.* target-moderator characteristics, flight path length and pulse width. The quantity $Z'(E,\vec{\eta},\vec{\kappa})$ represents the theoretical estimate of the observed transmission $T(E,\vec{\eta},\vec{\kappa})$ or reaction yield $Y(E,\vec{\eta},\vec{\kappa})$. Its calculation requires a theoretical model that includes a nuclear reaction formalism (*i.e.* R-matrix formalism) and models to account for various experimental effects. The theoretical model depends on a vector of resonance parameters and experimental parameters represented by $\vec{\eta}$ and $\vec{\kappa}$, respectively. The experimental parameter vector $\vec{\kappa}$ includes *e.g.* the sample temperature to reckon with the Doppler effect.

To account for inhomogeneites of the sample, the theoretical estimate of the transmission can be approximated by *e.g.*

$$T(E,\vec{\eta},\vec{\kappa}) = \left[\int e^{-\sum_k n'_k x \overline{\sigma}_{tot,k}} p(x) dx\right](1-f_h) + f_h, \qquad (33)$$

where f_h represents the fraction of holes in the sample. The average effective area density n'_k is related to the area density n_k, which is derived from measurements of mass and area, by $n'_k = n_k/f_h$. The variable x reflects the inhomogeneity of the sample. This variable is distributed as a log-normal distribution

$$p(x) = \frac{1}{x\sqrt{2\pi s^2}} \exp\left(-\frac{\left(\ln x + s^2/2\right)^2}{2s^2}\right), \qquad (34)$$

with average value one and a width parameter s^2 which is independent of k [90]. The area densities, parameter s^2 and holes fraction f_h are all elements of $\vec{\kappa}$. Examples of the use of this expression were already presented in section IV C.

For the analysis of the experimental yield resulting from a reaction experiment the theoretical expectation value can be expressed as

$$Y(E,\vec{\eta},\vec{\kappa}) = \sum_k \left[\epsilon'_{r,k}\left(F_{r0,k}Y_{0,k} + F_{rm,k}Y_{rm,k}\right) + K_{ns}Y_n\right], \qquad (35)$$

where Y_n is the neutron yield and the transmission in the calculation of the primary yields (neutron and capture) is calculated according to Eq. (33). The correction factors $F_{r0,k}$ and $F_{rm,k}$ are introduced to account for the escape probability of the reaction product and $\epsilon'_{r,k}$ for detection efficiencies which might be reaction dependent. These corrections together with the correction for neutron sensitivity are mainly used for the analysis of capture data. The expression in Eq. (35) supposes that the experimental yield is obtained without correcting for the γ-ray attenuation in the sample (*e.g.* using a weighting function for a homogeneous distribution in case of the PHWT) and the normalization is done for a well defined reaction or resonance. The factor $F_{\gamma 0,k}$ is introduced to correct for the γ-ray attenuation in case of primary yield events. Multiple scattering events are mostly supposed to be homogeneously distributed in the sample, such that $F_{\gamma m,k} = 1$. The relative efficiency factor $\epsilon'_{\gamma,k}$ depends on the neutron energy E_n and is given by

$$\epsilon'_{\gamma,k} = \frac{S_{n,k}\left[1 + \frac{m_k}{m_k+m_n}\frac{E_n}{S_{n,k}}\right]}{S_{n,N}\left[1 + \frac{m_N}{m_N+m_n}\frac{E_{n,N}}{S_{n,N}}\right]}, \qquad (36)$$

where $S_{n,N}$ and $E_{n,N}$ are related to the separation and neutron energy of the reaction or resonance used to normalize the experimental yield. Mostly the energy dependence is negligible, and Eq. (36) reduces to $\epsilon'_{\gamma,k} \approx S_{n,k}/S_{n,N}$.

The expressions of Eq. (33) and (35) are implemented in REFIT. The correction for γ-ray attenuation, detection efficiency and neutron sensitivity are given as additional input data files. In SAMMY a radial dependence of the

Author's personal copy

area density can be given as an input to account for sample inhomogeneities. However, the code does not include modules to account for the γ-ray attenuation and neutron sensitivity. On the other hand, it includes an option to calculate the reaction yields for simple geometries using the SAMSMC code [72]. The implementation of modules to derive resonance parameters by fitting experimental data within the CONRAD code is in progress at CEA Cadarache [212].

When the experimental yield and transmission are used as data input, the dead time and background can not be included in the model. The background can only be considered as a model parameter when the incoming neutron flux is given and the counts of the reaction experiment or sample-in measurement are fitted. Often a background parameter is included in the model. However, this parameter is only indirectly related to the background contributions discussed in the previous sections. In case the adjusted parameter deviates significantly from zero, one should not correct the data during the fitting but try to find which background component was not well estimated and redo the data reduction. The normalization factor can always be included as a model parameter. In case, however, the parameter is adjusted during the fitting and the adjusted value deviates from one, again a correction during the fit is definitely not recommended. To avoid bias effects one first has to identify the cause of this deviation and depending on the outcome redo the data reduction. Such a procedure might require an iterative interaction between experimentalists and evaluators.

1. *Synthetic data*

In this section the influence of experimental parameters on the covariances of resonance parameters is investigated. Covariance matrices obtained by propagating the experimental uncertainties using the methods (A, B, C and D) are compared. To study the impact of the different components separately, synthetic data have been generated, however, taking into account as much as possible the experimental conditions discussed in the previous sections. For the discussion transmission and capture experiments were considered. It should be noted that the final conclusions are also valid for any other reaction cross section data, *e.g.* fission.

In a reaction experiment, the normalization factor is one of the main components introducing a correlated uncertainty. Capture yields for the 4.9 eV s-wave resonance of ^{197}Au (ℓ = 0, J = 2, Γ_n = 15.2 meV and Γ_γ = 122.5 meV) have been generated for different peak uncertainties and three target thicknesses, including an extreme thin target for which self-shielding can be neglected and the yield is directly proportional to the cross section. The yields have been calculated for 980 data points between 4 eV and 6 eV. The Doppler broadening was included. However, the response function of the TOF spectrometer was neglected. Since the total width is larger than the Doppler broadening (which is about 50 meV FHWM), both Γ_n and Γ_γ can be determined from the observed profile. The uncorrelated uncertainty due to counting statistics was propagated together with a u_N/N = 2% normalization uncertainty. Method A and B, as expected, produced identical results. Since method B provides additional information on the experimental model parameters (in this example the normalization factor), the results obtained with method B are reported together with those of C and D in Table V.

Various conclusions can be drawn. The degree of correlation strongly depends on the target thickness and evidently on the relative contribution of the uncorrelated uncertainty component (or counting statistics). For low counting statistics significant differences between correlation coefficients derived by the different methods are noticed. When the reaction yield is directly proportional to the reaction cross section, *i.e.* in thin sample approximation, the four methods produce almost identical uncertainties, independent of the counting statistics. For extreme thin samples, the normalization uncertainty of 2% propagates completely to Γ_n, *i.e.* the smallest width which is mainly determined by the area of the resonance. The propagation to Γ_γ, the parameter determined from the broadening of the observed profile, is negligible and only visible for thick targets. With increasing sample thickness substantial differences are observed when comparing the results from different methods. Differences become distinct with increasing counting statistics, that is, with decreasing contribution of the uncorrelated uncertainty component. When CUP is used, the impact of the normalization uncertainty decreases strongly with increasing sample thickness. The thicker the sample, the more the uncertainties are determined by the counting statistics and they can become extremely small. The decrease in uncertainty with increasing sample thickness coincides with a decrease in uncertainty on the normalization factor. Using method C and D a complete different behavior with sample thickness is observed, the normalization uncertainty always propagates to the smallest width (Γ_n) and its influence even increases with sample thickness. The uncertainty on Γ_γ also increases with increasing thickness. By repeating the exercise with only the self-shielding term included in the generated capture yields, similar conclusions were drawn.

The results with CUP (method B) suggest that resonance parameters are best deduced from reaction yields obtained with thick samples. Indeed, from a theoretical point of view the results of a thick sample measurement are sensitive to the capture, total and even scattering cross section when multiple interaction events contribute as well. For a relatively thick target the full profile, including the peak and the wings, contains in principle enough information to determine $(N, \Gamma_\gamma, \Gamma_n)$. This statement is correct for an ideal homogeneous sample and a model that accounts correctly for the TOF-response, Doppler broadening, self-shielding, multiple interaction events, γ-ray attenuation and neutron sensitivity. The

Author's personal copy

TABLE V. Covariance data for the 4.9 eV resonance resulting from an analysis form synthetic data using methods B (CUP), C (MC-sampling) and D (marginalization). Results are given for 10%, 1% and 0.1% counting statistics uncertainty at the peak.

		$\lim_{n\to 0} Y \simeq n\sigma$			0.005 mm			0.01 mm		
		(B)	(C)	(D)	(B)	(C)	(D)	(B)	(C)	(D)
10 %	u_N/N	0.019			0.019			0.019		
	u_{Γ_n}/Γ_n	0.025	0.025	0.025	0.026	0.031	0.032	0.030	0.042	0.044
	$u_{\Gamma_\gamma}/\Gamma_\gamma$	0.018	0.018	0.017	0.018	0.022	0.022	0.022	0.031	0.036
	ρ(N,Γ_n)	-0.90			-0.91			-0.91		
	ρ(N,Γ_γ)	0.15			0.32			0.50		
	$\rho(\Gamma_n,\Gamma_\gamma)$	-0.23	-0.14	-0.26	-0.45	-0.15	-0.67	-0.67	-0.35	-0.90
1 %	u_N/N	0.019			0.015			0.009		
	u_{Γ_n}/Γ_n	0.022	0.022	0.023	0.018	0.030	0.029	0.013	0.037	0.040
	$u_{\Gamma_\gamma}/\Gamma_\gamma$	0.0030	0.0033	0.0033	0.005	0.011	0.011	0.006	0.020	0.026
	ρ(N,Γ_n)	-1.00			-1.00			-1.00		
	ρ(N,Γ_γ)	0.84			0.94			0.94		
	$\rho(\Gamma_n,\Gamma_\gamma)$	-0.85	-0.84	-0.86	-0.94	-0.97	-0.99	-0.96	-0.99	-1.00
0.1 %	u_N/N	0.019			0.002			0.001		
	u_{Γ_n}/Γ_n	0.022	0.021	0.023	0.003	0.026	0.029	0.001	0.039	0.040
	$u_{\Gamma_\gamma}/\Gamma_\gamma$	0.0030	0.0027	0.0028	0.001	0.009	0.011	0.001	0.021	0.026
	ρ(N,Γ_n)	-1.00			-1.00			-1.00		
	ρ(N,Γ_γ)	1.00			0.97			0.96		
	$\rho(\Gamma_n,\Gamma_\gamma)$	-1.00	-1.00	-1.00	-0.97	-1.00	-1.00	-0.97	-1.00	-1.00

results in Table III and Ref. [70] demonstrate that the models used for the calculation of the theoretical yield still show some limitations. Since uncertainty propagation based on CUP (methods A and B) supposes that the experimental data are perfectly described by the model, both methods will always produce optimistic covariances. On the other hand, the uncertainties derived by model C and D do not profit from the additional information on the normalization that can be deduced from the experimental data in this exercise. Consequently, for this example methods C and D will produce rather conservative uncertainties. Another striking effect is that for all the conditions considered in Table V, the uncertainty on Γ_γ is always smaller that the one on Γ_n. Since Γ_γ is derived from the observed shape of the resonance, such low uncertainties can only be trusted when all additional broadening effects are well described in the model. The strong impact of *e.g.* sample inhomogeneities on the observed profile is illustrated in Fig. 25. Hence, it requires a careful analysis of the quality of the fit.

To study the effect of an analysis of TOF cross section data combined with cross section data in the thermal energy region, capture yields were generated supposing that the capture cross section was the sum of the contribution of the 4.9 eV s-wave resonance and an additional contribution from a 1/v component. This 1/v component contributed 7.5% to $\sigma(n_{th},\gamma) = 98.7$ b at $E_n = 0.0253$ eV. The experimental data base consisted of a very accurate $\sigma(n_{th},\gamma) = 98.7 \pm 0.1$ b measured at 0.0253 eV and experimental yield of 200 data points from 100 meV to 10 eV with a 1% or 0.1% counting statistics uncertainty at the peak and a 2% normalization uncertainty. Two different yields were studied together with the data at 0.0253 eV, one for an extreme thin target, with a yield directly proportional to the capture cross section, and one for a sample with an area density of $n = 4 \times 10^{-5}$ at/b only accounting for the self-shielding and neglecting multiple interaction events. The relative uncertainties of the capture cross section, derived from the covariance matrices of the parameters, are plotted as a function of energy in Fig. 27. Results are given for an analysis of the yield with and without thermal point (TP) ($\sigma(n_{th},\gamma) = 98.7 \pm 0.1$ b). The results without thermal point, confirm the results of the previous exercise. For an extreme thin sample the uncertainties of $\sigma(n,\gamma)$ are practically identical for methods B, C and D and the normalization uncertainty u_N always fully propagates to the uncertainty of σ(n,γ). In case the resonance parameters are derived from a capture yield that is sensitive to self-shielding (sample thickness 0.01 mm), the normalization uncertainty u_N only fully propagates to the uncertainty of σ(n,γ) for method C and D. Once the thermal data is taken into account, the results are completely different. The uncertainties derived with the three methods are very similar and practically independent of sample thickness. The uncertainty on σ(n,γ) is strongly influenced by the 0.1% uncertainty of the thermal cross section. The effect of the thermal cross section evidently depends on the relative contribution of the s-wave resonance to the cross section at 0.0253 eV. This direct propagation of the uncertainty of the thermal cross section to the final result, which is reflected by a strong reduction in u_N as deduced

Author's personal copy

from method B, strongly relies on the reaction model that has been imposed. In case the additional contribution is not due to a 1/v contribution but due to a bound state (or negative resonance), the results are completely different as shown in Fig. 28. The results in Fig. 28 have been derived from a self-shielded yield Y_{exp} (with a 0.1% peak uncertainty) combined with $\sigma(n_{th},\gamma) = 98.7 \pm 0.1$ b. In the analysis only the Γ_γ of the bound state was supposed to be known. A comparison of Fig. 28 with Fig. 27 reveals a complete different behaviour of the uncertainties of the calculated capture cross section. Unfortunately, in most cases the experimental data do not provide enough information to differentiate between a $1/v$ contribution and a contribution due to bound states.

For all the results of method C and D a sequential analysis was applied, that is: first the capture data were analyzed by propagating the counting statistics and normalization by Monte Carlo or marginalization, subsequently $\sigma(n_{th},\gamma) = 98.7 \pm 0.1$ b was used to update the parameters. When the yield and thermal cross section data were analyzed simultaneously the results of marginalization differed significantly from those derived by MC-sampling.

The impact of the characteristics of the resonances was investigated by creating transmission and capture yield TOF data for a 10 m station and 2 resonances: (E_R = 1 eV, Γ_γ = 100 meV, Γ_n = 10 meV) and (E_R = 1 eV, Γ_γ = 10 meV, Γ_n = 100 meV). The sample thickness was adjusted to have a capture yield $Y_{exp} \approx 0.1$ and a transmission $T_{exp} \approx 0.35$. The additional broadening due to the TOF-response and Doppler effect was about 5 and 35 meV, respectively. The capture data were produced with a 1% counting statistics uncertainty in the peak and the transmission data with a 1% uncertainty in the transmission dip. Both T_{exp} and Y_{exp} were calculated for 220 data points symmetrically distributed around the resonance. The covariance matrix of the parameters were derived by propagating an additional correlated uncertainty of 0.25% on the area density, 2% due to the normalization of the capture data, 0.5% due to the normalization of the transmission data, 5 K on the sample temperature and 20% on the parameter ΔL determining the width of the TOF response function. The results are summarized in Table VI. The results from an analysis with method B show that only the uncertainty of the normalization of the transmission data improved. Since the capture data result from a thin sample, the normalization uncertainty on Y_{exp} propagates on the smallest width, when this parameter is deduced from the capture data. There is almost no increase in uncertainty due to the other experimental parameters, *e.g.* normalization on transmission data, T_{eff}, ΔL and n. The relative uncertainties of the resonance parameters determined from the width of the observed profiles are always very small. In case of capture data they are even comparable with the uncertainty of a Γ_n determined from transmission data, which are supposed to be more accurate. Even for the resonance (E_R = 1eV, Γ_γ = 10 meV, Γ_n = 100 meV) the uncertainty of Γ_γ when derived from the width of the transmission data is $\leq$ 4.5%, in case of CUP and MC-sampling. The correlation coefficients between the resonance parameters are completely related to the way how they have been derived from the experimental data. This is illustrated in Fig.29, which shows the correlation coefficient for the resonance (E_R = 1eV, Γ_γ = 100 meV, Γ_n = 10 meV) as a function of T_{exp}. They were derived from transmission data obtained with samples with different thicknesses.

2. *Experimental data*

In this section the full process starting from counting histograms to the production of resonance parameters is illustrated. The experimental yield of the 4.9 eV, 58.08 eV and 60.3 eV resonances is derived from capture measurements on a 0.01 mm thick metal ^{197}Au disc carried out at a 12.5 m station of GELINA using C_6D_6, as described in section VII C 3. The data reduction has been performed using the AGS package [23, 213], which is discussed in section IX A. The correlation matrix of the experimental yield close to the single resonance at 4.9 eV and the doublet at 58.08 eV and 60.3 eV are given in Fig. 30. For representation purposes they are given as function of neutron energy. For the translation of TOF into energy an average flight path length independent of energy was supposed. This figure illustrates how a more pronounced positive correlation is introduced by subsequently taking into account the uncertainties of dead time, background and normalization. A RSA was performed with REFIT to deduce the resonance parameters (Γ_γ, Γ_n) together with their covariance matrices. The resonance energies E_R were not adjusted. The propagation of the correlated uncertainty components due to dead time, background and normalization was done by CUP, MC-sampling and marginalization. The results are given in Table VII. In this table the covariance matrix when only the uncorrelated uncertainties are propagated are also given. The results obtained by MC-sampling and marginalization are similar. However, differences between correlation coefficients are observed. They produce more conservative covariances compared to those derived by CUP. This is predominately due to a reduction in uncertainty on the normalization when CUP is applied. This was confirmed by repeating the exercise only considering the correlated component due to the normalization.

C. Unresolved Resonance Region

In Ref. [14, 214] an evaluation for neutron induced reactions of ^{232}Th in the URR is presented. The independent parameters describing the average total and capture cross sections were: a scattering radius R' independent of ℓ, neutron strength functions $S_{\ell=0,1,2}$ and capture transmission coefficients $T_{\gamma,0}^{1/2+}$ and $T_{\gamma,0}^{1/2-}$ at zero energies for s- and p-waves, respectively. Those for d-waves were deduced from the transmission coefficient for s-waves and

Author's personal copy

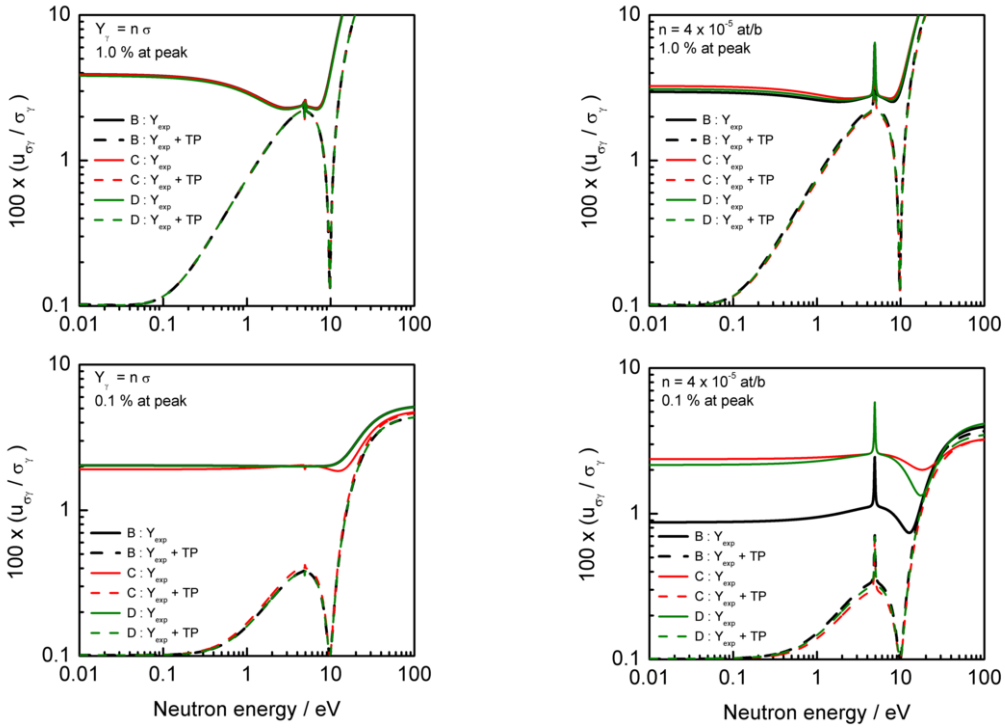

FIG. 27. The relative uncertainty of the capture cross section obtained from parameters which were derived from different experimental data sets. The data base consisted of experimental yields and an accurate capture cross section at 0.0253 eV (TP). The cross section was supposed to be the sum of a contribution of a s-wave resonance at 4.9 eV and a $1/v$-contribution.

TABLE VI. Covariance data for a 1 eV resonance with ($\Gamma_\gamma = 10$ meV, $\Gamma_n = 100$ meV) and ($\Gamma_\gamma = 100$ meV, $\Gamma_n = 10$ meV) derived from capture and transmission experiments. The results when only counting statistics are taken into account (1) are compared with results when other experimental effects are included based on CUP (2) and MC-sampling (3). See text for more details.

		Y_{exp}			T_{exp}		
		(1)	(2)	(3)	(1)	(2)	(3)
$\Gamma_\gamma = 100$ meV	$100 \times u_{\Gamma_\gamma}/\Gamma_\gamma$	0.2	0.3	0.4	0.3	0.4	1.7
$\Gamma_n = 10$ meV	$100 \times u_{\Gamma_n}/\Gamma_n$	0.1	2.2	2.3	0.2	0.4	1.6
	$\rho(\Gamma_n, \Gamma_\gamma)$	−0.02	−0.67	−0.74	0.51	0.58	0.97
	100 x u_N/N		2.0			0.1	
	100 x $u_{\Delta L}/\Delta L$		19.4			19.5	
$\Gamma_\gamma = 10$ meV	$100 \times u_{\Gamma_\gamma}/\Gamma_\gamma$	0.3	2.6	2.5	2.5	3.8	4.3
$\Gamma_n = 100$ meV	$100 \times u_{\Gamma_n}/\Gamma_n$	0.3	0.6	0.4	0.2	0.4	1.6
	$\rho(\Gamma_n, \Gamma_\gamma)$	−0.79	−0.92	−0.86	0.00	−0.29	0.48
	100 x u_N/N		1.6			0.1	
	100 x $u_{\Delta L}/\Delta L$		19.4			19.5	

their J dependence was determined from the level density. To comply with ENDF-6 format [215] restriction at that time, the scattering radius was not included as an adjustable parameter and a covariance matrix for $S_{\ell=0,1,2}$, $T_{\gamma,0}^{1/2+}$ and $T_{\gamma,0}^{1/2-}$ was derived by applying method A. Consequently, an informative prior of $u_{R'} = 0$ was supposed. This restriction could be partly released in the future development of the format [215]. Therefore, the covariance matrix was reanalysed with method B and D for two different priors, $u_{R'}/R' = 0\%$ and 100%, using the same experimental data base as in [14, 214], *i.e.* with $u_{N_{tot}}/N_{tot} = 1.0\%$ and $u_{N_\gamma}/N_\gamma = 1.5\%$ as normalization uncertainties on $\sigma(n, tot)$ and $\sigma(n, \gamma)$, respectively. These uncertainties resulted from a review of experimental data reported in the literature [14]. The uncertainty on the capture data resulted mainly from the measurements of

Author's personal copy

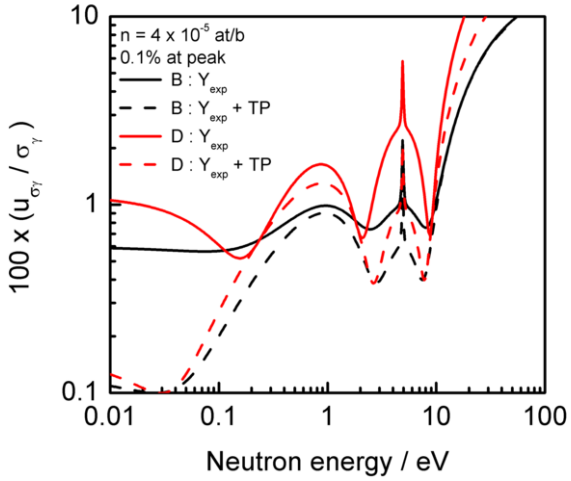

FIG. 28. The relative uncertainty of the capture cross section obtained from parameters which were obtained from an analysis of a capture yield with and without an accurate capture cross section at 0.0253 eV (TP). The cross section was supposed to be a sum of a contribution of a 4.9 eV s-wave resonance and a bound state.

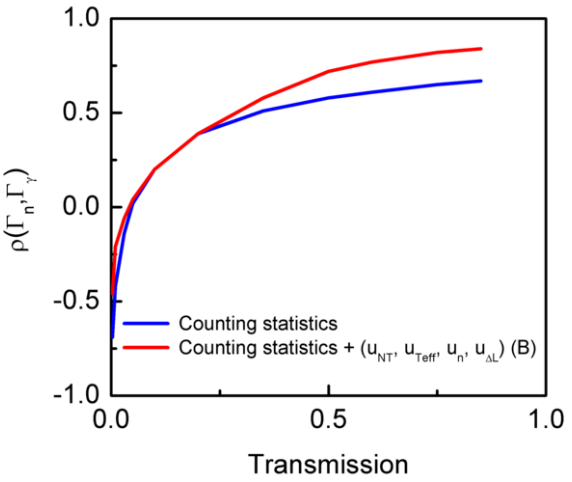

FIG. 29. The correlation coefficient $\rho(\Gamma_n, \Gamma_\gamma)$ as a function of transmission. The coefficient is given for an analysis accounting only for counting statistics and for additional uncertainties due to normalization N_T, temperature T_{eff}, resolution broadening ΔL and area density n, obtained by CUP.

Borella et al. [106].

For the analysis with $u_{R'} = 0$ as prior, the same covariance matrix as in Ref. [14, 214] was derived by using method B, however, with an additional information on $u_{N_{tot}}$ and u_{N_γ}. These uncertainties reduced to 0.58% and 1.48% for $\sigma(n, tot)$ and $\sigma(n, \gamma)$, respectively. The covariance matrix with $u_{R'}/R' = 100\%$ as prior is given in Table VIII. The results of method D based on a sequential

TABLE VII. Fitted ^{197}Au resonance parameters ($E_R^{(1)} = 4.9$ eV, $E_R^{(2)} = 58.08$ eV, $E_R^{(3)} = 60.3$ eV). The uncertainties and correlation matrix were obtained accounting only for counting statistics and including background and normalization uncertainties by CUP, MC-sampling and marginalization.

		$100\times$	$\rho(\theta,\theta')\times 100$					
θ	meV	(u_θ/θ)	$\Gamma_\gamma^{(1)}$	$\Gamma_n^{(1)}$	$\Gamma_\gamma^{(2)}$	$\Gamma_n^{(2)}$	$\Gamma_\gamma^{(3)}$	$\Gamma_n^{(3)}$
Only counting statistics								
$\Gamma_\gamma^{(1)}$	122.3	0.2	100	-77.3	0.0	0.0	-0.1	0.1
$\Gamma_n^{(1)}$	15.27	0.1		100	0.1	0.1	-0.6	0.6
$\Gamma_\gamma^{(2)}$	124.5	5.6			100	57.4	-13.0	12.5
$\Gamma_n^{(2)}$	4.61	1.0				100	-14.8	14.2
$\Gamma_\gamma^{(3)}$	99.36	6.0					100	-99.8
$\Gamma_n^{(3)}$	78.63	5.7						100
CUP								
$\Gamma_\gamma^{(1)}$	122.3	0.5	100	-94.7	3.8	-27.7	-7.1	-3.6
$\Gamma_n^{(1)}$	15.27	0.7		100	-3.3	30.6	7.9	3.7
$\Gamma_\gamma^{(2)}$	124.5	5.9			100	58.3	-8.0	7.8
$\Gamma_n^{(2)}$	4.61	1.2				100	-5.1	9.0
$\Gamma_\gamma^{(3)}$	99.36	6.1					100	-99.1
$\Gamma_n^{(3)}$	78.63	5.7						100
MC-sampling								
$\Gamma_\gamma^{(1)}$	122.4	2.8	100	-70.6	60.4	22.6	58.9	-68.6
$\Gamma_n^{(1)}$	15.27	3.8		100	6.1	35.1	-15.0	52.2
$\Gamma_\gamma^{(2)}$	125.0	25.4			100	64.5	60.9	-38.3
$\Gamma_n^{(2)}$	4.6	7.5				100	38.3	-7.4
$\Gamma_\gamma^{(3)}$	101.9	8.9					100	-88.4
$\Gamma_n^{(3)}$	79.0	7.7						100
Marginalization								
$\Gamma_\gamma^{(1)}$	122.3	2.7	100	-92.1	46.2	8.4	-47.3	-18.8
$\Gamma_n^{(1)}$	15.27	3.9		100	-10.0	29.6	58.8	11.3
$\Gamma_\gamma^{(2)}$	124.5	26.3			100	90.5	10.4	-20.8
$\Gamma_n^{(2)}$	4.61	6.2				100	33.4	-15.9
$\Gamma_\gamma^{(3)}$	99.36	7.7					100	-73.5
$\Gamma_n^{(3)}$	78.63	5.9						100

analysis were very similar. However, when the normalization uncertainty on both the total and capture cross section were propagated simultaneously by marginalization, a very particular covariance matrix was derived especially when $u_{R'}/R' = 0\%$ was used as a prior. This covariance matrix resulted in unrealistic high uncertainties for the calculated capture cross section. This observation together with the observation made on marginalization in the RRR are not understood. Hence, it calls for a further investigation of the marginalization procedure before its implementation for routine evaluation procedures.

When R' is also adjusted with a prior $u_{R'}/R' = 100\%$, the uncertainty on the calculated capture cross section increases slightly compared to the results of Ref. [14, 214]. However, the uncertainty on the total cross section in-

Author's personal copy

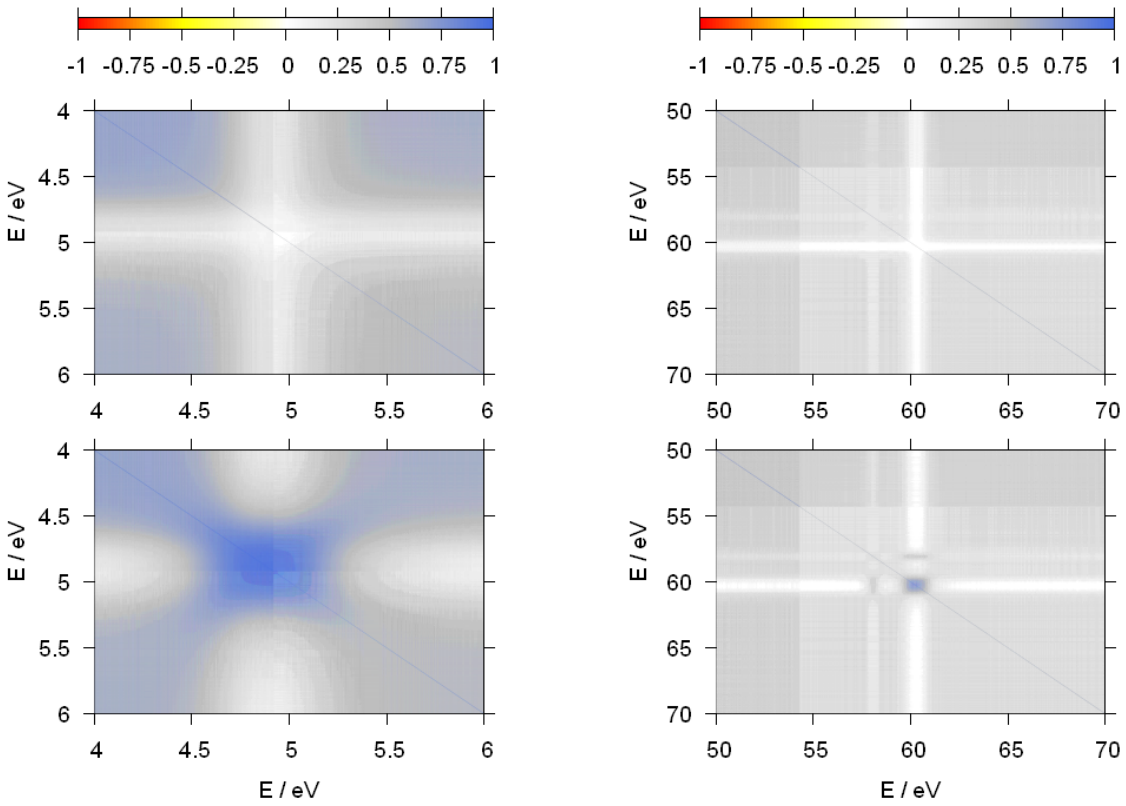

FIG. 30. The covariance matrix of the experimental yield resulting from capture measurements on a 1 mm thick Au sample at GELINA [198]. The covariance when only the dead time and background components are taken into account (up) is compared with the total covariance matrix (down), which includes the uncertainty of the normalization factor.

TABLE VIII. Normalization factors and average resonance parameters, together with their relative uncertainties u_θ and correlation matrix $\rho(\theta,\theta')$, derived from an analysis of total and capture cross section data for ^{232}Th in the URR [14].

			$\rho(\theta,\theta') \times 100$							
θ		$100 \times (u_\theta/\theta)$	N_T	N_c	R'	S_0	S_1	S_2	$T_{\gamma,0}^{1/2+}$	$T_{\gamma,0}^{1/2-}$
N_T	1	0.98	100	2.6	-81.0	-31.3	-19.0	-18.4	15.4	13.5
N_γ	1	1.48		100	8.7	-15.5	-22.5	6.6	-52.9	-49.8
R	9.8 fm	0.71			100	-27.7	-39.9	-30.1	25.1	22.3
S_0	0.878 10^{-4}	2.05				100	87.2	74.7	-62.4	-55.2
S_1	1.90 10^{-4}	4.25					100	75.5	-65.5	-54.6
S_2	1.27 10^{-4}	20.4						100	-59.4	-86.2
$T_{\gamma,0}^{1/2+}$	8.51 10^{-3}	4.18							100	69.5
$T_{\gamma,0}^{1/2-}$	8.18 10^{-3}	3.66								100

creases by more than 30%. This increase coincides with a difference in $u_{N_{tot}}$. When R' is not adjusted, and $u_{R'}$= 0% is supposed, this prior information is transferred in the fit to the normalization factor N_{tot} and results in a reduced uncertainty of the total cross section. In the analysis with R' as adjustable parameter, the sensitivity of the data to the scattering radius is not used to improve the knowledge of the normalization factor but to improve the scattering radius, which makes more sense. These results again confirm the strength and usefulness of method B to get an insight in the information that is provided by the experimental data.

Author's personal copy

IX. REPORTING AND DOCUMENTING TOF-CROSS SECTION DATA

The previous sections demonstrate that reporting the full experimental details is of primary importance to produce unbiased model parameters in the resonance region together with reliable covariance information. In particular reporting of the experimental reaction yields and transmissions needs to be supplemented with a full description of the experimental conditions and involved uncertainties. This can be accomplished by using the AGS (Analysis of Geel Spectra) concept and format which has been developed at the EC-JRC-IRMM for the data treatment of results of TOF measurements [23, 213].

A. Uncertainty Propagation Using the AGS-system

The basic concept of AGS relies on the idea of a separate bookkeeping of correlated and uncorrelated uncertainties throughout the data reduction process. A detailed description of the concept is given in Ref. [23].

Consider a spectrum $\vec{Z}$ that is deduced from p counting spectra $(\vec{Y}_1, \ldots, \vec{Y}_p)$ and the parameter vector $\vec{b}$ through the functional relationship $\vec{Z} = f(\vec{Y}_1, \ldots, \vec{Y}_p, \vec{b})$. Each of the spectra has a dimension n. The dimension of the parameter vector is m. Taking into account the specific property of counting spectra and supposing that the relationship f only involves channel-to-channel operations, the covariance matrix of $\vec{Z}$ can always be split into an uncorrelated and correlated component

$$\mathbf{V}_{\vec{Z}} = \underbrace{\sum_{j=1}^{p} \mathbf{D}_f(\vec{Y}_j)\mathbf{U}_{\vec{Y}_j}\mathbf{D}_f^T(\vec{Y}_j)}_{\text{uncorrelated}} + \underbrace{\mathbf{D}_f(\vec{b})\mathbf{V}_{\vec{b}}\mathbf{D}_f^T(\vec{b})}_{\text{correlated}}, \tag{37}$$

where $\mathbf{D}_f(\vec{b})$ is the sensitivity matrix of the operation f with respect to the parameter vector $\vec{b}$. The first term of Eq. (37) is a diagonal matrix containing solely the uncorrelated component of the covariance matrix of $\vec{Z}$ and can be denoted by $\mathbf{U}_{\vec{Z}}$. The second term contains the correlated uncertainty component stemming from the parameter covariance matrix $\mathbf{V}_{\vec{b}}$. Application of the Cholesky transformation on the covariance matrix $\mathbf{V}_{\vec{b}} = \mathbf{L}_{\vec{b}}\mathbf{L}_{\vec{b}}^T$ results in [23, 213]

$$\mathbf{V}_{\vec{Z}} = \mathbf{U}_{\vec{Z}} + \mathbf{D}_f(\vec{b})\mathbf{L}_{\vec{b}}\mathbf{L}_{\vec{b}}^T\mathbf{D}_f^T(\vec{b}). \tag{38}$$

By defining the $\mathbf{S}_Z$ matrix of $\vec{b}$ as $\mathbf{S}_Z = \mathbf{D}_f(\vec{b})\mathbf{L}_{\vec{b}}$, Eq. (38) can be replaced by

$$\mathbf{V}_{\vec{Z}} = \mathbf{U}_{\vec{Z}} + \mathbf{S}_Z\mathbf{S}_Z^T \tag{39}$$

Eq. (39) reveals that the full covariance information of $\vec{Z}$ can be contained in a vector $\vec{U}_{\vec{Z}}$ with length n and a matrix $\mathbf{S}_{\vec{Z}}$ of dimension (n x m). The former is the sum of all uncorrelated uncertainty components, while the latter represents the contribution of each component resulting in a correlated contribution [23, 213]. Subsequent channel-to-channel operations maintain fully the same format of Eq. (39) as demonstrated in [23].

This covariance representation results in a substantial reduction of storage space when the dimension n of the spectra is much larger than the total number m of correlated uncertainty components compared to the classical covariance matrix representation. The procedure also ensures that the covariance matrix is always well defined, *i.e.* symmetric and positive definite. The correlated and uncorrelated uncertainties are well separated, such that the impact of each part of the data reduction process resulting in a correlated uncertainty can be verified. In addition, AGS offers a convenient data structure [23] to include the correlated uncertainty components in the uncertainty propagation via the Monte Carlo scheme of Ref. [210] or the marginalization procedure of Ref. [211].

B. Reporting TOF-data in EXFOR

The EXFOR library was originally developed for low-energy neutron induced reaction data. The compilation of transmissions and capture yields for the library has been recognized as an important task of the International Network of Nuclear Reaction Data Centres (NRDC) since the NRDC 1978 Meeting [216]. In Ref. [217], the following recommendation was given :

"Data Centres should be ready to accept and exchange transmission and capture yield data. Experimentalists should be encouraged to send capture yield data as well as corrected cross sections to the Data Centres. Such data would then be available for re-analysis when improvements in analysis techniques are made."

A technical problem at that time was huge numbers of data points. For example, data tapes of neutron capture yields of chromium and iron isotopes measured at ORELA [218–221] and received at the IAEA Nuclear Data Section (NDS) contained about 2 million data lines which is more than the entire neutron EXFOR library at the end of 1977. The solution adopted by NRDC was to assign an EXFOR subentry number to each data set but store the data in a separated magnetic tape. This was a solution originally adopted for neutron transmissions of ytterbium isotopes measured at Columbia University Nevis synchrocyclotron and received at NNCSC (now NNDC). [222] The Yb transmission data stored in CSISRS-A tape were moved to a regular EXFOR entry in 1999, and they are still available. However, Cr and Fe capture yields received at the IAEA NDS and stored in a special data tape (EXFOR SUPPL NDS 001) are no longer available. Except for such exceptional cases, NRDC has usually compiled in EXFOR only resonance parameters published in articles and not transmissions and capture yields. Nowadays, inclusion of such volu-

Author's personal copy

minous data tables to a normal EXFOR entry is not a problem if the number of data line is less than 100 k. A capture measurement on ^{60}Ni [138] shows how useful a storage of transmission data is for normalization of experimental capture yields.

The NRDC 1978 Meeting also discussed another recommendation from Ref. [217]:

"A realistic assessment of the error in data is becoming increasingly important to evaluators. The errors quoted should be separated into correlated and uncorrelated components and accompanied by a descriptive statement on the nature of the correlations. This should not be taken as a request for a complete covariance matrix on all the quantities measured but more simply for a realistic statement on the salient features of correlations in the quoted errors."

This recommendation can be fulfilled if the data are compiled based on the AGS-concept (Eq. (39)).The EC-JRC-IRMM and IAEA NDS proposed compilation of TOF spectra and their covariance information with additionally submitted experimental information (*e.g.* response of TOF spectrometer, flight path length, detector and sample characteristics) in the "EXFOR template for TOF-spectra and covariance" for the EXFOR library [223]. The proposed format was approved in the NRDC 2011 Meeting [224], and two data sets of natural cadmium neutron transmission measured at GELINA [76] were compiled based on the approved coding rule. This EXFOR data set (EXFOR 23077.002) provides 25288 data points of neutron transmission at the incident neutron energy between 0.02 eV and 4.8 eV. Following the recommendation of Ref. [223], the experimental data are given as function of TOF boundaries and all experimental details to perform a resonance shape analysis are included.

X. SUMMARY AND CONCLUSIONS

The basic principles of transmission and reaction cross section measurements have been discussed. Components which have a significant contribution to the final covariance of the experimental observable, *i.e.* transmission and reaction yield, were identified and their uncertainties quantified. In case the fission channel can be neglected capture cross section data with an uncertainty of better than 2% can be produced. To reach such a low uncertainty special procedures are required to control and quantify the impact of systematic effects, in particular the normalization factor and different background components. In case of neutron induced charged particle reactions, including fission, similar uncertainties can be obtained. For total cross section measurements the uncertainty on the transmission can be reduced to 0.5%.

To deduce cross sections from the experimental data nuclear model parameters have to be determined by fitting experimental data. The theoretical model used in the fit includes the nuclear reaction formalism, *i.e.* R-matrix formalism in the resonance region, and models to describe various experimental effects in addition to background and normalization. To assess the resulting parameters together with their covariance a series of synthetic and experimental cases were investigated. The results illustrate that the covariance matrix of the model parameters is completely dependent on: the experimental conditions; the quality of the theoretical model describing the experimental data; the resonance structure and the method that is used to propagate the uncertainties.

A comparison of different methods applied to propagate the uncertainties has shown that a Monte Carlo scheme coupled to a least squares adjustment produces in general more conservative uncertainties compared to conventional uncertainty propagation (CUP). On the other hand CUP provides an additional insight in the information provided by the data. However, it relies completely on a perfect description of the experimental data by the model. Hence, a verification of the quality of the fit is always required. Since results obtained by the marginalization procedure are not completely understood, this procedure needs some further studies.

The data presented in this work also reveal the pronounced difference between uncertainties of parameters which are deduced from the area and of those deduced from the shape of the observed profile. The reliability of relatively low uncertainties for parameters which are deduced predominantly from the width of the observed profile has still to be investigated in more detail.

The examples given in this work show that propagating experimental uncertainties to derive reliable covariances for resonance parameters is a complex process. They can only be obtained if all the experimental conditions reflecting the production of the data are included in the analysis and the reliability of the model used in the adjustment process is verified. This requires that in the EXFOR library results of cross section measurements are reported with all the experimental details required to perform a proper covariance propagation. This can be accomplished by using the AGS format and concept.

ACKNOWLEDGMENTS

Our special thanks to all colleagues and students who have contributed to the data that was used in this paper and to K. Kauwenberghs for a careful reading of the manuscript. We are also grateful to the Nuclear Data Section of the IAEA and the Nuclear Energy Agency of the OECD for their interest and support and to D. Smith, M. Herman and P. Obložinský who initiated this work. This work was partly supported by the European Commission through the projects EFNUDAT (FP6-036434) and ERINDA (FP7-269499). One of the authors (A.R.J) acknowledges the support from the German Federal Ministry for Education and Research (02NUK13A). ORNL is managed by UT-Battelle, LLC, for the U.S. Department

Author's personal copy

of Energy under Contract No. DE-AC05-00OR22725. We also acknowledge the work of the anonymous referees for their valuable comments and suggestions which improved the original manuscript.

[1] F.H. Fröhner, "Evaluation and analysis of nuclear resonance data", JEFF Report 18, NEA/OECD (2000).
[2] E.P. Wigner, L. Eisenbud, "Higher angular momenta and long range interaction in resonance reactions", Phys. Rev. **72**, 29 – 41 (1947).
[3] A.M. Lane, R.G. Thomas,"R-matrix theory of nuclear reactions", Rev. Mod. Phys. **30**, 257 – 353 (1958).
[4] G.M. Hale, "Use of R-matrix methods in light element evaluations", Proc. Conf. on Nuclear Data Evaluation Methods and Procedures, 22 – 25 September 1980, New York, USA, Brookhaven National Laboratory BNL - NCS - 51363, Vol. 2, pp. 509 – 531 (1981).
[5] Z.P. Chen, Y.Y. Sun, R. Zhang and T.J. Liu, "Covariance propagation in R-matrix model fitting", High Energy Phys. And Nucl. Phys. **28**, 42 – 47 (2004).
[6] M.C. Moxon and J.B. Brisland, "GEEL REFIT, A least squares fitting program for resonance analysis of neutron transmission and capture data computer code", AEA-InTec-0630, AEA Technology, October (1991).
[7] N.M. Larson, "Updated users guide for SAMMY: Multilevel R-matrix fits to neutron data using Bayes' equations, Report ORNL/TM-9179/R8 and ENDF-364/R2, Oak Ridge National Laboratory, USA, (2008).
[8] L. Dresner, Proc. Int. Conf. on Neutron Reactions with the Nucleus , Columbia U. 1957, Report CU-157, p. 71 (1957).
[9] P. A. Moldauer, "Statistics and the Average Cross Sections", Nucl. Phys. A**344**, 185 – 195 (1980).
[10] H.M. Hofmann, J. Richert, J.W.Tepel, and W.A. Weidenmüller, "Direct reactions and Hauser-Feshbach theory", Annals of Physics, **90**, 403 – 435 (1975).
[11] F.H. Fröhner, SESH Computer Code, GA-8380, Gulf. General Atomic (1968).
[12] R. Capote, M. Herman, P. Obložinský, P. G. Young, S. Goriely, T. Belgya, A.V. Ignatyuk, A.J. Koning, S. Hilaire, V. A. Plujko, M. Avrigeanu, O. Bersillon, M. B. Chadwick, T. Fukahori, Zhigang Ge, Yinlu Han, S. Kailas, J. Kopecky, V. M. Maslov, G. Reffo, M. Sin, E. Sh. Soukhovistskii, and P. Talou, "RIPL reference input parameter library for calculation of nuclear reactions and nuclear data evaluations", Nucl. Data Sheets, **110**, 3107 – 3214 (2009).
[13] E.Sh. Soukhovitskii, R. Capote, J.M. Quesada, S. Chiba, "Dispersive coupled-channel analysis of nucleon scattering for ^{232}Th up to 200 MeV", Phys. Rev. C **72**, 024604 – 12 (2005).
[14] I. Sirakov, R. Capote, F. Gunsing, P. Schillebeeckx and A. Trkov, "An ENDF-6 compatible evaluation for neutron induced reactions of ^{232}Th in the unresolved resonance region", Ann. Nucl. En. **35**, 1223 – 1231 (2008).
[15] F. H. Fröhner, "Evaluation of the unresolved resonance range of ^{238}U", Nucl. Sci. Eng. **103**, 119 – 128 (1989)
[16] Z. Zhao, F. G. Perey, "The covariance matrix of derived quantities and their combination", ORNL/TM-12106, Oak Ridge National Laboratory (1992).
[17] G. D'Agostini, "On the use of the covariance matrix to fit correlated data", Nucl. Inst. Meth. **A346**, 306 (1994).
[18] S. Chiba and D. L. Smith, "Impacts of data transformations on least-squares solutions and their significance in data analysis and evaluation", J. Nucl. Sci. Tech. **31** , 770 – 781 (1994).
[19] F. H. Fröhner,"Assignment of uncertainties to scientific data", Nucl. Sci. Eng. **126**, 1 – 18 (1997).
[20] K. M. Hanson, T. Kawano, and P. Talou, "Probabilistic interpretation of Peelle's pertinent puzzle and its resolution", in proceedings of Int. Conf. Nuclear Data for Science and Technology, 26 Sep.–1 Oct., 2004, Santa Fe, NM, USA, AIP Conf. Proc. 769, pp. 304 – 307 (2004).
[21] A.D. Carlson, V.G. Pronyaev, D.L. Smith, N.M. Larson, Z. Chen, G.M. Hale, F.-J. Hambsch, E.V. Gai, Soo-Youl Oh, S.A. Badikov, T. Kawano, H.M. Hofman, H. Vonach, and S. Tagesen, "International evaluation of neutron cross section standards", Nuclear Data Sheets **110**, 3215 – 3324 (2009).
[22] D. Neudecker, R. Frühwirth, H. Leeb, "Peelle's Pertinent Puzzle: a fake due to improper analysis", Nucl. Sci. Eng. **170**, 54 – 60 (2012).
[23] B. Becker, C. Bastian, F. Emiliani, F. Gunsing, J. Heyse, K. Kauwenberghs, S. Kopecky, C. Lampoudis, C. Massimi, N. Otuka, P. Schillebeeckx, and I. Sirakov, "Data reduction and uncertainty propagation of time-of-flight spectra with AGS", accepted for publication in JINST (2012).
[24] Joint Committee for Guides in Metrology (JCGM/WG 1), "Evaluation of measurement data - guide to the expression of uncertainty in measurement, JCGM 100:2008", (2008).
[25] D. L. Smith and N. Otuka, "Experimental nuclear reaction data uncertainties: basic concepts and documentation", Nuclear Data Sheets **113**, 3006-3053 (2012).
[26] J.A. Harvey, "Experimental neutron resonance spectroscopy", Academic Press, New York and London, Ed. J. A. Harvey, (1970).
[27] F. G. P. Seidl, D.J. Hughes, H. Palevsky, J. S. Levin, W. Y. Kato and N. G. Sjöstrand, "Fast chopper time-of-flight measurement of neutron resonances", Phys. Rev. **95**, 476 – 499 (1954).
[28] F.W. K. Firk, "Neutron time-of-flight spectrometers", Nucl. Instr. Meth. **162**, 539 – 563 (1979).
[29] S. F. Mughabghab, "Atlas of neutron resonances: resonance parameters and thermal cross sections", Elsevier, Amsterdam (2006).
[30] L. Koester, H. Rauch and E. Seymann, "Neutron scattering lengths: A survey of experimental data and methods", At. Nucl. Data Tables **49**, 65 – 120 (1991).
[31] http://www.ncnr.nist.gov/resources/n-lengths/ (as on Aug. 2012).
[32] N.E. Holden and K.A. Holden, "Re-examination of 2200 meter/second cross section experiments for Neutron Capture and Fission Standards", Pure & Appl. Chem, **61**, 1505 – 1510 (1989).
[33] W. Dilg, W. Mannhart, E. Steichele and P. Arnold, "Precision neutron total cross section measurements on gold and cobalt in the 40 μeV - 5 meV range", Z. Phys.

Author's personal copy

264, 427 – 444 (1973).
[34] K.H. Böckhoff, A. D. Carlson, O. A. Wasson, J. A. Harvey and D. C. Larson,"Electron linear accelerators for fast neutron data measurements in support of fusion energy applications", Nucl. Sci. Eng. **106**, 192 – 207 (1990).
[35] J. Klug, E. Altstadt, C. Beckert, R. Beyer, D. Freiesleben, V. Galindo, E. Grosse, A.R. Junghans, D. Legrady, B. Naumann, K. Noack, G. Rusev, K.D. Schilling, R. Schlenk, R. Schneider, A. Wagner, and F.-P. Weiss, "Development of a neutron time-of-flight source at the ELBE accelerator", Nucl. Inst. Meth. A **577**, 641 – 653 (2007).
[36] P.E. Koehler, "Comparison of white neutron sources for nuclear astrophysics experiments using very small samples", Nucl. Inst. Meth. A **460**, 352 – 361 (2001).
[37] W. Mondelaers and P. Schillebeeckx, "GELINA, a neutron time-of-flight facility for neutron data measurements", Notizario **11**, 19 – 25 (2006).
[38] K. Kobayashi, S. Lee, S. Yamamoto and T. Kawano, "Neutron capture cross-section measurement of ^{99}Tc by linac time-of-flight and the resonance analysis", Nucl. Sci. Eng. **146**, 209 – 220 (2004).
[39] T.F. Wang, A.K.M.M.H. Meaze, M.U. Khandaker, M.S. Rahman, G.N. Kim, L.P. Zhu, H.H. Xia, Z.Y. Zhou, Y.D. Oh, H. Kang, M.H. Cho, I.S. Ko, and W. Namkung, "Measurement of the total neutron cross-section and resonance parameters of molybdenum using pulsed neutrons generated by an electron linac", Nucl. Instr. Meth. B **266**, 561 – 569 (2008).
[40] M.E. Overberg, B. E. Moretti, R.E. Slovacek, R.C. Block, "Photoneutron target development for the RPI linear accelerator", Nucl. Instr. Meth. A **438**, 253 – 264 (1999).
[41] K. Kino, M. Furusaka, F. Hiraga, T. Kamiyama, Y. Kiyanagi, K. Furutaka, S. Goko, H. Harada, M. Harada, T. Kai, A. Kimura, T. Kin, F. Kitatani, M. Koizumi, F. Maekawa, S. Meigo, S. Nakamura, M. Ooi, M. Ohta, M. Oshima, Y. Toh, M. Igashira, T. Katabuchi, and M. Mizumoto,"Measurement of energy spectra and spatial distributions of neutron beams provided by the ANNRI beam line for capture cross-section measurements at the J-PARC/MLF", Nucl. Instr. Meth. A **626-627**, 58 – 66 (2011).
[42] A. Kimura, T. Fujii, S. Fukutani, K. Furutaka, S. Goko, K. Y. Hara, H. Harada, K. Hirose, J. Hori, M. Igashira, T. Kamiyama, T. Katabuchi, T. Kin, K. Kino, F. Kitatani, Y. Kiyanagi, M. Koizumi, M. Mizumoto, S. Nakamura, M. Ohta, M. Oshima, K. Takamiya and Y. Toh, "Neutron-capture cross-sections of ^{244}Cm and ^{246}Cm measured with an array of large germanium detectors in the ANNRI at J-PARC/MLF", J. Nucl. Sci. Technol. **49**, 708 – 724 (2012).
[43] P.W. Lisowski, C. D. Bowman, G. J. Russell and S. A. Wender, "The Los Alamos National Laboratory spallation neutron sources", Nucl. Sci. Eng. **106**, 208 – 218 (1990).
[44] P.W. Lisowski and K.F. Schoenberg, "The Los Alamos neutron science center", Nucl. Inst. Meth. A **562**, 910 – 914 (2006).
[45] C. Borcea, P. Cennini, M. Dahlfors, A. Ferrari, G. Garcia-Munoz, P. Haefner, A. Herrera-Martinez, Y. Kadi, V. Lacoste, E. Radermacher, F. Saldana, V. Vlachoudis, L. Zanini, C. Rubbia, S. Buono, V. Dangendorf, R. Nolte, and M. Weierganz, "Results from the commissioning of the n_TOF spallation neutron source at CERN", Nucl. Instr. Meth. A **513**, 524 – 537 (2003).
[46] F. Gunsing et al. (n_TOF Collaboration), "Status and outlook of the neutron time-of-flight facility n_TOF at CERN", Nucl. Inst. Meth. B **261**, 925 – 929 (2007).
[47] K. Wisshak, K. Guber, F. Voss, and F. Käppeler, "Neutron capture in ^{148,150}Sm: A sensitive probe of the s-process neutron density", Phys. Rev. C **48**, 1401 – 1419 (1993).
[48] K. Wisshak, F. Voss, F. Käppeler, "Neutron Capture Cross Section of ^{232}Th", Nucl. Sci. Eng. **137**, 183 – 193 (2001).
[49] T. Ohsaki, Y. Nagai, M. Igashira, T. Shima, T.S. Suzuki, T. Kikuchi, T. Kobayashi, T. Takaoka, M. Kinoshita, Y. Nobuhara, "An NaI(Tl) spectrometer system for keV neutron radiative-capture reaction", Nucl. Instr. Meth. A**425**, 302 – 319 (1999).
[50] S. Mizuno, M. Igashira and K. Masuda, "Measurements of keV-neutron capture cross sections and capture gamma-ray spectra of ^{161,162,163}Dy", J. Nucl. Sci. Technol. **36**, 493 – 507 (1999).
[51] C. Coceva, R. Simonini, and D. K. Olsen, "Calculation of the ORELA neutron moderator spectrum and resolution function", Nucl. Instr. Meth. **211**, 459 – 467 (1983).
[52] D. Ene, C. Borcea, S. Kopecky, W. Mondelaers, A. Negret and A.J.M. Plompen, "Global characterisation of the GELINA facility for high-resolution neutron time-of-flight measurements by Monte Carlo simulations", Nucl. Instr. Meth. A **618**, 54 – 68 (2010).
[53] A. Michaudon, "The production of moderated neutron beams from pulsed accelerators", J. Nucl. En. **17** (part A/B), 165 –186 (1963).
[54] H. J. Groenewold and H. Groendijk, Physica **XIII**, 141 – 152 (1947).
[55] S. Ikeda and J. M. Carpenter,"Wide-energy-range, high-resolution measurements of neutron pulse shapes of polyethylene moderators", Nucl. Instr. Meth. A **239**, 536 – 544 (1985).
[56] P.E. Koehler,"A determination of the energy resolution at LANSCE", Nucl. Instr. Methd. A **350**, 511 – 516 (1994).
[57] C. Coceva, M. Frisoni, M. Magnani and A. Mengoni, "On the figure of merit in neutron time-of-flight measurements", Nucl. Instr. Meth. A **489**, 346 – 356 (2002).
[58] R. Beyer, E. Grosse, K. Heidel, J. Hutsch, A.R. Junghans, J. Klug, D. Légrády, R. Nolte, S. Röttger, M. Sobiella, A. Wagner, "Proton-recoil detectors for time-of-flight measurements of neutrons with kinetic energies from some tens of keV to a few MeV", Nucl. Instr. Methd. A **575**, 449 – 455 (2007).
[59] M.B. Chadwick, M. Herman, P. Obložinský et al., "ENDF/B-VII.1 nuclear data for science and technology: cross sections, covariances, fission product yields and decay data", Nucl. Data Sheets, **112**, 2887 - 2996 (2011).
[60] M.S. Moore, "Rate dependence of counting losses in neutron time-of-flight measurements, Nucl. Inst. Meth. **169**, 245 – 247 (1980).
[61] L.C. Mihailescu, A. Borella, C. Massimi and P. Schillebeeckx, "Investigations for the use of the fast digitizers with C_6D_6 detectors for radiative capture measurements at GELINA", Nucl. Instr. Meth. A **600**, 453 – 459 (2009).

Author's personal copy

[62] C. W. Reich and M. S. Moore, "Multilevel formula for the fission process", Phys. Rev. **111**, 929 – 933 (1958).
[63] H. E. Jackson and J. E. Lynn, "Resonant absorption of neutrons by crystals", Phys. Rev. 127, 461 – 468 (1962).
[64] W. E. Lamb, "Capture of neutrons by atoms in a crystal", Phys. Rev. **55**, 190 – 197 (1939).
[65] M. S. Nelkin, D. E. Parks, "Effects of chemical binding on nuclear recoil", Phys. Rev. **119**, 1060 – 1068 (1960).
[66] G.M. Borgonovi, D.H. Houston, J.U. Koppel, and E.L. Slaggie, "Crystal-binding effects on Doppler broadening of neutron absorption resonances", Phys. Rev. C **1**, 2054 – 2059 (1970).
[67] D. Naberejnev, C. Mounier, and R. Sanchez, "The influence of crystalline binding on resonant absorption", Nuc. Sci. Eng. **131**, 222 – 229 (1999).
[68] J.E. Lynn, W.J. Trela, and K. Meggers, "Neutron Doppler broadening studies of tantalum and tungsten metal", Nucl. Instr. Meth. B **192**, 318 – 330 (2002).
[69] C. Lampoudis, S. Kopecky, A. Plompen, P. Schillebeeckx, P. Siegler, F. Gunsing, C. Sage, O. Bouland, "Transmission and capture measurements for ^{241}Am at GELINA", J. Korean Phys. Soc. **59**, 1785 – 1788 (2011).
[70] P. Schillebeeckx, A. Borella, S. Kopecky, C. Lampoudis, C. Massimi, and M. Moxon, "Neutron resonance spectroscopy at GELINA", J. Korean Phys. Soc. **59**, 1563 – 1568 (2011).
[71] B. Becker, R. Dagan and G. Lohnert, "Proof and implementation of the stochastic formula for ideal gas, energy dependent scattering kernel", Annals Nucl. En. **36**, 470 – 474 (2009).
[72] N. Larson and K. Volev, "Validation of multiple-scattering corrections in the analysis code SAMMY", in PHYSOR 2002, Seoul, Korea, October 7–10, No. 14C-03 (10 pages) (2002).
[73] F. Gunsing et al. (n_TOF Collaboration), "Measurement of resolved resonances of ^{232}Th(n,γ) at the n_TOF facility at CERN", Phys. Rev. C **85**, 064601 (2012).
[74] R.E. MacFarlane and A.C. Kahler, "Methods for processing ENDF/B-VII with NJOY", Nucl. Data Sheets **111**, 2739 – 2890 (2010).
[75] X-5 Monte Carlo Team, "MCNP – A General Monte Carlo N-Particle Transport Code, Version 5", Report LANL, LA-UR-03-1987 (2003).
[76] S. Kopecky, I. Ivanov, M. Moxon, P. Schillebeeckx, P. Siegler and I. Sirakov, "The total cross section for the 0.178 eV resonance of ^{113}Cd", Nucl. Instr. Meth. B **267**, 2345 – 2350 (2009).
[77] J. A. Harvey and N. W. Hill "Scintillation detectors for neutron physics research", Nucl. Instr. Meth. **162**, 507 – 529 (1979).
[78] C. M. Perey, F. G. Perey, J. A. Harvey, N. W. Hill, N. M. Larson, R. L. Macklin, and D. C. Larson, "^{58}Ni + n transmission, differential elastic scattering, and capture measurements and analysis up to 813 keV", Phys. Rev. C **47**, 1143 – 1169 (1993).
[79] D.P. Barry, M.J. Trbovich, Y. Danon, R.C. Block, R.E. Slovacek, G. Leinweber, J.A. Burke and N.J. Drindak, "Neutron transmission and capture measurements and resonance parameter analysis of neodymium from 1 to 500 eV", Nucl. Sci. Eng. **153**, 8 – 25 (2006).
[80] F.J. Saglimen, Y. Danon, R.C. Block, M.J. Rapp, R.M. Bahran, G. Leinweber, D.P. Barry and N.J. Drindak, "A system for differential neutron scattering experiments in the energy range from 0.5 to 20 MeV", Nucl. Instr. Meth. A **620**, 401-409 (2010).
[81] D.C. Larson, N.M. Larson, J.A. Harvey, N.W. Hill, and C.H. Johnson, "Application of new techniques to ORELA neutron transmission measurements and their uncertainty analysis: the case of natural nickel from 2 keV to 20 MeV", ORNL Report, ORNL/TM-8203 (1983).
[82] D.B. Syme, "The black and white filter method for background determination in neutron time-of-flight spectrometry", Nucl. Instr. Meth. **198**, 357 – 364 (1982).
[83] M. C. Moxon and M. G. Sowerby, "A review of the U-238 resolved resonance parameters", AERE Report, AERE - R 10597, Harwell, Oxfordshire, August 1982.
[84] M. J. Rapp, "Design and construction of a large area detector system and neutron total cross section measurements in the energy range 0.4 to 20 MeV", PhD thesis, Rensselaer Polytechnic Institute Troy, New York, August 2011 (unpublished).
[85] C.H. Vincent, "Optimum sample thickness for total cross section measurements", Nucl. Inst. Meth. **219**, 440 (1984).
[86] V.F. Sears, "Optimum counting times in experiments governed by poisson statistics", Nucl. Inst. Meth. **B 12**, 430 – 433 (1985).
[87] M.E. Rose, M.M. Shapiro, "Statistical error in absorption experiments", Phys. Rev. **74**, 1853 – 1864 (1948).
[88] S. Kopecky, Ph.D Thesis, TU-Wien, 1995 (unpublished).
[89] Y. Danon and R.C. Block, "Minimizing the statistical error of resonance parameters and cross-sections derived from transmission measurements", Nucl. Inst. Meth. **A 485**, 585 – 595 (2002).
[90] S. Kopecky, P. Siegler and A. Moens, "Low energy transmission measurements of ^{240,242}Pu at GELINA and their impact on the capture width", Proc. Int. Conf. Nuclear Data for Science and Techn., Nice, France, April, 2007, pp. 623 – 626 (2007).
[91] P. A. Egelstaf, D. B. Gayther and K. P. Nicholson, "The slow-neutron resonance behavior of plutonium isotopes", J. Nuc. En. **6**, 303 – 321 (1958).
[92] R. E. Coté, L. M. Bollinger, R. F. Barnes, and H. Diamond, "Slow-Neutron Cross Sections of Pu^{240}, Pu^{242}, and Am^{243}", Phys. Rev. **114**, 505 – 509 (1959).
[93] G. F. Auchampauch, C. D. Bowman, M. S. Coops, and S. C. Fultz, "Neutron total cross section of Pu^{242}", Phys. Rev. **146**, 840 – 843 (1966).
[94] T. E. Young and S. D. Reeder, "Total neutron cross section of ^{242}Pu", Nucl. Sci. Eng. **40**, 389 – 395 (1970).
[95] G. Leinweber, D.P. Barry, M.J. Trbovich, J.A. Burke, N.J. Drindak, H.D. Knox, R.V. Ballad, R.C. Block, Y. Danon, and L.I. Severnyak, "Neutron capture and total cross-section measurements and resonance parameters of gadolinium", Nucl. Sci. Eng. **154**, 261 – 279 (2006).
[96] H.J. Rose and D.M. Brink, "Angular distributions of gamma rays in terms of phase-defined reduced matrix elements", Rev. Mod. Phys. **39**, 306 – 347 (1976).
[97] L.C. Mihailescu, L. Oláh, C. Borcea, and A.J.M. Plompen, "A new HPGe setup at Gelina for measurement of gamma-ray production cross-sections from inelastic neutron scattering", Nucl. Instr. Meth. A **531**, 375 – 391 (2004).
[98] A. Borella, G. Aerts, F. Gunsing, M. Moxon, P. Schillebeeckx and R. Wynants, "The use of C_6D_6 detectors for neutron induced capture cross-section measurements in

Author's personal copy

the resonance region", Nucl. Instr. Meth. A **577**, 626 – 640 (2007).

[99] C. Massimi et al. (the n_TOF collaboration), "^{197}Au cross section in the resonance region", Phys. Rev. C **81**, 044616 – 22 (2010).

[100] C. Lederer et al. (the n_TOF collaboration), "^{197}Au cross section in the unresolved resonance region", Phys. Rev. C **83**, 034608 – 11 (2011).

[101] J. Pancin et al. (the n_TOF collaboration), "Measurement of the n_TOF beam profile with a micromegas detector", Nucl. Instr. Meth. A **524**, 102 – 114 (2004).

[102] R. L. Macklin, N. W. Hill and B. J. Allen, "Thin ^{6}Li(n,α)T transmission flux monitor", Nucl. Instr. Meth. **96**, 509 – 513 (1971).

[103] S. Marrone et al. (the n_TOF collaboration), "A low background neutron flux monitor for the n_TOF facility at CERN", Nucl. Instr. Meth. A **517**, 389 – 398 (2004)

[104] G. Grosshoeg, "Neutron ionization chamber", Nucl. Instr. Meth. **162**, 125 – 160 (1979).

[105] D. M. Gilliam, G. P. Lamaze, M. S. Dewey abd G. L. Greene, "Mass assay and uniformity tests of boron targets by neutron beam methods", Nucl. Instr. Meth. A **334**, 149 – 153 (1993).

[106] A. Borella, K. Volev, A. Brusegan, P. Schillebeeckx, F. Corvi, N. Koyumdjieva, N. Janeva and A.A. Lukyanov, "Determination of the ^{232}Th(n,γ) cross section from 4 to 140 keV at GELINA", Nucl. Sci. Eng. **152**, 1 – 14 (2006).

[107] A. Borella, F. Gunsing, M. Moxon, P. Schillebeeckx and P. Siegler, "High-resolution neutron transmission and capture measurements of the nucleus ^{206}Pb", Phys. Rev. C **76**, 014605 – 18 (2007).

[108] G. Giorginis and V. Khriatchkov, "The effect of particle leaking and its implications for measurements of the (n,α) reaction on light elements by using ionization chambers", Nucl. Instr. Meth. A **538**, 550 – 558 (2005).

[109] D. M. Gilliam, G. L. Greene and G. P. Lamaze, "Absolute neutron counting based on B-10 alpha-gamma coincidence methods", Nucl. Instr. Meth. A **284**, 220 – 222 (1989).

[110] R.L. Macklin and J.H. Gibbons, "Capture-cross-section studies for 30-220-keV neutron using a new technique", Phys. Rev. **159**, 1007 – 1012 (1967).

[111] S. Wang, M. Lubert, Y. Danon, N. C. Francis, R. C. Block, F. Bečvář, M. Krtička, "The RPI multiplicity detector response to γ-ray cascades following neutron capture in ^{149}Sm and ^{150}Sm", Nucl. Instr. Meth. A **513** 585 – 595 (2003).

[112] S. Yamamoto, Y. Fujita, T. Shibata and S. Selvi, "Characteristics of BGO scintillator for use in neutron capture cross section measurements", Nucl. Instr. Meth. A **249**, 484 – 490 (1986).

[113] O. Shcherbakov, K. Furutaka, S. Nakamura, H. Harada, and K. Kobayashi, "A BGO detector system for studies of neutron capture by radioactive nuclides", Nucl. Instr. Meth. A **517**, 269 – 284 (2004).

[114] O. Shcherbakov, K. Furutaka, S. Nakamura, H. Sakane, K. Kobayashi, S. Yamamoto, J. Hori, and H. Harada, " Measurement of neutron capture cross section of ^{237}Np from 0.02 to 100 eV", J. Nucl. Sci. Techn. **42** (No.2), 135 – 144 (2005).

[115] H. W. Schmitt, "Sample scattering corrections in neutron beam experiments", ORNL-2883 (1960).

[116] H. Harada, S. Goko, A. Kimura, M. Ohta, M. Oshima, F. Kitatani, Y. Toh, K. Furutaka, T. Kin, M. Koizumi, S. Nakamura, M. Igashira, T. Katabuchi, M. Mizumoto, T. Ohsaki, J. Hori, T. Fujii, K. Takamiya, J. Goto, Y. Kiyanagi, K. Kino, M. Furusaka, F. Hiraga and T. Kamiyama,"Study of neutron capture reactions using the 4π Ge spectrometer", J. Korean Phys. Soc., **59**, 1547 – 1552 (2011).

[117] D. B. Gayther, "International intercomparison of fast neutron fluence-rate measurements using fission chamber transfer instruments", Metrologia **27**, 221 – 231 (1990).

[118] S. A. Wender, S. Balestrini, A. Brown, R. C. Haight, C. M. Laymon, T. M. Lee, P. W. Lisowski, W. McCorkle, R. O. Nelson and W. Parker, "A fission ionization detector for neutron flux measurements at a spallation source", Nucl. Instr. Meth. A **336**, 226 – 231 (1993).

[119] C. Budtz-Jørgensen, H.-H. Knitter, Ch. Straede, F.-J. Hambsch and R. Vogt, "A twin ionization chamber for fission fragment detection", Nucl. Instr. Meth. A **258**, 209 – 220 (1987).

[120] S. Andriamonje, M. Calviani, Y. Kadi, R. Losito, V. Vlchoudis, E. Berthounieux, F. Gunsing, A. Giganon, Y. Giomataris, C. Guerrero, R. Sarmento, (the n_TOF collaboration), "A transparant detector for n_TOF neutron beam monitoring", J. Korean Phys. Soc. **59**, 1597 – 1600 (2011).

[121] R. L. Macklin, J. Halperin, and R. R. Winters, "Absolute neutron capture yield calibration", Nucl. Instr. Meth. **164**, 213 – 214 (1979).

[122] J. Heyse, C. Wagemans, L. De Smet, O. Serot, J. Wagemans, and J. Van Gils, "High resolution measurement of the ^{234}U(n,f) cross section in the neutron energy range from 0.5 eV to 100 keV", Nucl. Sci. Eng. **156**, 211 – 218 (2007).

[123] C. Paradela et al. (The n_TOF collaboration), "Neutron-induced fission cross section of ^{234}U and ^{237}Np measured at the CERN neutron time-of-flight (n_TOF) facility", Phys. Rev. C **82**, 034601 – 11 (2010).

[124] M. Calviani et al. (The n_TOF collaboration), "A fast ionization chamber for fission cross-section measurements at n_TOF", Nucl. Instr. Meth. A **594**, 220 – 227 (2008).

[125] K. H. Guber, R. R. Spencer, L. C. Leal, J. A. Harvey, N. W. Hill, G. Dos Santos, R. O. Sayer and D. C. Larson, "New high-resolution fission cross-section measurements of ^{233}U in the 0.4-eV to 700-keV energy range", Nucl. Sci. Eng. **135**, 141 – 149 (2000).

[126] F. Tovesson and T.S. Hill, "Neutron induced fission cross section of ^{237}Np from 100 keV to 200 MeV", Phys. Rev. C **75**, 034610 – 8 (2007).

[127] L. De Smet, C. Wagemans, G. Goeminne, J. Heyse, and J. Van Gils, "Experimental determination of the ^{36}Cl(n,p)^{36}S and ^{36}Cl(n,α)^{33}P reaction cross section and the consequence on the origin of ^{36}S", Phys. Rev. C **75**, 034617 – 8 (2007).

[128] P. E. Koehler, S. M. Graff, H. A. O'Brien, Yu. M. Gledenov, and Yu. P. Popov,"^{36}Cl(n,p)^{36}S cross section from 25 meV to 800 keV and the nucleosynthesis of the rare isotope ^{36}S", Phys. Rev. C **47**, 2107 – 2112 (1993).

[129] P. E Koehler, J. A Harvey, and N. W Hill, "Two detectors for (n,p) and (n,α) measurements at white neutron sources", Nucl. Instr. Meth. A **361**, 270 – 276 (1995).

Author's personal copy

[130] Yu. M. Gledenov, P. E. Koehler, J. Andrzejewski, K. H. Guber, and T. Rauscher, "^{147}Sm(n,α) cross section measurements from 3 eV to 500 keV: Implications for explosive nucleosynthesis reaction rates", Phys. Rev. C **62**, 042801(R) – 4 (2000).

[131] P. Schillebeeckx, A. Borella, J. C. Drohe, R. Eykens, S. Kopecky, C. Massimi, L. C. Mihailescu, A. Moens, M. Moxon, and R. Wynants,"Target requirements for neutron-induced cross-section measurements in the resonance region", Nucl. Instr. Meth. A **613**, 378 – 385 (2010).

[132] C. Wagemans, P. Schillebeeckx, and J.P. Bocquet,"Measurement of the Thermal Neutron Induced Fission Cross Section of ^{243}Am", Nucl. Sci. Eng. **101**, 293 – 297 (1989).

[133] F. Corvi, "The measurement of neutron capture cross sections via prompt gamma-ray detection", Proc. Specialists Meeting on Measurement, Calculation and Evaluation of Photon Production Data, eds. C. Coceva et al., Bologna Nov. 9-11, 1994, Report NEA/NSC/DOC (95)1, pp. 229 – 246.

[134] U. Abbondanno et al. (the n_TOF collaboration), "The data acquisition system of the neutron time-of-flight facility n_TOF at CERN", Nucl. Instr. Meth. A **538**, 692 – 702 (2005).

[135] L. C. Mihailescu, C. Borcea and A. J. M. Plompen, "Data acquisition with a fast digitizer for large volume HPGe detectors", Nucl. Instr. Meth. A **578**, 298 – 305 (2007).

[136] C. Massimi, A. Borella, S. Kopecky, C. Lampoudis, M. C. Moxon, P. Schillebeeckx and G. Vannini, "Neutron resonance parameters of ^{197}Au from transmission, capture and self-indication measurements", J. Korean Phys. Soc. **59**, 1689 – 1692 (2011).

[137] G. Aerts et al. (The n_TOF collaboration), "Neutron capture cross section of ^{232}Th measured at the n_TOF facility at CERN in the unresolved resonance region up to 1 MeV", Phys. Rev. C **73**, 054610 – 10 (2006).

[138] F. Corvi, G. Fioni, F. Gunsing, P. Mutti and L. Zanini, "Resonance neutron capture in ^{60}Ni below 450 keV", Nucl. Phys. A **697**, 581 – 610 (2002).

[139] C. Guerrero *et al.*, (n_TOF Collaboration), "Measurement and resonance analysis of the ^{237}Np neutron capture cross section", Phys. Rev. C **85**, 044616 – 15 (2012).

[140] R. L. Macklin, R. B. Perez, G. de Saussure and R. W. Ingle, "High energy resolution measurement of the ^{238}U neutron capture yield from 1 to 100 keV", Ann. Nucl. Energy **18**, 567 – 583 (1991).

[141] C. Guerrero et al. (the n_TOF collaboration), "Characterization of the new n_TOF neutron beam: Fluence, profile, and resolution", **59**, 1624 – 1627 (2011).

[142] H. Beer, F. Corvi, and P. Mutti, "Neutron capture of the bottleneck isotopes ^{138}Ba and ^{208}Pb, s-process studies, and the r-process abundance distribution", Ap. J. **474**, 843 – 861 (1997).

[143] P. E. Koehler, R.R. Winters, K.H. Guber, T. Rauscher, J.A. Harvey, S. Raman, R.R. Spencer, J.C. Blackmon, D.C. Larson, D.W. Bardayan, and T.A. Lewis, "High-resolution neutron capture and transmission measurements, and the stellar neutron-capture cross section of ^{88}Sr", Phys. Rev. C **62**, 055803 – 15 (2000).

[144] R. L. Macklin, J. Halperin and R. R. Winters, "Neutron capture by ^{208}Pb at stellar temperatures", Astrophys. J. **217**, 222 – 226 (1977).

[145] B.J.Allen, A.R. de L. Musgrove, and R.L. Macklin, "Neutron sensitivity of capture gamma ray detectors", Proceedings of a Specialists Meeting on Neutron Data of Structural Materials for Fast Reactors, Geel, Belgium, 1977, pp. 506 – 529 (1977).

[146] R. Plag, M. Heil, F. Käppeler, P. Pavlopoulos, R. Reifarth, and K. Wisshak, "An optimized C_6D_6 detector for studies of resonance-dominated (n,γ) cross-sections", Nucl. Instr. Meth. A **496**, 425 – 436 (2003).

[147] K. Wisshak and F. Käppeler, "Determination of the capture width of the 27.7-keV s-wave neutron resonance in Iron-56", Nucl. Sci. Eng. **77**, 58 – 70 (1981).

[148] T. Kikuchi, Y. Nagai, T. S. Suzuki, T. Shima, T. Kii, M. Igashira, A. Mengoni, and T. Otsuka, "Nonresonant direct p- and d-wave neutron capture by ^{12}C", Phys. Rev. C **57**, 2724 – 2730 (1998).

[149] C. Coceva, "Radiative transitions from neutron capture in ^{53}Cr resonances", Nuovo Cimento A **107**, 85 – 116 (1994).

[150] E.T. Jurney and H.T. Motz, "Thermal neutron capture in D and ^{16}O", Proc. of the Int. Conf. on Nuclear Physics with Reactor Neutrons, Argonne National Laboratory, 15 - 17 October, 1963, pp. 236 – 242 (1963).

[151] S. Raman, E.T. Jurney, J.W. Starner, and J.E. Lynn, "Thermal-neutron capture by silicon isotopes", Phys. Rev. C **46**, 972 – 983 (1992).

[152] A. Borella, T. Belgya, S. Kopecky, F. Gunsing, M. Moxon, M. Rejmund, P. Schillebeeckx and L. Szentmiklósi, "Determination of the ^{209}Bi(n,γ)^{210}Bi and ^{209}Bi(n,γ)^{210m,g}Bi reaction cross sections in a cold neutron beam", Nucl. Phys. A**850**, 1 – 21 (2011).

[153] Zs. Révay, T. Belgya and G.L. Molnár, "New prompt k_0 and partial cross section values measured in the cold neutron beam of Budapest Research Rector", J. Radional. Nucl. Chem. **265**, 169 – 173 (2005).

[154] M. Mizumoto and M. Sugimoto, "The influence of water absorption in samples for neutron capture cross section measurements", Nucl. Instr. Meth. A **282**, 324 – 328 (1989).

[155] J. C. Blackmon, S. Raman, J. K. Dickens, R. M. Lindstrom, R. L. Paul and J. E. Lynn, "Thermal-neutron capture by ^{208}Pb", Phys. Rev. C **65** 045801 – 9 (2002).

[156] R. Köhler, J. A. Wartena, H. Weigmann, L. Mewissen, F. Poortmans, J. P. Theobald and S. Raman, "Nuclear structure of ^{208}Pb from ^{207}Pb + n resonances", Phys. Rev. C **35**, 1646 – 1660 (1987).

[157] S. Nakamura, H. Harada, S. Raman and P. E. Koehler, "Thermal-neutron capture cross section of palladium-107", J. Nucl. Sci. Technol. **44**, 103 – 108 (2007).

[158] S. Nakamura, H. Harada, S. Raman and P. E. Koehler, "Thermal-neutron capture cross section of zirconium-91 and zirconium-93", J. Nucl. Sci. Technol. **44**, 21 – 28 (2007).

[159] T. Belgya, "Improved accuracy of γ-ray intensities from basic principles for the calibration reaction ^{14}N(n,γ)^{15}N", Phys. Rev. C **74**, 024603 (2006).

[160] F. Bečvář, "Simulation of γ cascades in complex nuclei with emphasis on assessment of uncertainties of cascade-related quantities", Nucl. Instr. Meth. A **417**, 434 – 449 (1998).

[161] J. L. Tain and D. Cano - Ott, "The influence of the unknown de-excitation pattern in the analysis of γ-decay total absorption spectra", Nucl. Inst. Meth. A **571**, 719 – 727 (2012).

Author's personal copy

[162] G. Schramm, R. Massarczyk, A. R. Junghans, T. Belgya, R. Beye, E. Birgersson, E. Grosse, M. Kempe, Z. Kis, K. Kosev, M. Krtička, A. Matic, K. D. Schilling, R. Schwengner, L. Szentmiklósi, A. Wagner and J. L. Weil, "Dipole strength in ^{78}Se below the neutron separation energy from a combined analysis of ^{77}Se(n,γ) and ^{78}Se(γ,γ') experiments", Phys. Rev. C **85**, 014311 –14 (2012)

[163] B. C. Diven, J. Terrell and A. Hemmendinger, "Radiative capture cross sections for fast neutrons", Phys. Rev. **120**, 556 – 569 (1960).

[164] J. H. Gibbons, R. L. Macklin, P. D. Miller and J. H. Neiler, "Average radiative capture cross sections for 7- to 170-keV neutrons", Phys. Rev. **122**, 182 – 201 (1961).

[165] E. Haddad, R. B. Walton, S. J. Friesenhahn and W. M. Lopez, "A high efficiency detector for neutron capture cross section measurements", Nucl. Instr. Meth. **31**, 125 – 138 (1964).

[166] R. W. Hockenbury, Z. M. Bartolome, J. R. Tatarczuk, W. R. Moyer and R. C. Block, "Neutron radiative capture in Na, Al, Fe, and Ni from 1 to 200 keV", Phys. Rev. **178**, 1746 – 1769 (1969).

[167] D. Kompe, "Capture cross-section measurements of some medium- and heavy-weight nuclei in the keV region", Nucl. Phys. A**133**, 513 – 536 (1969).

[168] B. C. Diven, J. Terrell and A. Hemmendinger, "Capture-to-fission ratios for fast neutrons in U^{235}", Phys. Rev. **109**, 144 – 150 (1958).

[169] J. C. Hopkins and B. C. Diven, "Neutron capture to fission ratios in ^{233}U, ^{235}U, ^{239}Pu", Nucl. Sci. Eng. **12**, 169 – 177 (1962).

[170] L. W. Weston, G. de Saussure and R. Gwin, "Ratio of capture to fission in U^{235} at keV neutron energies", Nucl. Sci. Eng. **20**, 80 – 87 (1964).

[171] G. de Saussure, L. W. Weston, R. Gwin, J. E. Russell and R. W. Hockenbury, "Measurement of the U^{235} neutron capture-to-fission ratio, α, for incident neutron energies from 3.25 eV to 1.8 keV", Nucl. Sci. Eng. **23**, 45 – 57 (1965).

[172] L. W. Weston, R. Gwin, G. de Saussure, R. R. Fullwood and R. W. Hockenbury, "Measurement of the neutron induced fission and capture cross sections for ^{235}U in the energy region 0.4 to 2000 eV", Nucl. Sci. Eng. **34**, 1 – 12 (1968).

[173] R. Gwin, L. W. Weston, G. de Saussure, R. W. Ingle, J. H. Todd, F. E. Gillespie, R. W. Hockenbury and R. C. Block, "Measurements of the neutron fission and absorption cross sections of ^{239}Pu over the energy region 0.02 eV to 30 keV", Nucl. Sci. Eng. **40**, 306 – 316 (1970).

[174] L. W. Weston, R. Gwin, G. de Saussure, R. W. Ingle, R. W. Hockenbury and R. C. Block, "Neutron fission and capture cross-section measurements for Uranium-233 in the energy region 0.002 to 1 eV", Nucl. Sci. Eng. **42**, 143 – 149 (1970).

[175] R. Gwin, L. W. Weston, G. de Saussure, R. W. Ingle, J. H. Todd, F. Gillespie, R. W. Hockenbury and R. C. Block, "Simultaneous measurement of the neutron fission and absorption cross sections of Plutonium-239 over the energy region 0.02 eV to 30 keV", Nucl. Sci. Eng. **45**, 25 – 36 (1971).

[176] R. B. Perez, G. de Saussure, E. G. Silver, R. W. Ingle and H. Weaver, "Simultaneous measurements of the neutron fission and capture cross sections for Uranium-235 for neutron energies from 8 eV to 10 keV", Nucl. Sci. Eng. **52**, 46 – 72 (1973).

[177] R. Gwin, E. G. Silver, R. W. Ingle and H. Weaver, "Measurement of the neutron capture and fission cross sections of ^{239}Pu and ^{235}U, 0.02 eV to 200 keV, the neutron capture cross section of ^{197}Au, 10 to 50 keV, and neutron fission cross sections of ^{233}U, 5 to 200 keV", Nucl. Sci. Eng. **59**, 79 – 105 (1976).

[178] R. E. Bandl, H. Miessner, and F. H. Fröhner, "A measurement of the capture-to-fission cross section ratios of Uranium-235 and Plutonium-239 with a new technique", Nucl. Sci. Eng. **48**, 324 – 330 (1972).

[179] G.V. Muradyan, Yu. V. Adamchuk, Yu. G. Shchepkin and M.A. Voskanyan, "Multiplicity spectrometer for measuring neutron cross sections", Nucl. Sci. Eng. **90**, 60 -74 (1985).

[180] K. Wisshak, K. Guber, F. Käppeler, J. Krisch, H. Müller, G. Rupp and F. Voss, "The Karlsruhe 4π barium fluoride detector", Nucl. Instr. Meth. A **292**, 595 – 618 (1990).

[181] C. Guerrero et al. (the n_TOF collaboration), "The n_TOF Total Absorption Calorimeter for neutron capture measurements at CERN", Nucl. Instr. Meth. A **608** 424 – 433 (2009).

[182] B. Baramsai, G. E. Mitchell, U. Agvaanluvsan, F. Bečvář, T. A. Bredeweg, A. Chyzh, A. Couture, D. Dashdorj, R. C. Haight, M. Jandel, A. L. Keksis, M. Krtička, J. M. O'Donnell, R. S. Rundberg, J. L. Ullmann, D. J. Vieira and C. L. Walker, "Neutron resonance parameters in ^{155}Gd measured with the DANCE γ-ray calorimeter array", Phys. Rev. C **85**, 024622 – 13 (2012).

[183] M. Heil, R. Reifarth, M.M. Fowler, R.C. Haight, F. Käppeler, R.S. Rundberg, E.H. Seabury, J.L. Ullmann, J.B. Wilhelmy and K. Wisshak, "A 4π BaF_2 detector for (n,γ) cross-section measurements at a spallation neutron source", Nucl. Instr. Meth. A **459**, 229 – 246 (2001).

[184] J. Goto, H. Harada, F. Kitatani, Y. Nagai, M. Oshima, M. Segawa and Y. Toh, "Design of a 4$\pi$$LaBr_3$(Ce) spectrometer for neutron capture cross section measurements", J. Korean Phys. Soc. **59**, 1585 - 1588 (2011).

[185] K. Wisshak, F. Käppeler and G. Schatz, "Calculated efficiency of a 4π detector of BGO or BaF_2 for monoenergetic gamma rays and gamma cascades following neutron capture", Nucl. Instr. Meth. **221**, 385 – 392 (1984).

[186] M. Jandel, T. A. Bredeweg, E. M. Bond, M. B. Chadwick, R. R. Clement, A. Couture, J. M. O'Donnell, R. C. Haight, T. Kawano, R. Reifarth, R. S. Rundberg, J. L. Ullmann, D. J. Vieira, J. B. Wilhelmy, J. M. Wouters, U. Agvaanluvsan, W. E. Parker, C. Y. Wu and J. A. Becker, "Neutron capture cross section of ^{241}Am", Phys. Rev. C **78**, 034609 – 15 (2008).

[187] C. Guerrero, D. Cano-Ott, E. Mendoza, J. L. Tain, A. Algora, E. Berthoumieux, N. Colonna, C. Domingo-Pardo, E. Gonzalez-Romero, M. Heil, D. Jordan, F. Käppeler, C. Lampoudis, T. Martinez, C. Massimi, R. Plag, "Monte Carlo simulation of the n_TOF Total Absorption Calorimeter", Nucl. Instr. Meth. A **671**, 108 - 117 (2012).

[188] T. A. Bredeweg, M. M. Fowler, J. A. Becker, E. M. Bond, M. B. Chadwick, R. R. C. Clement, E. -I. Esch, T. Ethvignot, T. Granier, M. Jandel, R. A. Macri, J. M. O'Donnell, R. Reifarth, R. S. Rundberg, J. L. Ullmann, D. J. Vieira, J. B. Wilhelmy, J. M. Wouters and C. Y. Wu, "Simultaneous measurement of (n,γ) and (n,fission)

Author's personal copy

cross sections with the DANCE 4π BaF_2 array", Nucl. Instr. Meth. B **261**, 986 – 989 (2007).

[189] C. Guerrero et al. (the n_TOF collaboration), "Simultaneous measurement of neutron-induced capture and fission reactions at CERN", Eur. Phys. J. A **48**, 29 – (2012).

[190] E. Berthoumieux et al. (the n_TOF collaboration), "Simultaneous measurement of the neutron capture and fission yields of ^{233}U", Proc. Int. Conf. on Nuclear Data for Science and Technology, Nice, 22 - 27 April, 2007, pp. 571 – 574 (2007).

[191] N. Yamamuro, T. Hayase, T. Doi, Y. Fujita, K. Kobayashi and R. C. Block, "Reliability of the weighting function for the pulse height weighting technique", Nucl. Instr. Meth. **133**, 531 – 536 (1976).

[192] M.C. Moxon and E.R. Rae, "A gamma-ray detector for neutron capture cross-section measurements", Nucl. Instr. Meth. **24**, 445 – 455 (1963).

[193] K. Wisshak, F. Käppeler, G. Reffo and F. Fabbri, "Neutron capture in s-wave resonances of Iron-56, Nickel-58 and Nickel-60", Nucl. Sci. Eng. **86**, 168 – 183 (1984).

[194] F. Corvi, C. Bastian and K. Wisshak, "Neutron capture in the 1.15-keV resonance of ^{56}Fe using Moxon-Rae detectors", Nucl. Sci. Eng. **93**, 348 – 356 (1986).

[195] K. Kobayashi, S. Lee, S. Yamamoto, H. J. Cho and Y. Fujita, "Measurement of neutron capture cross section of ^{237}Np by linac time-of-flight method and with linac-driven lead slowing-down spectrometer", J. Nucl. Sci. Techn. **39**, 111 – 119 (2002).

[196] K.H. Guber, H. Derrien, L.C. Leal, G. Arbanas, D. Wiarda, P.E. Koehler, and J.A. Harvey, "Astrophysical reaction rates for ^{58,60}Ni(n,γ) from new capture cross section measurements", Phys. Rev. C **82**, 057601 – 4 (2010).

[197] N. V. Kornilov, "Capture cross section measurements with a total energy BGO-detector", Nucl. Instr. Meth. A **379**, 317 – 322 (1996).

[198] C. Massimi, B. Becker, S. Kopecky, C. Lampoudis, R. Massarczyk, M. Moxon, V. Pronyaev, P. Schillebeeckx, I. Sirakov, K. Volev, and R. Wynants, to be published.

[199] F.G. Perey, J.O. Johnson, T.A. Gabriel, R.L. Macklin, R.R. Winters, J.H. Todd, and N.H. Hill, "Responses of C_6D_6 and C_6F_6 γ-ray detectors and the capture in the 1.15-keV resonance of ^{56}F", Proc. of the International Conference on Nuclear Data for Science and Technology, Mito, Japan, 1988, pp. 379 – 382 (1988).

[200] J.N. Wilson, B. Haas, S. Boyer, D. Dassie, G. Barreau, M. Aiche, S. Czajkowski, C. Grosjean, A. Guiral, "Measurements of (n,γ) neutron capture cross-sections with liquid scintillator detectors", Nucl. Instr. Meth. A **511** 388 – 399 (2003).

[201] U. Abbondanno et al. (The n_TOF collaboration), "New experimental validation of the pulse height weighting technique for capture cross-section measurements", Nucl. Instr. Meth. A **521**, 454 –467 (2004).

[202] C. Domingo-Pardo et al. (the n_TOF collaboration), "Measurement of the radiative neutron capture cross section of ^{206}Pb and its astrophysical implications", Phys. Rev. C **76**, 045805 – 10 (2007).

[203] F. Corvi, G. Fioni, F. Gasperini and P.B. Smith, "The weighting function of a neutron capture detection system", Nucl. Sci. Eng. **107**, 272 – 283 (1991).

[204] K. Wisshak, G. Walter and F. Käppeler, "Self-absorption of neutron capture gamma-rays in gold samples", Nucl. Instr. Meth. **219**, 136–140 (1984).

[205] F.G. Perey, "Status of the parameters of the 1.15-keV resonance of ^{56}Fe", Proc. Intern. Conf. Nuclear Data for Basic and Applied Science, Santa Fe, New Mexico, pp. 1523 – 1528 (1985).

[206] R. L. Macklin, "A self-calibrated neutron capture measurement of the 1.15-keV resonance of iron", Nucl. Sci. Eng. **95**, 200 – 205 (1987).

[207] F. Corvi, L. Calabretta, M. Merla, T. van der Veen and M. S. Morre, "Measurement of neutron capture cross section and alpha of ^{235}U from 2 to 85 keV", Proc. ANL-83-4 NEANDC(US)-214, (1983).

[208] T. Hauschild, M. Jentschel, "Comparison of maximum likelihood estimation and chi-square statistics applied to counting experiments", Nucl. Instr. Meth. A **457**, 384–401 (2001).

[209] L.C. Mihailescu, I. Sirakov, R. Capote, A. Borella, K.H. Guber, S. Kopecky, L.C. Leal, P. Schillebeeckx, P. Siegler, E. Soukhovitskii and R. Wynants,"Evaluation of the ^{103}Rh neutron cross-section data in the unresolved resonance region for improved criticality safety", Proc. Int. Conf. on Nuclear Data for Science and Technology, Nice, 22 - 27 April, 2007, pp. 649 – 652 (2007).

[210] C. De Saint Jean, G. Noguere, B. Habert and B. Iooss, "A Monte Carlo approach to nuclear model parameter uncertainties propagation", Nucl. Sci. Eng. **161**, 363 – 370 (2009).

[211] B. Habert, C. De Saint Jean, G. Noguere, L. Leal, Y. Rugama, "Retroactive generation of covariance matrix of nuclear model parameters using marginalization techniques", Nucl. Sci. Eng. **166**, 276 – 287 (2010).

[212] C. De Saint Jean, B. Habert, G. Noguere, D. Bernard, J. M. Ruggieri, L. Leal and H. Derrien, "Covariances for ^{239}Pu induced cross section in the resonance region using the CONRAD code", J. Korean Phys. Soc. **59**, 1280 – 1283 (2011).

[213] C. Bastian, "General procedures and computational methods for generating covariance matrices", Proc. Int. Symposium on Nuclear Data Evaluation Methodology, Brookhaven National Laboratory, USA, October 12-16, 1992, pp. 642 – 649 (1992).

[214] R. Capote, L. Leal, P. Liu, T. Liu, P. Schillebeeckx, M. Sin, I. Sirakov and A. Trkov, "Evaluated nuclear data for nuclides within the thorium-uranium fuel cycle", Technical Report IAEA Nuclear Data Section, STI/PUB/1435, (2010).

[215] Cross Sections Evaluation Working Group, ENDF-6 Format Manuals. Data Formats and Procedures for the Evaluated Nuclear Data Files ENDF/B-VI and ENDF/B-VII. In: A.Trkov, M.Herman and D.Brown (Ed.), 2011, Report BNL-90365-2009-Rev.2, NNDC, BNL, Upton, New York (2011).

[216] P. Johnston (ed.), "Summary record of the third meeting of nuclear reaction data centres, Paris, France, 19-23 June 1978", INDC(NDS)-99, OECD Nuclear Energy Agency (1978).

[217] K.H. Böckhoff (ed.), Proc. of a Specialists' Meeting on Neutron Data of Structural Materials for Fast Reactors, Geel, Belgium, 5-8 December, 1977, Pergamon Press, Oxford, pp. 789 – 802 (1977).

[218] M.J. Kenny, B.J. Allen, A.R. de L. Musgrove, R.L. Macklin, J. Halperin, "Neutron capture by the chromium isotopes", AAEC/E400, Australian Atomic Energy Commission Research Establishment, Lucas

Author's personal copy

Heights (1977). EXFOR 30393 and 30429.

[219] B.J. Allen, A.R. de L. Musgrove, J.W. Boldeman, M.J. Kenny, R.L. Macklin, "Resonance neutron capture in ^{56}Fe", Nucl. Phys. **A269**, 408 – 428 (1976). EXFOR 30355 and 30430.

[220] B.J. Allen, A.R. de L. Musgrove, J.W. Boldeman, R.L. Macklin, "Valence neutron capture in ^{54}Fe", Nucl. Phys. A **283**, 37 – 44 (1977). EXFOR 30355 and 30430.

[221] B.J. Allen, A.R. de L. Musgrove, R. Taylor, R.L. Macklin, "Neutron capture cross section of ^{57}Fe", Proc. of a Specialists' Meeting on Neutron Data of Structural Materials for Fast Reactors, Geel, Belgium, 5-8 December, 1977, Pergamon Press, Oxford, pp. 476 – 496 (1977). EXFOR 30424 and 30430.

[222] H.I. Liou, H.S. Camarda, G. Hacken, F. Rahn, J. Rainwater, M. Slagowitz, S. Wynchank, "Neutron resonance spectroscopy. XI. The separated isotopes of Yb", Phys. Rev. C **7**, 823 – 839 (1973). EXFOR 10081.

[223] N. Otuka, A. Borella, S. Kopecky, C. Lampoudis, and P. Schillebeeckx, "Database for time-of-flight spectra with their covariances", J. Korean Phys. Soc. **59**, 1314 – 1317 (2011).

[224] N. Otuka (ed.), "Summary report on the IAEA technical meeting on the international network of nuclear reaction data centres, Vienna, Austria, 23-24 May, 2011", INDC(NDS)-0593, IAEA (2011).